Application of Sr-Nd-Pb isotopes to the late Quaternary Paleoceanography of the Atlantic Ocean

Dissertation zur Erlangung des Grades

"Doktor der Naturwissenschaften"

am Fachbereich Chemie, Pharmazie und Geowissenschaften

vorgelegt von

M.Sc. Ran Wei

geboren in Heilongjiang

Johannes Gutenberg-Universität Mainz

angefertigt am Max-Planck-Institut für Chemie

Mainz, 2016

Datum der mündlichen Prüfung: November 24th, 2016

I hereby declare that I wrote the dissertation submitted without any unauthorized external assistance and used only sources acknowledged in the work. All textual passages which are appropriated verbatim or paraphrased from published and unpublished texts as well as all information obtained from oral sources are duly indicated and listed in accordance with bibliographical rules. In carrying out this research, I complied with the rules of standard scientific practice as formulated in the statutes of the Johannes Gutenberg University, Mainz, to ensure standard scientific practice.

October 20th, 2016

Ran Wei

Abstract

The Atlantic Meridional Overturning Circulation (AMOC) plays a crucial role in distributing heat around the globe and impacts strongly on Earth's climate. The long-lived radiogenic systems Sm-Nd, Rb-Sr and Th-U-Pb have been developed and used extensively in oceanography as robust tracers of water mass provenance and water mass mixing, in particular, in relation to variability in the AMOC and its correlation with climate change and glacial-interglacial cycles. These applications of the Sr-Nd-Pb radiogenic isotope systems to paleoceanography are explored here by analyzing hydrogenetic components and terrigenous phases from Atlantic deep-sea sediment cores.

The reconstruction of paleocurrents has long been a subject of paleoceanographic research. Many of these studies have focused on documenting variations in North Atlantic Deep Water (NADW) intensity on millennial and glacial-interglacial timescales. Changes in AMOC strength and formation of NADW during the Last Glacial Maximum (LGM) still remain very uncertain despite being discussed and argued about in many studies. Here, we present Sr and Nd radiogenic isotope records of Fe-Mn oxide leachates of bulk sediment - which reflect the composition of deep water - from cores located in the South Atlantic, to reconstruct past variability in NADW circulation over the last glacial cycle. The Fe-Mn leachate ε_{Nd} records show a coherent decreasing trend from glacial radiogenic values towards less radiogenic values during the Holocene. Our results, along with published multi-proxy records, suggest that (a) a shallower Southern Component Water penetration northwards during the LGM, (b) there was continuous production and export of Northern Component Water over the last 24 kyr, and (c) the AMOC was reinvigorated progressively to its full strength today over the Holocene period.

A second study presented here uses the radiogenic isotopic compositions of Sr, Nd and Pb hosted in detrital minerals extracted from ocean sedimentary cores to infer the provenance

of air-borne dust deposited into the equatorial Atlantic, and to discuss these data in relation to glacial-interglacial climate forcing. The down-core Sr-Nd-Pb isotopes in the detrital fraction from a core located on the Sierra Leone Rise (SLR), in the eastern tropical Atlantic, imply that the predominant dust sources are located in Mauritania, Northern Mali and the Bodélé Depression. The eolian inputs from the Mali and Bodélé sources are present in roughly equal proportions throughout the past 180 kyr. However, more Mauritanian dust input, having a more radiogenic Pb isotopic composition, is found during African Humid Periods, when vegetation spread northwards and many now-dry lakes were filled, suppressing dust emission from the Mali and Bodélé Depression regions. Dust delivery to the SLR occurs mainly during the boreal winter by wet deposition, and is blocked during the summer monsoon months as the Intertropical Convergence Zone migrates northwards.

In the western equatorial Atlantic, we have investigated the detrital fraction of a sediment core located on the Ceara Rise (CR), which reflects suspended load output from the Amazon River plume entering the western Atlantic. Systematic variations are seen in the detrital fraction Sr-Nd-Pb isotope records from this core: these variations correlate extremely well with glacial-interglacial cycles. Within the catchment, terrigenous supply is from the highland Andes (in the west) and the lowland Guiana Shield (in the east), and there is a greater contribution from the highland Andes during glacial versus interglacial periods. Good correlations are observed between isotopic compositions, relative sea level and Northern Hemisphere summer insolation, showing that climate within the Amazon Basin as a whole was strongly modulated over glacial-interglacial cycles, exerting control on the provenance of the suspended load delivered by the Amazon River.

In summary, this thesis provides new insights into changes in AMOC strength over the last glacial cycle. Further, it is shown how North African eolian dust blown into the Eastern Atlantic was affected by climate over the past 200 kyr; similarly, we have obtained new

insights into how the suspended load off the Amazon River changed in provenance over the past several glacial-interglacial cycles.

Zusammenfassung

Die Atlantik meridionale Umwältzbewegung (AMOC; engl.: Atlantic Meridional Overturning Circulation) spielt eine entscheidende Rolle, Hitze um den Globus zu verteilen und hat starke Auswirkungen auf das Klima der Erde. Die langlebigen radiogenischen Isotopensysteme Sm-Nd, Rb-Sr und Th-U-Pb wurden entwickelt und finden in der Ozeanographie Anwendungen als robuste Tracer von Wassermassen, deren Herkunft und Wassermassenmischungsprozessen, insbesondere in Bezug auf die Variabilität der AMOC und Korrelationen mit Klimawandel und Glazial-Interglazial-Zyklen. Diese Anwendungen der Sr-Nd-Pb Isotopensysteme zu Paläozeanographie werden hier durch Analysen von hydrogenetischen Komponenten und terrestrische Phasen (kontinentaler Detritus) in Atlantik Tiefseesedimentbohrkernen realisiert.

Die Rekonstruktion von Paläoströmen ist ein zentrales Thema der paläozeanographischen Forschung. Viele dieser Studien konzentrierten sich auf die Erforschung von Schwankungen der Nord-Atlantik-Tiefwasser (NADW; engl.: North Atlantic Deep Water) Strömungsintensität auf tausendjährigen und glazial-interglazialen Zeitskalen. Änderungen in AMOC Stärke und ob die Bildung von NADW während des letzten glazialen Maximums (LGM) stattgefunden hat, bleiben immerhin trotz heftige Diskussion und Argumentation aus vielen Studien relativ ungewiss. Wir präsentieren Sr- und Nd-Radiogen-Isotopendaten für Fe-Mn-Oxid-Phasen, die die Zusammensetzung von tiefem Wasser wiederspiegeln, aus Sedimentärablagerungen, die aus Ozeanbohrkernen im Südatlantik gewonnen waren; hier wurde die Variabilität der NADW-Zirkulation durch die letzte Eiszeit rekonstruiert. Die Fe-Mn-Oxid ε_{Nd}-Daten zeigen einen progressiv abnehmenden Trend von glazialen radiogenischen Werten bis zu weniger radiogen während des Holozäns. Veröffentlichte Multi-Proxy-Daten zusammen mit unseren Ergebnissen deuten darauf hin, dass (a) Süd-Komponent Tiefwasser (SCW; engl.: Southern Component Water)

drang nach Norden flacher während des LGM ein, (b) es gab kontinuierliche Produktion und Export von Nord-Komponent Tiefwasser (NCW; engl.: Northern Component Water) während der letzten 24 kyr, und (c) die AMOC erreicht ihre volle heutige Stärke nach und nach über die Holozän-Zeit.

Eine zweite Studie, die hier präsentiert wird, handelt sich um die radiogene Isotopenzusammensetzung von Sr, Nd und Pb in detritalen Restmineralien, die aus Ozeansedimentkernen westlich vom Nordafrika extrahiert wurden. Dies wurde gemacht, um die Herkunft vom luftgetragenen Staub in den äquatorialen Atlantik stammend aus Nordafrika zu erkunden in Zusammenhang mit glazial-interglazialen Klimaänderungen. Der Bohrkern befindet sich an der Sierra Leone Erhöhung (SLR; engl.: Sierra Leone Rise) im östlichen tropischen Atlantik. Mit der Bohrkerntiefe zeigt die Sr-Nd-Pb-Isotopie der detritalen Fraktionen, dass sich die Hauptquellen für den Staub in Mauretanien, Nord Mali und die Bödele-Tiefe (Chad) befinden. Der eolische Material aus den Quellen von Mali und Bodélé liegen über die vergangenen 180 kyr in etwa gleichen Proportionen vor. Doch mehr Staub aus Mauretanien, der eine noch radiogenischer Pb-Isotopenzusammensetzung aufweist, wird während der afrikanischen Feucht-Perioden (AHP; engl.: African Humid Periods) gefunden. Zu diesen Zeiten wurde die Sahel-Vegetation noch nördlicher ausgebreitet und viele Seen, die heutzutage ausgetrocknet sind, wurden gefüllt. Dies hatte zu Folge, dass die Staubemissionen von den Mali- und Bodélé-Tiefe-Regionen unterdrückt wurden. Staubzufuhr zu die SLR kommt vor allem während des borealen Winters vor, durch Nassabscheidung (Regen), und wird während der Sommer-Monsun-Monate hauptsächlich geblockt, wenn die intertropikalische Konvergenzzone nördlich wandert.

Im westlichen äquatorialen Atlantik haben wir die detritale Fraktion eines Ozeansedimentbohrkerns, der sich auf der Ceara Erhöhung (CR; engl.: Ceara Rise) befindet, untersucht. Dies beinhaltet hauptsächlich die Sedimentlast der Amazonas-Fluss-Plume, wenn dies im westlichen Atlantik gelangt. Die radiogenische Sr-Nd-Pb-Isotopenmessungen, die

wir im CR-Bohrkern dokumentieren, variieren systematisch und korrelieren extrem gut mit globalen Glazial-Interglazial-Zyklen. Das Sediment aus dem Amazonas-Einzugsgebiet stammt aus zwei Hauptquellen: den Anden Hochland (im Westen) und dem Tiefland Guiana-Schild (im Osten); weiter gibt es ein deutlich größerer Beitrag aus dem Hochland Anden in Eiszeiten gegenüber Warmzeiten. Gute Korrelationen sind eindeutig zwischen Sr-Nd-Pb Isotopenzusammensetzungen, relativem Meeresspiegel und Sommer Einstrahlung in der nördlichen Hemisphäre. Diese Beobachtung zeigt, dass das Klima im Amazonas-Becken im ganzen stark durch die Glazial-Interglazial-Zyklen moduliert und abhängig ist. Dies ubt letztendlich eine entscheidende Kontrolle über die Herkunft der sedimentären Last geliefert durch den Amazonas zum atlantischen Ozean.

Zusammenfassend liefert diese Arbeit einen neuen Einblick in Veränderungen der AMOC-Stärke im letzten Eiszeitzyklus. Ferner zeigen wir wie eolischer Nordafrikastaub, der in den Ostatlantik geblasen wird, durch Klimaänderungen in der nordafrikanischen Region in den letzten 200 kyr beeinflusst war. Wir haben auch neue Einblicke ergattert, inwieweit sich die Herkunft des Materials in der Sedimentlast des Amazonas-Flusses während die letzten einigen Glazial-Interglazial-Zyklen verändert hat.

Dedication

This dissertation is dedicated to my parents, Zhensheng Wei and Dongying Yu for their unconditional love and support for me throughout my whole life.

我谨将此论文集献给我的父母，魏震声和于冬颖，以感谢他们这一生对我无条件的支持和爱护。

Table of Contents

Chapter 1

Introduction

1.1 Radiogenic isotope systems as geochronometers and tracers

Radiogenic isotopes are produced in the process of radioactive decay from nuclei of excited and/or unstable atoms transforming, ultimately, to more stable nuclei, along with the emission of particles and radiation. The physical laws of conservation of energy momentum, angular momentum, spin and parity govern which particles are emitted and the partitioning of energy and momentum between them.

There are four types of decay of relevance in the Earth system. (1) In α-decay, there is emission of an α-particle (helium nucleus) and usually one or more ɣ-rays (high energy photons). (2) β-decay involves emission of an electron - effectively converting a neutron to a proton in the nucleus - and usually accompanied by ɣ-rays. (3) Electron capture of a shell electron effectively changes a proton into a neutron, with emission of X-rays. Lastly (4) spontaneous fission of $^{238}_{92}$U and $^{244}_{94}$Pu results in the production of two highly unstable nuclides of uneven size, which then decay further by β-decay and emission of neutrons. The original nucleus is called the parent isotope and that produced after radioactive decay is the daughter isotope, and its abundance is normally assayed relative to a stable isotope of the daughter element. Depending on the different half-lives involved (the time taken for half of the parent isotope to decay in the daughter isotope), radioactive decays can be subdivided into long-lived and short-lived ones. Long-lived radiogenic (daughter) isotopes are extensively used in geochemistry because the isotopes of the daughter element are not fractionated during partial melting or crystallization, allowing us to gain insight into ancient and modern processes involving the parent and daughter elements over time: the changes in the isotopic composition of the daughter element simply depend on the starting isotopic composition, the

relative abundances of parent and daughter isotope and the time available for radioactive decay to take place.

The variations in isotopic composition that occur are generally very small and require precise measurement. Technical developments in mass spectrometry and more sensitive instrumentation lead to greater precision in the isotope ratios measured. Radioactive decay systems are commonly used (a) in studying the distribution of isotopes in the Earth system, such as their abundance in different geologic bodies, their migration and enrichment patterns as a result of geological processes, in order to investigate the origin, evolution and history of geological materials; and (b) establishing geological timescales in studying the evolution of the Earth and the Solar System. The long-lived radioactive decay systems Rb-Sr, Sm-Nd, Re-Os, Th-U-Pb and Lu-Hf (Table 1.1) are regarded as the most important tools for providing precise ages of geological events and as tracers of geological processes (Faure, 1986; Dickin, 2005; White, 2013).

Table 1.1 Geological used parameters for long-lived radioactive decay systems.

Decay system	Parent/daughter	Isotope ratio	Present day	Decay mode	Half-life (Ga)	Decay constant (yr^{-1})	Common application	Parent isotope	Daughter isotope
Rb-Sr	$^{87}Rb/^{87}Sr$	$^{87}Sr/^{86}Sr$	0.705	β	48.8	1.42×10^{-11}	age dating tracer	^{87}Rb	^{87}Sr
Sm-Nd	$^{147}Sm/^{143}Nd$	$^{143}Nd/^{144}Nd$	0.512638	α	106	6.54×10^{-12}	age dating tracer	^{147}Sm	^{143}Nd
Re-Os	$^{187}Re/^{187}Os$	$^{187}Os/^{186}Os$	1.04	β	42.8	1.62×10^{-11}	dating ores tracer	^{187}Re	^{187}Os
			Initial solar system						
Th-U-Pb	$^{238}U/^{206}Pb$	$^{206}Pb/^{204}Pb$	9.307	α	4.47	1.55125×10^{-10}	tracer model age	^{238}U	^{206}Pb
	$^{235}U/^{207}Pb$	$^{207}Pb/^{204}Pb$	10.294	α	0.704	9.8485×10^{-10}		^{235}U	^{207}Pb
	$^{232}Th/^{208}Pb$	$^{208}Pb/^{204}Pb$	29.476	α	14.01	4.9475×10^{-11}		^{232}Th	^{208}Pb
Lu-Hf	$^{176}Lu/^{176}Hf$	$^{176}Hf/^{177}Hf$	0.27978	β	35.4	1.94×10^{-11}	tracer	^{176}Lu	^{176}Hf

The use of radiogenic isotopes to measure the age of rocks (i.e. geochronology) was first published in 1907 by Bertram Borden Boltwood based upon the U-Pb decay system (Boltwood, 1907), which suggested that the Earth is only 2000 Ma old. Pb isotopes are

commonly used in dating rocks and provide some of the best constraints on the age of the Earth. Two different Pb isotopes (^{206}Pb and ^{207}Pb) are produced from the radioactive decay of two different uranium isotopes (^{238}U and ^{235}U) respectively, so two independent geochronometers are present in the sample parent-daughter element pair. This allows the use of the Pb-Pb isochron method of dating which does not require knowledge of the U/Pb ratio.

Nowadays, the generally accepted age of the Earth is close to 4.5 Ga. This age comes from radioactive dating of lunar rocks and meteorites based on the general model describing the evolution of Pb isotopes in meteorites, the Earth and the Solar System (Hofmann, 2001; Dalrymple, 2004). The foundations of this model were originally proposed independently by Gerling (Gerling, 1942), Holmes (Holmes, 1946), and Houtermans (Houtermans, 1946), and was further developed and applied to meteorites and the Earth by Clair Patterson (Patterson, 1956). In Patterson's classic paper, he showed that the Pb isotopic ratio of natural Earth materials containing different amounts of uranium should fall on a straight-line isochron when ^{207}Pb/^{204}Pb is plotted against ^{206}Pb/^{204}Pb, on the assumption that the Pb isotopic compositions were uniform in all planetary bodies and meteorites at the time of their original formation (Patterson, 1956). This ultimately leads to the development of isochrons, in which two isotopes are plotted against each other to calculate an age for a mineral or rock.

By the beginning of the 1970s, dating on whole rocks older than 50 Ma with the help of Rb-Sr isochrons had come into general use, making use of the decay of very long half-life ^{87}Rb. The Rb-Sr method requires rocks or minerals to have remained closed systems, suffering no loss or gain of Rb or Sr, since their formation. In other words, the Rb-Sr "age" indicates the true age of the minerals only if the rocks have not been disturbed subsequently.

The Precambrian rocks (3600 - 3900 Ma) of West Greenland, which were dated by the Rb-Sr and Pb-Pb decay systems, were considered the oldest rocks on Earth in the 1970s based upon a number of geochronological studies (Black et al., 1971; Moorbath et al., 1972; Kalsbeek, 1997). Shortly thereafter, the use of Sm-Nd system was first used as a chronometer

for dating the Juvinas and Stannern achondrites, lunar basalts and terrestrial rocks; the system is based on the decay of ^{147}Sm to ^{143}Nd with a half-life of 106 Ga (Lugmair, 1974; Lugmair and Scheinin, 1975; Lugmair et al., 1975; DePaolo and Wasserburg, 1976; Jacobsen and Wasserburg, 1980).

Due to the fact that isotopes of the daughter elements are not fractionated during physical, chemical or biological processes, the radiogenic isotopic compositions are "conservative" during geological processes. For example, the isotopic compositions of magmas reflect those of the mantle source of the magmas. Thus, radiogenic isotopes have been widely used as tracers in igneous petrology, to study continental evolution and in mantle geochemistry. Their utility in paleoceanography has become increasingly important, especially in addressing sediment provenance and ocean circulation, with the first studies appearing in 1960s (Chow and Patterson, 1962; Dasch, 1969; Faure, 1986).

The residence time of Nd, Pb, and Hf in seawater is shorter or on the order of the turnover time of the oceans (~1500 years), which means these elements are not well-mixed in the ocean as a whole. The radiogenic isotope variability of these elements in the oceans has been inferred from measurements of seawater, calcium carbonate, authigenic fractions in deep-sea sediments, and in Fe-Mn nodules and crusts; the Nd, Pb and Hf isotopic compoisitions are a quasi-conservative water mass tracer through the whole of the world's oceans (White et al., 1986; Abouchami and Goldstein, 1995; von Blanckenburg et al., 1996; Abouchami et al., 1997; Frank, 2002; Goldstein and Hemming, 2003; Piotrowski et al., 2005; Gutjahr et al., 2007; Piotrowski et al., 2012; Osborne et al., 2014; Jonkers et al., 2015). Because dissolved Hf has not been extensively measured in the world's ocean, and Pb isotopes in the modern ocean are contaminated by anthropogenic input, Nd isotopes are the most prominent tracer used to investigate paleocirculation in the oceans (Frank, 2002; Goldstein and Hemming, 2003).

Similarily, radiogenic isotopes have proven to be particularly robust tracers of geographic provenance and transport pathways of atmospheric dust and terrigenous sediments, providing effectively an "isotopic fingerprint" of the material (Biscaye et al., 1974; Grousset et al., 1988; Parra et al., 1997; Bayon et al., 2002; Abouchami and Zabel, 2003; Franzese et al., 2006; Franzese et al., 2009; Meyer et al., 2011; Reyes et al., 2014; Li et al., 2015; Molina-Kescher et al., 2016). "Isotopic fingerprinting" is possible because the isotopic compositions retain the signature of their source rocks throughout erosion, transport, deposition and diagenesis, allowing them to serve as highly effective provenance tracers. For this reason, Pb, Sr and Nd isotopic compositions have been used extensively to pin-point dust sources and dust delivery on a global scale (Grousset and Biscaye, 2005; Stuut et al., 2005; Cole et al., 2009; Abouchami et al., 2013; Scheuvens et al., 2013; Kumar et al., 2014; Miller et al., 2014; Újvári et al., 2015; Blakowski et al., 2016).

Radiogenic isotopes are also a powerful tool for examining elemental mass balances and mixing between sources, and have often been used to investigate mixing processes in paleoceanography (Faure, 1986). A particular good example of this approach, based upon Nd isotopes, is to monitor the evolution of ocean water mass mixing and provide constrains on the ocean circulation pattern; this has as its basis the observation that different water masses appear to have distinct and characteristic Nd isotopic compositions (von Blanckenburg, 1999; Frank et al., 2003; Goldstein and Hemming, 2003; Piotrowski et al., 2004; van de Flierdt et al., 2004; Piotrowski et al., 2005; Pahnke et al., 2008; Piotrowski et al., 2012; Garcia-Solsona et al., 2014; Howe et al., 2016).

There is large variability in radiogenic isotopic compositions of Pb, Nd and Sr in different continental source regions of river-borne sediments and atmospheric dusts due to the varied geology and age structure of the continental land masses. Thus, the radiogenic isotopic compositions of terrestrially-derived material in deep-sea sediments can constrain in continental weathering regimes resulting from changes in continental climate and changes in

global wind patterns over time (Abouchami and Zabel, 2003; Franzese et al., 2006; Lupker et al., 2010; Stumpf et al., 2011; Kumar et al., 2014; Rodrigo-Gámiz et al., 2015; van der Lubbe et al., 2016).

1.2 Thermohaline circulation

The gross overturn of the world's oceans is described as the "thermohaline circulation" in that it is driven by differences in sea water density arising from changes in temperature (thermal expansion, evaporative cooling), and salinity (evaporation, formation of ice, freshwater inputs) (Rahmstorf, 2002, 2003). The thermohaline circulation is also called, variously, the meridional overturning circulation, the great ocean conveyor, and the global conveyor belt. The abyssal circulation scheme was first proposed by Stommel and Arons (Stommel and Arons, 1959a, b) and further developed during the last thirty years into the classic and oversimplified pattern shown in Fig. 1.1 (Gordon, 1986; Broecker, 1991; Sarnthein et al., 1994; Ganachaud and Wunsch, 2000; Rahmstorf, 2002, 2003; Marshall and Speer, 2012). Surface winds trigger the warm surface waters to move northward; along this path, the water mass density increases due to evaporative cooling. At high latitudes, this high-density water sinks in the Greenland-Iceland-Norwegian (GIN) seas area, once heat is released to the atmosphere, resulting in the formation of North Atlantic Deep Water (NADW) (Rahmstorf, 2002). High-density NADW - identified by its high salinity, high $\delta^{13}C$ and low nutrient contents - then flows very slowly southwards into the deep abyssal ocean basins at a depth between 2 km and 5 km. In the South Atlantic, NADW flows over the southern-derived Antarctic Bottom Water (AABW, low $\delta^{13}C$ and high nutrients), and then splits into two, taking routes into the Indian Ocean and the Pacific around the tip of South Africa. Thermohaline upwelling regions in the Indian Ocean and Bering Strait bring these deep water masses back to intermediate and surface layers of the ocean, where they feed into the slow surface return flow back to the Atlantic Ocean again, closing the loop. This closed system

circulation redistributes energy and matter along it path around the globe; hence, the thermohaline circulation plays a critical role in modulating the Earth's climate.

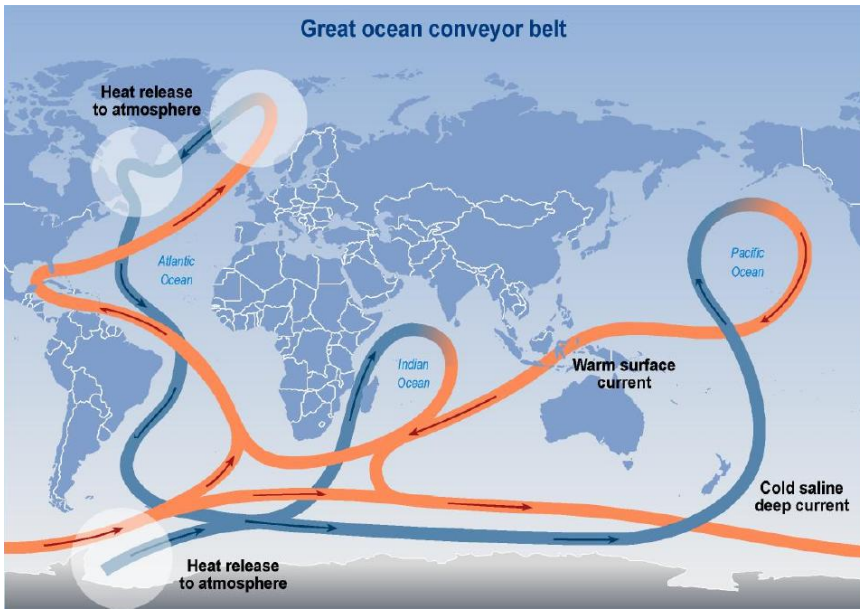

Fig. 1.1 The schematic diagram of great ocean conveyor belt (Broecker, 1991). The shaded area represents the shallow warm ocean currents back into the North Atlantic, other parts (not shaded) represent the deep cold and salty water flowing out the North Atlantic.

The thermohaline circulation is influenced by climate and in turn influents climate. The ocean contains the largest active pool of carbon on Earth (Falkowski et al., 2000). The carbon mainly enters the ocean as dissolved inorganic carbon. This carbon is stored for a longer time in the deep ocean compared to the surface layer, where it exchanges rapidly with the atmosphere. The thermohaline circulation is instrumental in modulating carbon exchange between these two layers, and also affects carbon solubility (Broecker and Maier-Reimer, 1992; Stocker and Schmittner, 1997). This is because cold saline waters absorb CO_2 more efficiently from the atmosphere; thus the formation of high-density cold NADW at high latitudes has a very important influence on sequestration of atmospheric CO_2 by the ocean overall.

Stocker and Schmittner (1997) have suggested that the thermohaline circulation is sensitive to atmospheric CO_2 levels and depends on the rate of change of the atmospheric CO_2

concentration. A four-fold increase in atmospheric CO_2 would collapse and deepen the thermohaline circulation, prevent nutrient ventilation to the upper ocean and influence the carbon cycle (Manabe and Stouffer, 1993; Toggweiler and Samuels, 1995). Ocean acidification by CO_2 absorption would also occur with consequences for ocean biosystems (Kleypas et al., 1999; Langdon et al., 2000).

An important role of the thermohaline circulation is supplying heat to polar regions - amounting to approximately 1 PW of heat - as well as regulating the amount of sea ice (Trenberth and Caron, 2001). The North Atlantic regions would be as much as 5 °C colder if the thermohaline circulation (Gulf Stream) were to collapse (Siedler et al., 2001; Steffen et al., 2006). The North Atlantic Drift – a branch of the thermohaline circulation - brings warm water, humid air and abundant rainfall further north, warming Europe and the northeastern Atlantic compared to countries in the western Atlantic at the same latitude such as Labrador. A slowdown and/or shutdown of the thermohaline circulation would be associated with reduction in North Atlantic heat transport and formation of NADW, and would lead to a dramatic drop in temperature in Europe, together with an increase in sea ice cover in the North Atlantic (Broecker, 1998; Marotzke, 2000; Vellinga and Wood, 2002; Jacob et al., 2005). The climate over northeastern North America would be similarly affected. Such as a shutdown of AMOC would lead to a substantial cooling in North Atlantic sea surface temperature, which further would inhibited moisture flux into central North America (Bromwich et al., 2004; Pu et al., 2012).

Another factor that affects the thermohaline circulation is the hydrological balance in the North Atlantic region. Here, changes in fresh water inputs to the North Atlantic have a modulating effect on the formation of NADW, and thus the strength of the thermohaline circulation, by altering the ocean water density in the Nordic seas (Schmittner and Clement, 2002; Rennermalm et al., 2006; Lorenzo et al., 2009; Nummelin et al., 2016).

1.3 Marine sedimentary records

In undisturbed sediment cores from the ocean floor, as well as Fe-Mn crusts, the materials were laid down sequentially layer upon layer over time. Thus, as progresses from the present surface into the core or crust, layers that were once at the surface in the geological past can be sampled. Provided that the core or crust has a good age model (i.e. the geological age versus depth), one can construct a record of inputs and conditions, at that location in the past. Such marine sedimentary records can be used as archives of events, paleo-climate, ocean chemistry and global biogeochemical cycles, among others, depending on what is measured.

Biogenic, authigenic and terrigenous phases are the three major components in marine sediments, which basically reflect biological, chemical and physical processes, respectively. Authigenic components are oceanic inorganic minerals that precipitate directly from seawater carrying a "seawater signal", which can reveal details of the deep water circulation, for example. Terrigenous components entering the oceans in the form of atmospheric dusts and riverine suspended particulates have an ultimate source as weathering and erosion products of rocks on land, and provide information about provenance, weathering processes, and transport mechanisms. Biogenic sediments are composed of the accumulated remains (e.g. shells, tests, fish debris) of marine organisms on the ocean floor that grew in the surface ocean. Such materials can supply information on the primary production, nutrient supply and conditions (e.g. temperature) in the surface ocean.

Radiogenic isotopic compositions of Sr, Nd and Pb from marine sediments have been used extensively as a paleoceanographic proxy for reconstructing past changes in deep water circulation (deep water sourcing), sediment provenance and transport mechanisms. Various authigenic marine sedimentary components have been used, such as fish debris and fish teeth (Martin and Scher, 2004; Roberts et al., 2010), cleaned foraminifera (Piotrowski et al., 2012; Stumpf et al., 2015), uncleaned foraminifera (Winter et al., 1997; Roberts et al., 2010), deep sea corals (van de Flierdt et al., 2006; Wilson et al., 2015a), and leachated authigenic Fe-Mn

oxide coatings (Bayon et al., 2002; Gutjahr et al., 2008; Pahnke et al., 2008; Osborne et al., 2014), Fe-Mn crusts (Abouchami and Goldstein, 1995; Abouchami et al., 1997; Burton et al., 1997; Abouchami and Galer, 1998; Abouchami et al., 1999; Vlastélic et al., 2001; Foster and Vance, 2006). This allows us to observe radiogenic isotope changes over glacial-interglacial cycles on timescales of millennial to tens of millions of years (O'Nions et al., 1978; Goldstein and O'Nions, 1981; Bayon et al., 2002).

There are a large number of Nd and Pb isotope records available, including from the North Atlantic (Frank et al., 2002; Gutjahr et al., 2008; Muiños et al., 2008), the Equatorial Atlantic (Frank et al., 2002; Frank et al., 2003), and in the South Atlantic from the Cape Basin (Rutberg et al., 2000; Piotrowski et al., 2004, 2005; Piotrowski et al., 2008; Piotrowski et al., 2012) and the Angola Basin (Bayon et al., 2002). Together, these radiogenic isotope records show that the relative proportion of North Atlantic Deep Water (NADW) and Antarctic Bottom Water (AABW) varied in a systematic way through glacial-interglacial cycles. Negre et al. (2010) were the first to propose that a reversed flow pattern in the Atlantic deep water existed during the Last Glacial Maximum (LGM), and this idea has been supported by further studies involving comparison of contemporaneous records of NADW and AABW (Piotrowski et al., 2012; Jonkers et al., 2015).

Climate plays a dominant role governing the intensity of continental weathering and erosion as well as the location of sources of dust and the quantity of discharge from rivers into the oceans. Radiogenic Sr-Nd-Pb isotopic compositions of the residual fraction of marine sediments has been used in many studies for constraining continental sources of these materials and reconstructing paleocurrent pathways (Grousset et al., 1988; Grousset et al., 1992; Revel et al., 1996; Parra et al., 1997; Walter et al., 2000; Weldeab et al., 2002; Jung et al., 2004; Grousset and Biscaye, 2005; Rutberg et al., 2005; Franzese et al., 2006; Cole et al., 2009; Franzese et al., 2009; Pourmand et al., 2014).

In the central South Atlantic, dust inputs are principally from Patagonia, the Falkland Islands, the Antarctic Peninsula and East Antarctica, and their relative contributions depend on geography and climate, while ocean currents transport and redistribute this continentally-derived terrigenous material (Walter et al., 2000). Franzese et al. (2006; 2009) have used Sr isotopes in the detrital fraction of marine sediments from the Cape Basin (tip of South Africa) to show that sediment carried by the Agulhas Current has a radiogenic Sr isotopic composition which originated from old continental terrains on the eastern coast of Africa, and might possibly be useful in tracing the path of the Agulhas Current system. In combination with other proxies, this suggests that there was a reduced Agulhas leakage during the LGM and that the Agulhas Current was weaker, in agreement with low sea surface temperatures during the glacial periods in the Cape Basin (Peeters et al., 2004).

Changes in AMOC strength and formation of NADW during the LGM compared to that of the present day have been hotly debated in many studies and still remain controversial and very uncertain. One important objective of this thesis was to reconstruct the past circulation changes in the Atlantic deep water circulation over last 24 kyrs. For this purpose, Nd and Sr isotopic compositions of Fe-Mn leachates in two South Atlantic sediment core archives located in the Cape Basin were used for tracing past variability in the deep water circulation. In particular, we aim to reconstruct the advection and mixing of the principal northern and southern deep water masses (NADW vs. AABW) over time. We can further test the hypothesis of "a reversed flow pattern during the LGM" in the Atlantic basin proposed by Negre et al. (2010). Our leachate dataset was verified by additionally measuring ε_{Nd} in fish debris and mixed planktonic foraminifera from the same core sites. These issues are presented and discussed in Chapter 2.

The eastern and western Atlantic receive a far larger input of continentally-derived material than most other oceanic regions (Prospero et al., 1981; Duce et al., 1991). In the eastern Atlantic this takes the form of large quantities of North African dust blown in from

sources located in the Sahara and Sahel regions. By contrast, in the western Atlantic, the terrigenous material is supplied as suspended load of the Amazon river, the largest river on Earth by discharge. Changes in the mean position of the Intertropical Convergence Zone (ITCZ) during glacial-interglacial cycles potentially have a strong impact on the ocean circulation, the hydrological cycle and continental aridity. In Chapters 3 and 4, we will be examining how global climate changes of this sort impacted on the supply and sources of terrigenous material delivered to the eastern and western Atlantic, respectively.

In Chapter 3, the temporal changes in Sr-Nd-Pb isotopic compositions recorded in detrital phases extracted from a sediment core located on the Sierra Leone Rise (eastern equatorial Atlantic) were measured. These radiogenic isotope data provide valuable information on the pattern of Saharan dust exported to the eastern equatorial Atlantic in response to climate changes occurring over the past 180 kyrs, based upon the fact that the terrigenous material at the Sierra Leone Rise originates exclusively from North African sources (Curry and Lohmann, 1986; Zabel et al., 1999; Abouchami and Zabel, 2003; Funk et al., 2004). In the western equatorial Atlantic (Chapter 4), the suspended particulates discharged by the Amazon plume were investigated over time. We measured radiogenic isotopic compositions of the detrital fraction of a sedimentary core located in the Ceara Rise, and present a 200-kyr record. These data enable us to fingerprint the provenance of detrital material delivered to this core site within the Amazon watershed and, to reconstruct how this changed in response to past climate variations.

These two studies show clearly that the provenance of terrigenous inputs varies and responds strongly to Pleistocene climate cycles. Overall, Chapters 2, 3 and 4 of this dissertation contribute to a better understanding of the relationships between atmospheric circulation, ocean circulation, terrestrial aridity and global climate over recent Earth history.

Reference

Abouchami, W., Galer, S., 1998. The provinciality of Pb isotopes in Pacific Fe-Mn deposits. Mineral. Mag. 62A, 1-2.

Abouchami, W., Galer, S.J.G., Koschinsky, A., 1999. Pb and Nd isotopes in NE Atlantic Fe–Mn crusts: Proxies for trace metal paleosources and paleocean circulation. Geochimica et Cosmochimica Acta 63, 1489-1505.

Abouchami, W., Goldstein, S.L., 1995. A lead isotopic study of circum-antarctic manganese nodules. Geochimica et Cosmochimica Acta 59, 1809-1820.

Abouchami, W., Goldstein, S.L., Galer, S.J.G., Eisenhauer, A., Mangini, A., 1997. Secular changes of lead and neodymium in central Pacific seawater recorded by a Fe-Mn crust. Geochimica et Cosmochimica Acta 61, 3957-3974.

Abouchami, W., Näthe, K., Kumar, A., Galer, S.J.G., Jochum, K.P., Williams, E., Horbe, A.M.C., Rosa, J.W.C., Balsam, W., Adams, D., Mezger, K., Andreae, M.O., 2013. Geochemical and isotopic characterization of the Bodélé Depression dust source and implications for transatlantic dust transport to the Amazon Basin. Earth and Planetary Science Letters 380, 112-123.

Abouchami, W., Zabel, M., 2003. Climate forcing of the Pb isotope record of terrigenous input into the Equatorial Atlantic. Earth and Planetary Science Letters 213, 221-234.

Bayon, G., German, C.R., Boella, R.M., Milton, J.A., Taylor, R.N., Nesbitt, R.W., 2002. An improved method for extracting marine sediment fractions and its application to Sr and Nd isotopic analysis. Chemical Geology 187, 179-199.

Biscaye, P.E., Chesselet, R., Prospero, J.M., 1974. Rb-Sr, $^{87}Sr/^{86}Sr$ isotope system as an index of provenance of continental dusts in the open Atlantic ocean. Journal de Recherches Atmospheriques 8, 819-829.

Black, L.P., Gale, N.H., Moorbath, S., Pankhurst, R.J., McGregor, V.R., 1971. Isotopic dating of very early Precambrian amphibolite facies gneisses from the Godthaab district, West Greenland. Earth and Planetary Science Letters 12, 245-259.

Blakowski, M.A., Aciego, S.M., Delmonte, B., Baroni, C., Salvatore, M.C., Sims, K.W.W., 2016. A Sr-Nd-Hf isotope characterization of dust source areas in Victoria Land and the McMurdo Sound sector of Antarctica. Quaternary Science Reviews 141, 26-37.

Boltwood, B.B., 1907. Ultimate disintegration products of the radioactive elements; Part II, Disintegration products of uranium. American Journal of Science Series 4 Vol. 23, 78-88.

Broecker, W.S., 1991. The great conveyor belt. Oceanography 4, 11.

Broecker, W.S., 1998. Paleocean circulation during the Last Deglaciation: A bipolar seesaw? Paleoceanography 13, 119-121.

Broecker, W.S., Maier-Reimer, E., 1992. The influence of air and sea exchange on the carbon isotope distribution in the sea. Global Biogeochemical Cycles 6, 315-320.

Bromwich, D.H., Toracinta, E.R., Wei, H., Oglesby, R.J., Fastook, J.L., Hughes, T.J., 2004. Polar MM5 simulations of the winter climate of the Laurentide Ice Sheet at the LGM. Journal of Climate 17, 3415-3433.

Burton, K.W., Ling, H.-F., O'Nions, R.K., 1997. Closure of the Central American Isthmus and its effect on deep-water formation in the North Atlantic. Nature 386, 382-385.

Chow, T.J., Patterson, C.C., 1962. The occurrence and significance of lead isotopes in pelagic sediments. Geochimica et Cosmochimica Acta 26, 263-308.

Cole, J.M., Goldstein, S.L., deMenocal, P.B., Hemming, S.R., Grousset, F.E., 2009. Contrasting compositions of Saharan dust in the eastern Atlantic Ocean during the last deglaciation and African Humid Period. Earth and Planetary Science Letters 278, 257-266.

Curry, W.B., Lohmann, G.P., 1986. Late Quaternary carbonate sedimentation at the Sierra Leone Rise (eastern equatorial Atlantic Ocean). Marine Geology 70, 223-250.

Dalrymple, G.B., 2004. Ancient Earth, Ancient Skies: The Age of Earth and Its Cosmic Surroundings. Stanford University Press.
Dasch, E.J., 1969. Strontium isotopes in weathering profiles, deep-sea sediments, and sedimentary rocks. Geochimica et Cosmochimica Acta 33, 1521-1552.
DePaolo, D., Wasserburg, G., 1976. Nd isotopic variations and petrogenetic models. Geophysical Research Letters 3, 249-252.
Dickin, A.P., 2005. Radiogenic Isotope Geology. Cambridge University Press.
Duce, R.A., Liss, P.S., Merrill, J.T., Atlas, E.L., Buat-Menard, P., Hicks, B.B., Miller, J.M., Prospero, J.M., Arimoto, R., Church, T.M., Ellis, W., Galloway, J.N., Hansen, L., Jickells, T.D., Knap, A.H., Reinhardt, K.H., Schneider, B., Soudine, A., Tokos, J.J., Tsunogai, S., Wollast, R., Zhou, M., 1991. The atmospheric input of trace species to the world ocean. Global Biogeochemical Cycles 5, 193-259.
Falkowski, P., Scholes, R.J., Boyle, E., Canadell, J., Canfield, D., Elser, J., Gruber, N., Hibbard, K., Högberg, P., Linder, S., Mackenzie, F.T., Moore III, B., Pedersen, T., Rosenthal, Y., Seitzinger, S., Smetacek, V., Steffen, W., 2000. The global carbon cycle: A test of our knowledge of Earth as a system. Science 290, 291-296.
Faure, G., 1986. Principles of isotope geology. Wiley.
Foster, G.L., Vance, D., 2006. Negligible glacial-interglacial variation in continental chemical weathering rates. Nature 444, 918-921.
Frank, M., 2002. Radiogenic isotopes: tracers of past ocean circulation and erosional input. Reviews of Geophysics 40.
Frank, M., van de Flierdt, T., Halliday, A.N., Kubik, P.W., Hattendorf, B., Günther, D., 2003. Evolution of deepwater mixing and weathering inputs in the central Atlantic Ocean over the past 33 Myr. Paleoceanography 18, 1091.
Frank, M., Whiteley, N., Kasten, S., Hein, J.R., O'Nions, K., 2002. North Atlantic Deep Water export to the Southern Ocean over the past 14 Myr: Evidence from Nd and Pb isotopes in ferromanganese crusts. Paleoceanography 17, 1022.
Franzese, A.M., Hemming, S.R., Goldstein, S.L., 2009. Use of strontium isotopes in detrital sediments to constrain the glacial position of the Agulhas Retroflection. Paleoceanography 24, PA2217.
Franzese, A.M., Hemming, S.R., Goldstein, S.L., Anderson, R.F., 2006. Reduced Agulhas Leakage during the Last Glacial Maximum inferred from an integrated provenance and flux study. Earth and Planetary Science Letters 250, 72-88.
Funk, J.A., von Dobeneck, T., Wagner, T., Kasten, S., 2004. Late Quaternary sedimentation and early diagenesis in the Equatorial Atlantic Ocean: Patterns, trends and processes deduced from rock magnetic and geochemical records, in: Wefer, G., Mulitza, S., Ratmeyer, V. (Eds.), The South Atlantic in the Late Quaternary. Springer Berlin Heidelberg, pp. 461-497.
Ganachaud, A., Wunsch, C., 2000. Improved estimates of global ocean circulation, heat transport and mixing from hydrographic data. Nature 408, 453-457.
Garcia-Solsona, E., Jeandel, C., Labatut, M., Lacan, F., Vance, D., Chavagnac, V., Pradoux, C., 2014. Rare earth elements and Nd isotopes tracing water mass mixing and particle-seawater interactions in the SE Atlantic. Geochimica et Cosmochimica Acta 125, 351-372.
Gerling, E., 1942. Age of the Earth according to radioactivity data, Doklady (Proc Russian Acad Sci), pp. 259-261.
Goldstein, S.L., Hemming, S.R., 2003. Long-lived isotopic tracers in oceanography, paleoceanography, and ice-sheet dynamics, in: Turekian, H.D.H.K. (Ed.), Treatise on Geochemistry. Elsevier, Oxford, pp. 453-489.
Goldstein, S.L., O'Nions, R.K., 1981. Nd and Sr isotopic relationships in pelagic clays and ferromanganese deposits. Nature 292, 324-327.

Gordon, A.L., 1986. Interocean exchange of thermocline water. Journal Geophysical Research 91, 5037-5046.
Grousset, F.E., Biscaye, P.E., 2005. Tracing dust sources and transport patterns using Sr, Nd and Pb isotopes. Chemical Geology 222, 149-167.
Grousset, F.E., Biscaye, P.E., Revel, M., Petit, J.-R., Pye, K., Joussaume, S., Jouzel, J., 1992. Antarctic (Dome C) ice-core dust at 18 k.y. B.P.: Isotopic constraints on origins. Earth and Planetary Science Letters 111, 175-182.
Grousset, F.E., Biscaye, P.E., Zindler, A., Prospero, J., Chester, R., 1988. Neodymium isotopes as tracers in marine sediments and aerosols: North Atlantic. Earth and Planetary Science Letters 87, 367-378.
Gutjahr, M., Frank, M., Stirling, C.H., Keigwin, L.D., Halliday, A.N., 2008. Tracing the Nd isotope evolution of North Atlantic Deep and Intermediate Waters in the western North Atlantic since the Last Glacial Maximum from Blake Ridge sediments. Earth and Planetary Science Letters 266, 61-77.
Gutjahr, M., Frank, M., Stirling, C.H., Klemm, V., van de Flierdt, T., Halliday, A.N., 2007. Reliable extraction of a deepwater trace metal isotope signal from Fe–Mn oxyhydroxide coatings of marine sediments. Chemical Geology 242, 351-370.
Hofmann, A.W., 2001. Lead isotopes and the age of the Earth - a geochemical accident. Geological Society, London, Special Publications 190, 223-236.
Holmes, A., 1946. An estimate of the age of the Earth. Nature 157, 5.
Houtermans, F.G., 1946. Die Isotopenhäufigkeiten im natürlichen Blei und das Alter des Urans. Naturwissenschaften 33, 185-186.
Howe, J.N.W., Piotrowski, A.M., Noble, T.L., Mulitza, S., Chiessi, C.M., Bayon, G., 2016. North Atlantic Deep Water production during the Last Glacial Maximum. Nat Commun 7.
Jacob, D., Goettel, H., Jungclaus, J., Muskulus, M., Podzun, R., Marotzke, J., 2005. Slowdown of the thermohaline circulation causes enhanced maritime climate influence and snow cover over Europe. Geophysical Research Letters 32, L21711.
Jacobsen, S.B., Wasserburg, G.J., 1980. Sm-Nd isotopic evolution of chondrites. Earth and Planetary Science Letters 50, 139-155.
Jonkers, L., Zahn, R., Thomas, A., Henderson, G., Abouchami, W., François, R., Masque, P., Hall, I.R., Bickert, T., 2015. Deep circulation changes in the central South Atlantic during the past 145 kyrs reflected in a combined $^{231}Pa/^{230}Th$, neodymium isotope and benthic $\delta^{13}C$ record. Earth and Planetary Science Letters 419, 14-21.
Jung, S., Mezger, K., Hoernes, S., 2004. Shear zone-related syenites in the Damara belt (Namibia): the role of crustal contamination and source composition. Contrib Mineral Petrol 148, 104-121.
Kalsbeek, F., 1997. Age determinations of Precambrian rocks from Greenland: past and present. Geology of Greenland Survey Bulletin 176, 55-59.
Kleypas, J.A., Buddemeier, R.W., Archer, D., Gattuso, J.-P., Langdon, C., Opdyke, B.N., 1999. Geochemical consequences of increased atmospheric carbon dioxide on coral reefs. Science 284, 118-120.
Kumar, A., Abouchami, W., Galer, S.J.G., Garrison, V.H., Williams, E., Andreae, M.O., 2014. A radiogenic isotope tracer study of transatlantic dust transport from Africa to the Caribbean. Atmospheric Environment 82, 130-143.
Langdon, C., Takahashi, T., Sweeney, C., Chipman, D., Goddard, J., Marubini, F., Aceves, H., Barnett, H., Atkinson, M.J., 2000. Effect of calcium carbonate saturation state on the calcification rate of an experimental coral reef. Global Biogeochemical Cycles 14, 639-654.
Li, T., Xu, Z., Lim, D., Chang, F., Wan, S., Jung, H., Choi, J., 2015. Sr–Nd isotopic constraints on detrital sediment provenance and paleoenvironmental change in the

northern Okinawa Trough during the late Quaternary. Palaeogeography, Palaeoclimatology, Palaeoecology 430, 74-84.
Lorenzo, M.N., Taboada, J.J., Iglesias, I., 2009. Sensitivity of thermohaline circulation to decadal and multidecadal variability. ICES Journal of Marine Science: Journal du Conseil 66, 1439-1447.
Lugmair, G., 1974. Sm-Nd ages: a new dating method. Meteoritics 9, 369.
Lugmair, G., Scheinin, N., 1975. Sm-Nd systematics of the Stannern meteorite. Meteoritics 10, 447-448.
Lugmair, G.W., Scheinin, N.B., Marti, K., 1975. Search for extinct ^{146}Sm, 1. The isotopic abundance of ^{142}Nd in the Juvinas meteorite. Earth and Planetary Science Letters 27, 79-84.
Lupker, M., Aciego, S.M., Bourdon, B., Schwander, J., Stocker, T.F., 2010. Isotopic tracing (Sr, Nd, U and Hf) of continental and marine aerosols in an 18th century section of the Dye-3 ice core (Greenland). Earth and Planetary Science Letters 295, 277-286.
Manabe, S., Stouffer, R.J., 1993. Century-scale effects of increased atmospheric CO_2 on the ocean-atmosphere system. Nature 364, 215-218.
Marotzke, J., 2000. Abrupt climate change and thermohaline circulation: Mechanisms and predictability. Proceedings of the National Academy of Sciences 97, 1347-1350.
Marshall, J., Speer, K., 2012. Closure of the meridional overturning circulation through Southern Ocean upwelling. Nature Geoscience 5, 171-180.
Martin, E.E., Scher, H.D., 2004. Preservation of seawater Sr and Nd isotopes in fossil fish teeth: bad news and good news. Earth and Planetary Science Letters 220, 25-39.
Meyer, I., Davies, G.R., Stuut, J.-B.W., 2011. Grain size control on Sr-Nd isotope provenance studies and impact on paleoclimate reconstructions: An example from deep-sea sediments offshore NW Africa. Geochemistry, Geophysics, Geosystems 12, Q03005.
Miller, J., Mackin, G., Miller, S.M.O., 2014. Application of geochemical tracers to fluvial sediment. Springer International Publishing.
Molina-Kescher, M., Frank, M., Tapia, R., Ronge, T.A., Nürnberg, D., Tiedemann, R., 2016. Reduced admixture of North Atlantic Deep Water to the deep central South Pacific during the last two glacial periods. Paleoceanography.
Moorbath, S., O'nions, R., Pankhurst, R., Gale, N., McGregor, V., 1972. Further rubidium-strontium age determinations on the very early Precambrian rocks of the Godthaab district, West Greenland. Nature 240, 78-82.
Muiños, S.B., Frank, M., Maden, C., Hein, J.R., van de Flierdt, T., Lebreiro, S.M., Gaspar, L., Monteiro, J.H., Halliday, A.N., 2008. New constraints on the Pb and Nd isotopic evolution of NE Atlantic water masses. Geochemistry, Geophysics, Geosystems 9.
Negre, C., Zahn, R., Thomas, A.L., Masque, P., Henderson, G.M., Martinez-Mendez, G., Hall, I.R., Mas, J.L., 2010. Reversed flow of Atlantic deep water during the Last Glacial Maximum. Nature 468, 84-88.
Nummelin, A., Ilicak, M., Li, C., Smedsrud, L.H., 2016. Consequences of future increased Arctic runoff on Arctic Ocean stratification, circulation, and sea ice cover. Journal of Geophysical Research: Oceans 121, 617-637.
O'Nions, R.K., Carter, S.R., Cohen, R.S., Evensen, N.M., Hamilton, P.J., 1978. Pb, Nd and Sr isotopes in oceanic ferromanganese deposits and ocean floor basalts. Nature 273, 435-438.
Osborne, A.H., Newkirk, D.R., Groeneveld, J., Martin, E.E., Tiedemann, R., Frank, M., 2014. The seawater neodymium and lead isotope record of the final stages of Central American Seaway closure. Paleoceanography 29, 715-729.
Pahnke, K., Goldstein, S.L., Hemming, S.R., 2008. Abrupt changes in Antarctic Intermediate Water circulation over the past 25,000 years. Nature Geoscience 1, 870-874.

Parra, M., Faugères, J.-C., Grousset, F., Pujol, C., 1997. Sr-Nd isotopes as tracers of fine-grained detrital sediments: the South-Barbados accretionary prism during the last 150 kyr. Marine Geology 136, 225-243.

Patterson, C., 1956. Age of meteorites and the earth. Geochimica et Cosmochimica Acta 10, 230-237.

Peeters, F.J.C., Acheson, R., Brummer, G.-J.A., de Ruijter, W.P.M., Schneider, R.R., Ganssen, G.M., Ufkes, E., Kroon, D., 2004. Vigorous exchange between the Indian and Atlantic oceans at the end of the past five glacial periods. Nature 430, 661-665.

Piotrowski, A.M., Galy, A., Nicholl, J.A.L., Roberts, N., Wilson, D.J., Clegg, J.A., Yu, J., 2012. Reconstructing deglacial North and South Atlantic deep water sourcing using foraminiferal Nd isotopes. Earth and Planetary Science Letters 357–358, 289-297.

Piotrowski, A.M., Goldstein, S.L., Hemming, S.R., Fairbanks, R.G., 2004. Intensification and variability of ocean thermohaline circulation through the last deglaciation. Earth and Planetary Science Letters 225, 205-220.

Piotrowski, A.M., Goldstein, S.L., Hemming, S.R., Fairbanks, R.G., 2005. Temporal relationships of carbon cycling and ocean circulation at glacial boundaries. Science 307, 1933-1938.

Piotrowski, A.M., Goldstein, S.L., R, H.S., Fairbanks, R.G., Zylberberg, D.R., 2008. Oscillating glacial northern and southern deep water formation from combined neodymium and carbon isotopes. Earth and Planetary Science Letters 272, 394-405.

Pourmand, A., Prospero, J.M., Sharifi, A., 2014. Geochemical fingerprinting of trans-Atlantic African dust based on radiogenic Sr-Nd-Hf isotopes and rare earth element anomalies. Geology 42, 675-678.

Prospero, J.M., Glaccum, R.A., Nees, R.T., 1981. Atmospheric transport of soil dust from Africa to South America. Nature 289, 570-572.

Pu, B., Vizy, E.K., Cook, K.H., 2012. Warm season response over North America to a shutdown of the Atlantic Meridional Overturning Circulation and CO_2 increases. Journal of Climate 25, 6701-6720.

Rahmstorf, S., 2002. Ocean circulation and climate during the past 120,000 years. Nature 419, 207-214.

Rahmstorf, S., 2003. Thermohaline circulation: The current climate. Nature 421, 699-699.

Rennermalm, A.K., Wood, E.F., Déry, S.J., Weaver, A.J., Eby, M., 2006. Sensitivity of the thermohaline circulation to Arctic Ocean runoff. Geophysical Research Letters 33, L12703.

Revel, M., Cremer, M., Grousset, F.E., Labeyrie, L., 1996. Grain-size and Sr-Nd isotopes as tracer of paleo-bottom current strength, Northeast Atlantic Ocean. Marine Geology 131, 233-249.

Reyes, A.V., Carlson, A.E., Beard, B.L., Hatfield, R.G., Stoner, J.S., Winsor, K., Welke, B., Ullman, D.J., 2014. South Greenland ice-sheet collapse during Marine Isotope Stage 11. Nature 510, 525-528.

Roberts, N.L., Piotrowski, A.M., McManus, J.F., Keigwin, L.D., 2010. Synchronous deglacial overturning and water mass source changes. Science 327, 75-78.

Rodrigo-Gámiz, M., Martínez-Ruiz, F., Chiaradia, M., Jiménez-Espejo, F.J., Ariztegui, D., 2015. Radiogenic isotopes for deciphering terrigenous input provenance in the western Mediterranean. Chemical Geology 410, 237-250.

Rutberg, R.L., Goldstein, S.L., Hemming, S.R., Anderson, R.F., 2005. Sr isotope evidence for sources of terrigenous sediment in the southeast Atlantic Ocean: Is there increased available Fe for enhanced glacial productivity? Paleoceanography 20, PA1018.

Rutberg, R.L., Hemming, S.R., Goldstein, S.L., 2000. Reduced North Atlantic Deep Water flux to the glacial Southern Ocean inferred from neodymium isotope ratios. Nature 405, 935-938.

Sarnthein, M., Winn, K., Jung, S.J.A., Duplessy, J.-C., Labeyrie, L., Erlenkeuser, H., Ganssen, G., 1994. Changes in East Atlantic deepwater circulation over the last 30,000 years: eight time slice reconstructions. Paleoceanography 9, 209-267.

Scheuvens, D., Schütz, L., Kandler, K., Ebert, M., Weinbruch, S., 2013. Bulk composition of northern African dust and its source sediments — A compilation. Earth-Science Reviews 116, 170-194.

Schmittner, A., Clement, A.C., 2002. Sensitivity of the thermohaline circulation to tropical and high latitude freshwater forcing during the last glacial-interglacial cycle. Paleoceanography 17.

Siedler, G., Gould, J., Church, J.A., 2001. Ocean circulation and climate: Observing and modelling the global ocean. Elsevier Science.

Steffen, W., Sanderson, R.A., Tyson, P.D., Jäger, J., Matson, P.A., Moore, B., Oldfield, F., Richardson, K., Schellnhuber, H.J., Turner, B.L., 2006. Global change and the Earth system: A planet under pressure. Springer.

Stocker, T.F., Schmittner, A., 1997. Influence of CO_2 emission rates on the stability of the thermohaline circulation. Nature 388, 862-865.

Stommel, H., Arons, A.B., 1959a. On the abyssal circulation of the world ocean - I. Stationary planetary flow patterns on a sphere. Deep Sea Research (1953) 6, 140-154.

Stommel, H., Arons, A.B., 1959b. On the abyssal circulation of the world ocean - II. An idealized model of the circulation pattern and amplitude in oceanic basins. Deep Sea Research (1953) 6, 217-233.

Stumpf, R., Frank, M., Schönfeld, J., Haley, B.A., 2011. Climatically driven changes in sediment supply on the SW Iberian shelf since the Last Glacial Maximum. Earth and Planetary Science Letters 312, 80-90.

Stumpf, R., Kraft, S., Frank, M., Haley, B., Holbourn, A., Kuhnt, W., 2015. Persistently strong Indonesian Throughflow during marine isotope stage 3: evidence from radiogenic isotopes. Quaternary Science Reviews 112, 197-206.

Stuut, J.-B., Zabel, M., Ratmeyer, V., Helmke, P., Schefuß, E., Lavik, G., Schneider, R., 2005. Provenance of present-day eolian dust collected off NW Africa. Journal of Geophysical Research: Atmospheres 110, D04202.

Toggweiler, J., Samuels, B., 1995. Effect of Drake Passage on the global thermohaline circulation. Deep Sea Research Part I: Oceanographic Research Papers 42, 477-500.

Trenberth, K.E., Caron, J.M., 2001. Estimates of meridional atmosphere and ocean heat transports. Journal of Climate 14, 3433-3443.

Újvári, G., Stevens, T., Svensson, A., Klötzli, U.S., Manning, C., Németh, T., Kovács, J., Sweeney, M.R., Gocke, M., Wiesenberg, G.L.B., Markovic, S.B., Zech, M., 2015. Two possible source regions for central Greenland last glacial dust. Geophysical Research Letters 42, 10,399-310,408.

van de Flierdt, T., Frank, M., Halliday, A.N., Hein, J.R., Hattendorf, B., Günther, D., Kubik, P.W., 2004. Deep and bottom water export from the Southern Ocean to the Pacific over the past 38 million years. Paleoceanography 19.

van de Flierdt, T., Robinson, L.F., Adkins, J.F., Hemming, S.R., Goldstein, S.L., 2006. Temporal stability of the neodymium isotope signature of the Holocene to glacial North Atlantic. Paleoceanography 21, PA4102.

van der Lubbe, H.J.L., Frank, M., Tjallingii, R., Schneider, R.R., 2016. Neodymium isotope constraints on provenance, dispersal, and climate-driven supply of Zambezi sediments along the Mozambique Margin during the past ~45,000 years. Geochemistry, Geophysics, Geosystems 17, 181-198.

Vellinga, M., Wood, R.A., 2002. Global climatic impacts of a collapse of the Atlantic thermohaline circulation. Climatic Change 54, 251-267.

Vlastélic, I., Abouchami, W., Galer, S.J.G., Hofmann, A.W., 2001. Geographic control on Pb isotope distribution and sources in Indian Ocean Fe-Mn deposits. Geochimica et Cosmochimica Acta 65, 4303-4319.

von Blanckenburg, F., 1999. Tracing past ocean circulation? Science 286, 1862-1863.

von Blanckenburg, F., O'Nions, R.K., Heinz, J.R., 1996. Distribution and sources of pre-anthropogenic lead isotopes in deep ocean water from FeMn crusts. Geochimica et Cosmochimica Acta 60, 4957-4963.

Walter, H.J., Hegner, E., Diekmann, B., Kuhn, G., Rutgers van der loeff, M.M., 2000. Provenance and transport of terrigenous sediment in the south Atlantic Ocean and their relations to glacial and interglacial cycles: Nd and Sr isotopic evidence. Geochimica et Cosmochimica Acta 64, 3813-3827.

Weldeab, S., Emeis, K.-C., Hemleben, C., Siebel, W., 2002. Provenance of lithogenic surface sediments and pathways of riverine suspended matter in the Eastern Mediterranean Sea: evidence from $^{143}Nd/^{144}Nd$ and $^{87}Sr/^{86}Sr$ ratios. Chemical Geology 186, 139-149.

White, W.M., 2013. Geochemistry. Wiley.

White, W.M., Patchett, J., BenOthman, D., 1986. Hf isotope ratios of marine sediments and Mn nodules: evidence for a mantle source of Hf in seawater. Earth and Planetary Science Letters 79, 46-54.

Wilson, D., van de Flierdt, T., Bridgestock, L., Paul, M., Rehkamper, M., Robinson, L., Adkins, J., 2015. Exploring Pb isotopes in deep-sea corals: Measurement by TIMS and application to the deglacial Southern Ocean. Goldschmidt Conference Abstract.

Winter, B.L., Johnson, C.M., Clark, D.L., 1997. Strontium, neodymium, and lead isotope variations of authigenic and silicate sediment components from the Late Cenozoic Arctic Ocean: Implications for sediment provenance and the source of trace metals in seawater. Geochimica et Cosmochimica Acta 61, 4181-4200.

Zabel, M., Bickert, T., Dittert, L., Haese, R.R., 1999. Significance of the sedimentary Al:Ti ratio as an indicator for variations in the circulation patterns of the equatorial North Atlantic. Paleoceanography 14, 789-799.

Chapter 2

Deep circulation changes in the South Atlantic since the Last Glacial Maximum from Nd isotope and multi-proxy records

R. Wei[1]*,W. Abouchami[1,2,3], R. Zahn[4,5,6] , P. Masque[5,6,7,8]

[1] Max Planck Institute for Chemistry, Biogeochemistry Department, P.O. Box 3060, 55020 Mainz, Germany

[2] Institut für Mineralogie, Westfälische Wilhelms Universität, Münster, Germany

[3] Institut de Physique du Globe de Paris, Sorbonne Paris Cité, Université Paris Diderot, UMR 7154 CNRS, 75238 Paris, France

[4] Institució Catalana de Recerca i Estudis Avançats, Barcelona, Spain

[5] Institut de Ciència i Tecnologia Ambientals, Universitat Autònoma de Barcelona, Cerdanyola del Vallès, Spain

[6] Departament de Física, Universitat Autònoma de Barcelona, Cerdanyola del Vallès, Spain

[7] Oceans Institute and School of Physics, The University of Western Australia, Crawley, WA, Australia.

[8] School of Natural Sciences and Centre for Marine Ecosystems Research, Edith Cowan University, Joondalup, WA, Australia.

*Corresponding author. Tel: +49 (6131) 305 6601: Email: ran.wei@mpic.de

This chapter is published as Wei R., Abouchami W., Zahn R. and et al., 2016. Deep circulation changes in the South Atlantic since the Last Glacial Maximum from Nd isotope and multi-proxy records. Earth and Planetary Science Letters 434, 18-29.

Abstract

We report down-core sedimentary Nd isotope (ε_{Nd}) records from two South Atlantic sediment cores, MD02-2594 and GeoB3603-2, located on the western South African continental margin. The core sites are positioned downstream of the present-day flow path of North Atlantic Deep Water (NADW) and close to the Southern Ocean, which makes them suitable for reconstructing past variability in NADW circulation over the last glacial cycle. The Fe-Mn leachates ε_{Nd} records show a coherent decreasing trend from glacial radiogenic values towards less radiogenic values during the Holocene. This trend is confirmed by ε_{Nd} in fish debris and mixed planktonic foraminifera, albeit with an offset during the Holocene to lower values relative to the leachates, matching the present-day composition of NADW in the Cape Basin. We interpret the ε_{Nd} changes as reflecting the glacial shoaling of Southern Ocean waters to shallower depths combined with the admixing of southward flowing Northern Component Water (NCW). A compilation of Atlantic ε_{Nd} records reveals increasing radiogenic isotope signatures towards the south and with increasing depth. This signal is most prominent during the Last Glacial Maximum (LGM) and of similar amplitude across the Atlantic basin, suggesting continuous deep water production in the North Atlantic and export to the South Atlantic and the Southern Ocean. The amplitude of the ε_{Nd} change from the LGM to Holocene is largest in the southernmost cores, implying a greater sensitivity to the deglacial strengthening of NADW at these sites. This signal impacted most prominently the South Atlantic deep and bottom water layers that were particularly deprived of NCW during the LGM. The ε_{Nd} variations correlate with changes in $^{231}Pa/^{230}Th$ ratios and benthic $\delta^{13}C$ across the deglacial transition. Together with the contrasting $^{231}Pa/^{230}Th$: ε_{Nd} pattern of the North and South Atlantic, this indicates a progressive reorganization of the AMOC to full strength during the Holocene.

Keywords: Nd isotopes, deep circulation, Holocene, Last Glacial Maximum, South Atlantic

Highlights

- Depth gradient in ε_{Nd} consistent with glacial shallowing of southern waters
- Continuous southward export of Northern Component Water during the past 24 kyrs
- Northward glacial penetration of southern waters supported by multi-proxy records
- The AMOC progressively reinvigorates to full strength during the Holocene

2.1 Introduction

The Atlantic Meridional Overturning Circulation (AMOC) refers to a portion of the large-scale ocean circulation that is driven by a combination of wind forcing, buoyancy exchanges and cross-isopycnal mixing (Munk and Wunsch, 1998; Kuhlbrodt et al., 2007). These processes critically impact Earth's climate, and the documentation of the AMOC behavior through time has been a major goal of modern observational and paleoceanographic studies (Elliot et al., 2002; Hirschi et al., 2003; McManus et al., 2004; Raymo et al., 2004). The AMOC transports surface water out of the Southern Hemisphere and releases heat to the atmosphere in the Greenland-Iceland-Norwegian (GIN) seas (Nordic Seas) (Rahmstorf, 2002), where convective overturning leads to the formation of North Atlantic Deep Water (NADW). NADW is exported to the Southern Hemisphere flowing above the southern-derived Antarctic Bottom Water (AABW) (Dickson and Brown, 1994), and propagates into the deep Indian and Pacific Oceans. A compensating return flow of upper layer water from the Pacific and Indian Oceans toward the North Atlantic feeds NADW production. A substantial portion of this return flow occurs via the advection of Agulhas Current water and the Antarctic Circumpolar Current (ACC) (Gordon, 1986; Gordon et al., 1992; Beal et al., 2011).

Nutrient-based proxy records such as benthic foraminiferal Cd/Ca and $\delta^{13}C$ indicate that past restructuring and vertical redistribution of the ocean's nutrient inventory may have shaped glacial-interglacial climatic cycles by impacting the CO_2 exchange between the ocean and atmosphere (Broecker and Denton, 1990). These data compellingly indicate that the ventilation of the deep Atlantic with well-oxygenated NADW was substantially reduced and deep-reaching convective activity in the North Atlantic Ocean was much weaker during the Last Glacial Maximum (LGM) than at present (Hodell et al., 2003; Lynch-Stieglitz et al., 2007; Hesse et al., 2011; Oppo and Curry, 2012). Compilation of these proxies further suggests penetration of high-nutrient (low $\delta^{13}C$, high Cd) southern waters far into the North Atlantic and shoaling of the boundary between NADW and AABW by 1-2 km during glacial

periods (Curry and Oppo, 2005; Marchitto and Broecker, 2006; Yu et al., 2008; Lund et al., 2011; Lippold et al., 2012; Gebbie, 2014). The significance of the $\delta^{13}C$ gradients as signaling changes in water sources remains, however, a matter of debate due to the potential biases introduced by nutrient remineralisation at the seafloor and variable carbon isotope fractionation during air-sea gas exchanges in the past (Broecker and Maier-Reimer, 1992; Zahn and Keir, 1994; Matsumoto and Lynch-Stieglitz, 1999; Mackensen and Licari, 2004; Charles et al., 2010; Gebbie, 2014).

Radiogenic Nd and Sr isotopes have proven to be useful tracers of changes in ocean circulation patterns (Revel et al., 1996; Abouchami et al., 1997; Burton and Vance, 2000; Rutberg et al., 2000), terrigenous provenance and transport mechanism of continental and volcanic detritus (Biscaye and Dasch, 1971; Nakai et al., 1993; Asahara et al., 1999; Walter et al., 2000). In particular, the short residence time of Nd in seawater (approximately 300 to 1000 years) relative to the turnover rate of the oceans (~1500 years) (Elderfield et al., 1988; Tachikawa et al., 1999) makes Nd isotopes particularly useful proxies to trace water mass origins and advection through the ocean's interior (Piepgras et al., 1979; Jeandel, 1993; Hemming et al., 1998). In addition, Nd isotopes are not fractionated by biogenic processes in the water column, which makes them particularly valuable for studies of the ocean's past states of circulation and overturning. By contrast, the oceanic residence time of Sr is much longer (~2.5Ma) (Palmer and Elderfield, 1985; Hodell et al., 1990) as reflected in the global homogenous and constant seawater $^{87}Sr/^{86}Sr$ ratio of ~0.7092.

Several studies have shown that Nd isotopes (expressed as ε_{Nd}, which is the deviation in part per ten thousands from the CHUR (Chondritic Uniform Reservoir)) in Fe-Mn oxide precipitates match relatively well that of ambient seawater (see Goldstein and Hemming, 2003). Modern seawater shows distinctive ε_{Nd} for NADW (ε_{Nd} = -13.5) (Piepgras and Wasserburg, 1980, 1987) and PAC (Pacific Deep Water) (ε_{Nd} = -4) (Piepgras and Wasserburg, 1980; Piepgras and Jacobsen, 1988), reflecting the composition of the surrounding terrains,

mainly old continental crust in the North Atlantic and young volcanism in the Pacific. High resolution Nd isotope records of Fe-Mn crusts and corals indicate that the past composition of water masses remained relatively constant through the last glacial cycle (Abouchami et al., 1997; van de Flierdt et al., 2006; Foster et al., 2007), underscoring the potential of ε_{Nd} as a tracer of changes in thermohaline circulation on millennial and glacial-interglacial time scales.

Existing sedimentary Nd isotope records are mainly from the Southeast Atlantic and North Atlantic within the deep western boundary current region. These records all point to an increased northward flow of AABW with reduced northern-sourced water influence during the LGM (Rutberg et al., 2000; Bayon et al., 2002; Bayon et al., 2004; Piotrowski et al., 2004, 2005; Gutjahr et al., 2008; Roberts et al., 2010; Piotrowski et al., 2012; Skinner et al., 2013). Complementary analysis of a dynamical proxy that is sensitive to changes in deep water flow rate ─ the uranium series isotope ratio $^{231}Pa/^{230}Th$ ─ provided so far an inconclusive picture, with some studies suggesting the glacial AMOC was at least as vigorous as today (Yu et al., 1996; Lippold et al., 2012), while others infer less than a 30-40% slowdown of the AMOC (*McManus et al.*, 2004) and a prominent northward flow of Southern Component Water (SCW) during the LGM (Negre et al., 2010). These scenarios are in agreement with reconstructions from benthic foraminiferal $\delta^{13}C$, a nutrient-based proxy widely used in stable isotope paleoceanography.

Here we present down-core sedimentary Nd isotope records of Fe-Mn leachates from two South Atlantic cores, MD02-2594 (34˚43'S, 17˚20'E, water depth 2,440 m) and GeoB3603-2 (35˚08'S, 17˚33'E, water depth 2,840 m), which are located on the southwest African continental margin of the Cape Basin. The two cores are positioned downstream along the present-day flow path of NADW and close to the Southern Ocean (Fig. 2.1), a suitable location for reconstructing past variability in deep water circulation in relation with the intensity of deep convection in the North Atlantic and Southern Ocean and the magnitude of inter-basin water exchange between the Indian and Atlantic Oceans. Available nutrient-

based and temperature/salinity-sensitive proxy records of core MD02-2594 indicate an overall prominent influence of SCW and reduced through flow of high-salinity Agulhas Water transporting Indian Ocean water into the South Atlantic Ocean during glacial periods (Martínez-Méndez et al., 2010; Negre et al., 2010; Caley et al., 2014; Dyez et al., 2014; Kasper et al., 2014). Faunal and geochemical evidence from nearby sediment core GeoB3603-2 also suggest variability of the Agulhas Leakage in relation with changes of AMOC and climate (Esper et al., 2004; Peeters et al., 2004; Martínez-Méndez et al., 2010; Koutsodendris et al., 2014; Mejía et al., 2014; Scussolini et al., 2015). Of particular interest is the $^{231}Pa/^{230}Th$ record of MD02-2594, which led Negre et al. (2010) to propose that the water flow in the abyssal Atlantic was reversed during the LGM, a hypothesis that received further support from a recent $^{231}Pa/^{230}Th$ study in the open South Atlantic (Jonkers et al., 2015). In our study, we combine multiple proxy records (ε_{Nd}, $\delta^{13}C$, $^{231}Pa/^{230}Th$) from the Atlantic to test for AMOC variability and evaluate the hypotheses that have been put forward for the deep circulation changes during the LGM. The significance of the observed variations are discussed in terms of changes in mixing proportions of northern- and southern-sourced deep waters reaching the South Atlantic versus changes in the water masses isotopic "endmember" compositions. The scenarios for the LGM dynamics of the AMOC are discussed by examining the relationship between Nd isotopes, a tracer of water mass origins (North Atlantic *vs.* Pacific), and $^{231}Pa/^{230}Th$ ratios a proxy of deep water flow rate, hence the AMOC strength.

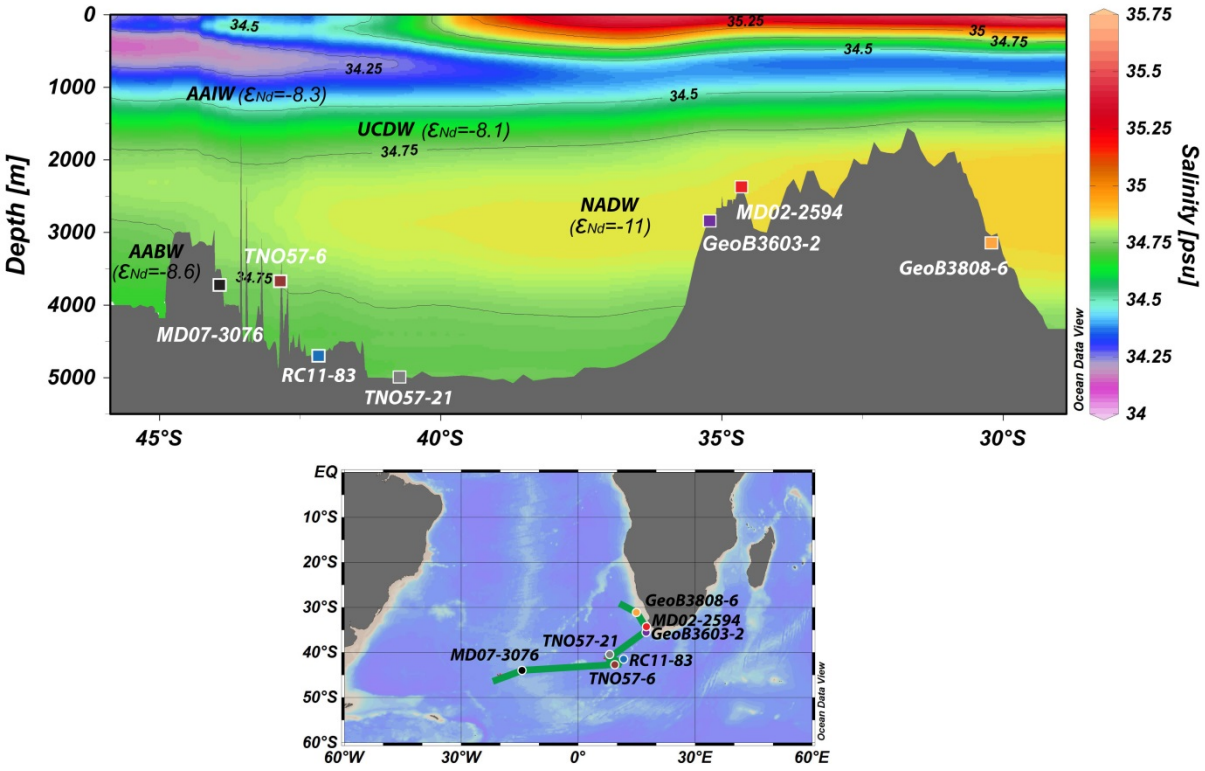

Fig. 2.1 Salinity transect from the tip of South Africa to the western slope of the Mid-Atlantic Ridge showing the core locations from this study (MD02-2594 and GeoB3603-2) and South Atlantic sites with published records used in this study for comparison (Rutberg et al., 2000; Piotrowski et al., 2004, 2005; Skinner et al., 2013; Jonkers et al., 2015). Water mass ε_{Nd} values are reported for North Atlantic Deep Water (NADW), Antarctic Bottom Water (AABW), Upper Circumpolar Deep Water (UCDW) and Antarctic Intermediate Water (AAIW). Figure prepared using Ocean Data View software (Schlitzer, 2014).

2.2 Material and methods

We report Nd and Sr isotope data on the dispersed Fe-Mn oxides of cores MD02-2594 and GeoB3603-2 from the southwest African continental margin in the Cape Basin (Southeast Atlantic) for the period 0-24 kyr, along with data on mixed planktonic foraminifera species and fish debris (Table 2.1). The age model for core MD02-2594 was derived using a combination of radiocarbon dating and graphical correlation of the benthic $\delta^{18}O$ record (Martínez-Méndez et al., 2010). For core GeoB3603-2, the $\delta^{18}O$ record of benthic foraminifera *Cibicides wuellerstorfi* served as stratigraphic control to develop the age model using standard orbital tuning (Peeters et al., 2004).

Table 2.1 Nd and Sr isotope ratios in core MD02-2594 (**a**) and GeoB3603-2 (**b**).

"*" refer to samples duplicated and for which the weighed mean are plotted in the figures.

Depth in core (cm)	Age (cal-kyr BP)	$^{143}Nd/^{144}Nd$ (2σ)	ε_{Nd} (2σ)	$^{87}Sr/^{86}Sr$ (2σ)
MD02-2594				
Bulk sediment Fe-Mn leachate				
5-6	0.3	0.512190 (10)	-8.74 ± 0.20	0.709271 (5)
12-13	0.7	0.512172 (13)	-9.09 ± 0.25	0.709302 (6)
22-23	1.2	0.512184 (14)	-8.86 ± 0.28	0.709305 (7)
32-33	1.8	0.512183 (15)	-8.88 ± 0.30	0.709297 (12)
50-51*	2.8	0.512197 (10)	-8.60 ± 0.20	0.709280 (7)
60-61	3.5	0.512194 (10)	-8.67 ± 0.19	0.709322 (12)
75-76	4.6	0.512180 (10)	-8.93 ± 0.20	0.709321 (14)
82-83	5.0	0.512202 (9)	-8.51 ± 0.17	0.709315 (7)
88-89	5.5	0.512194 (22)	-8.66 ± 0.42	0.709294 (14)
98-99	6.1	0.512178 (12)	-8.97 ± 0.24	0.709356 (6)
112-113	7.1	0.512194 (8)	-8.67 ± 0.15	0.709268 (11)
125-126	7.8	0.512194 (14)	-8.67 ± 0.27	0.709302 (10)
135-136	8.4	0.512172 (10)	-9.10 ± 0.19	0.709306 (6)
140-141	8.6	0.512193 (13)	-8.69 ± 0.26	0.709312 (11)
155-156	9.5	0.512175 (10)	-9.02 ± 0.19	0.709311 (11)
160-161	9.7	0.512174 (14)	-9.05 ± 0.28	0.709329 (11)
165-166	10.0	0.512166 (13)	-9.20 ± 0.26	0.709374 (6)
170-171	10.3	0.512136 (14)	-9.79 ± 0.27	0.709299 (11)
180-181	10.9	0.512184 (10)	-8.85 ± 0.19	0.709254 (11)
192-193*	11.6	0.512172 (26)	-9.09 ± 0.51	0.709296 (7)
205-206	12.3	0.512185 (8)	-8.84 ± 0.15	0.709173 (7)
215-216	13.1	0.512200 (12)	-8.54 ± 0.23	0.709284 (12)
222-223	13.7	0.512198 (17)	-8.59 ± 0.33	0.709277 (7)
235-236	14.9	0.512223 (9)	-8.10 ± 0.17	0.709393 (6)
245-246	15.8	0.512210 (7)	-8.34 ± 0.13	0.709548 (7)
252-253	16.5	0.512226 (11)	-8.05 ± 0.22	0.709282 (11)
265-266	17.4	0.512219 (6)	-8.17 ± 0.11	0.709115 (7)
270-271	17.7	0.512245 (6)	-7.66 ± 0.11	0.709244 (10)
273-274*	17.7	0.512232 (6)	-7.92 ± 0.11	0.709245 (7)
283-284	18.3	0.512293 (7)	-6.73 ± 0.14	0.709414 (9)
297-298	19.6	0.512266 (6)	-7.27 ± 0.11	0.709557 (7)
305-306*	20.8	0.512267 (6)	-7.24 ± 0.12	0.709188 (3)
315-316	22.7	0.512285 (7)	-6.88 ± 0.14	0.709547 (6)
323-324	24.1	0.512250 (6)	-7.57 ± 0.13	0.709401 (6)

Continued **Table 2.1**

Depth in core (cm)	Age (cal-kyr BP)	$^{143}Nd/^{144}Nd$ (2σ)	ε_{Nd} (2σ)	$^{87}Sr/^{86}Sr$ (2σ)
Fine <63 µmFe-Mn leachates				
35-36	2.0	0.512196 (7)	-8.63 ± 0.14	0.709390 (7)
75-76	4.6	0.512203 (15)	-8.48 ± 0.29	0.709286 (6)
135-136	8.4	0.512191 (16)	-8.71 ± 0.32	0.709315 (6)
165-166	10.0	0.512220 (16)	-8.16 ± 0.31	0.709284 (6)
285-286	18.4	0.512271 (8)	-7.15 ± 0.15	0.709258 (6)
295-296	18.8	0.512253 (8)	-7.50 ± 0.15	0.709298 (6)
305-306	20.8	0.512266 (14)	-7.26 ± 0.27	0.709364 (6)
315-316	22.7	0.512253 (9)	-7.51 ± 0.18	0.709280 (6)
Bulk sediment				
5-6	0.3	0.512118 (5)	-10.15 ± 0.11	0.709732 (7)
50-51	2.8	0.512138 (10)	-9.76 ± 0.19	0.709697 (8)
192-193*	11.6	0.512123 (5)	-10.04 ± 0.10	0.709503 (4)
205-206	12.3	0.512151 (7)	-9.50 ± 0.14	0.709446 (7)
265-266*	17.4	0.512177 (6)	-8.98 ± 0.12	0.709472 (4)
273-274*	17.7	0.512210 (5)	-8.13 ± 0.10	0.709454 (7)
305-306*	20.8	0.512150 (6)	-9.52 ± 0.11	0.709476 (7)
Planktonic foraminifera				
98-99	6.1	0.512140 (16)	-9.72 ± 0.31	0.709193 (7)
112-113	7.1	0.512174 (18)	-9.05 ± 0.36	0.709184 (6)
140-141	8.6	0.512140 (29)	-9.72 ± 0.58	0.709188 (6)
283-284	18.3	0.512248 (8)	-7.62 ± 0.16	0.709186 (6)
297-298	19.6	0.512233 (7)	-7.90 ± 0.13	0.709177 (6)
GeoB3603-2				
Bulk sediment Fe-Mn leachate				
2	1.0	0.512207 (9)	-8.42 ± 0.17	0.709289 (7)
5	2.5	0.512189 (9)	-8.76 ± 0.18	0.709293 (7)
7	3.3	0.512188 (10)	-8.78 ± 0.20	0.709281 (6)
10	5.4	0.512177 (9)	-8.99 ± 0.18	0.709309 (5)
13	7.4	0.512186 (7)	-8.82 ± 0.14	0.709293 (7)
18	10.7	0.512192 (12)	-8.71 ± 0.25	0.709264 (7)
20	11.9	0.512183 (7)	-8.88 ± 0.13	0.709302 (6)
23	13.5	0.512219 (8)	-8.17 ± 0.15	0.709271 (7)
25	14.9	0.512223 (6)	-8.09 ± 0.12	0.709260 (7)
29	16.9	0.512250 (6)	-7.58 ± 0.12	0.709252 (7)
32	18.6	0.512251 (6)	-7.56 ± 0.13	0.709244 (7)
37	20.6	0.512261 (10)	-7.36 ± 0.20	0.709220 (6)
40	21.7	0.512268 (6)	-7.22 ± 0.13	0.709264 (7)
Fish debris				
5	2.5	0.512121 (8)	-10.09 ± 0.15	0.709154 (6)
7	3.3	0.512112 (8)	-10.26 ± 0.16	0.709173 (4)
32	18.6	0.512223 (7)	-8.10 ± 0.14	0.709137 (5)
37	20.6	0.512233 (7)	-7.90 ± 0.14	0.709079 (6)

About 50 to 80 mg of bulk sediment was weighed and a leaching procedure slightly modified from previous studies (Chester and Hughes, 1967; Rutberg et al., 2000; Bayon et al., 2002) was used to remove sequentially the carbonates and Fe-Mn oxides, leaving behind the residual detrital fraction. The leaching procedure was also performed on the sieved fraction (< 63μm) of a few samples of core MD02-2594 to test for grain-size effect on the leachate Nd isotopic signal (Table 2.1). Full details about the leaching protocol are reported in Supplementary Material S1. In addition, a few isotopic analyses were obtained on the bulk sediment (Table 2.1) and compared to those of the "terrigenous" and "authigenic" fractions, mainly to evaluate the effectiveness of the leaching procedure in separating those two signals (see Supplementary Material S2). Following on similar previous studies, Sr isotope ratios were measured to test the faithfulness of the Fe-Mn leachates as recording past seawater Nd isotopic compositions, with the premise that the $^{87}Sr/^{86}Sr$ ratios in the leachates are close to that of modern seawater (0.7092). We note, however, that the validity of this approach has been questioned (see Gutjahr et al., 2007).

Several studies have meanwhile shown that the "seawater" Nd isotope signal recorded by Fe-Mn leachates may be biased (Martin and Scher, 2004; Roberts et al., 2010; Elmore et al., 2011; Piotrowski et al., 2012; Osborne et al., 2014), due to boundary exchange processes near continental margins (Lacan and Jeandel, 2005) or reversible scavenging (Siddall et al., 2008). These processes may alter the ambient seawater ε_{Nd}, via release of Nd from particles, and could potentially have affected our Fe-Mn leachates data, especially in view of the proximity of our cores sites to the South African continental margin. To ensure that terrigenous inputs did not impact the ε_{Nd} of the Fe-Mn oxides in the local sediments, possibly offsetting it from that of ambient seawater, mixed planktonic foraminifera and fossil fish debris were hand-picked from the >70 μm sieved fraction whenever available. For each core, four samples were selected to cover the LGM and Holocene sections. For core MD02-2594, no fish debris were found and only mixed planktonic foraminifera (ca. 1 to 5 mg) were

analysed at depths corresponding to 6.1, 7.1, 8.6, 18.3 and 19.6 kyr BP. For core GeoB3603-2, fish debris (10-20 fragments) were hand-picked from the 2.5, 3.3, 18.6 and 20.6 kyr BP depths. Details about the cleaning procedure are reported in Supplementary Material S1.

Table 2.2 Duplicate Nd and Sr isotopic analysis in bulk sediment Fe-Mn leachates and bulk sediment from core MD02-2594.

Depth in core (cm)	$^{143}Nd/^{144}Nd$ (2σ)	ε_{Nd} (2σ)	$^{87}Sr/^{86}Sr$ (2σ)
Bulk sediment Fe-Mn leachate			
50-51	0.512211 (15)	-8.33 ± 0.29	0.709289 (11)
50-51	0.512184 (18)	-8.86 ± 0.34	——
50-51	0.512185 (27)	-8.83 ± 0.53	0.709274 (9)
192-193	——	——	0.709319 (12)
192-193	——	——	0.709286 (8)
273-274	0.512223 (8)	-8.10 ± 0.16	——
273-274	0.512241 (8)	-7.75 ± 0.16	——
305-306	0.512265 (12)	-7.27 ± 0.23	0.709142 (11)
305-306	0.512268 (7)	-7.22 ± 0.14	0.709191 (3)
Bulk sediment			
192-193	0.512117 (6)	-10.16 ± 0.13	0.709507 (5)
192-193	0.512136 (11)	-9.80 ± 0.22	0.709499 (6)
192-193	0.512131 (11)	-9.90 ± 0.22	——
265-266	0.512179 (7)	-8.95 ± 0.13	——
265-266	0.512169 (14)	-9.15 ± 0.27	——
273-274	0.512218 (7)	-8.19 ± 0.14	——
273-274	0.512228 (9)	-8.00 ± 0.18	——
305-306	0.512150 (6)	-9.52 ± 0.12	——
305-306	0.512151 (15)	-9.50 ± 0.29	——

The Nd and Sr isotopic measurements were performed by thermal ionization mass spectrometry (ThermoFisher, TRITON). Strontium was loaded onto single tungsten filaments along with a TaF_5 activator and oxidized in air and the $^{87}Sr/^{86}Sr$ ratios corrected for instrumental fractionation by normalizing to $^{86}Sr/^{88}Sr = 0.1194$. Replicate measurements of NIST SRM 987 yielded 0.710261± 22 (2SD, N = 31) during different sets of measurements. Nd isotopic compositions were determined as NdO^+ species, which involves loading the Nd sample in dilute HNO_3 on a tungsten filament and "sandwiching" with 1 µl of TaF_5 solution following the method described in Rampone et al. (2003). The $^{143}Nd/^{144}Nd$ ratios after oxygen

stripping were corrected for fractionation using $^{146}Nd/^{144}Nd = 0.7219$. Multiple measurements of 5 ng loads of the La Jolla Nd standard resulted in a value of 0.511851±11 (2SD, N = 47) during the period of analysis. The external reproducibility based on duplicate samples analyses is ± 0.23 ε_{Nd} units (see Table 2.2). Total Nd and Sr procedural blanks were of 3 pg and 24 pg, respectively.

2.3 Results

2.3.1 Comparison of Fe-Mn leachates, detrital and bulk sediment Nd isotopic records

The Fe-Mn leachates, detrital fractions and bulk sediments of core MD02-2594 exhibit distinct ε_{Nd} values (Fig. 2.2a), indicating that the leaching procedure efficiently separates the "authigenic" and "terrigenous" isotope signals (see Supplementary Material S2). Furthermore, the good agreement between ε_{Nd} in the Fe-Mn leachates (hereafter $\varepsilon_{Ndleach}$) extracted from the sieved samples (<63 μm fraction) and those from the bulk sediment of core MD02-2594 indicates that 1) the leaching procedure yields reproducible isotopic results and 2) grain-size has little effect on the leachates ε_{Nd} values (see Table 2.2 and Fig. 2.2a).

Despite the occasional occurrence of slightly elevated $^{87}Sr/^{86}Sr$ in the leachates compared to the modern seawater value (~0.7092) (see Table 2.1, Fig. 2.2b), in particular during the LGM and Heinrich Event 1 (H1), these are not associated with significant changes in ε_{Nd} (Fig. 2.2a). This observation indicates that the processes (dissolution of biogenic opal or carbonate or pore water infiltration, detrital contamination during leaching) that could affect Sr isotopes had little effect on the Nd isotope signal recorded by the Fe-Mn oxides leachates, in agreement with previous studies (Bayon et al., 2002; Bayon et al., 2004).

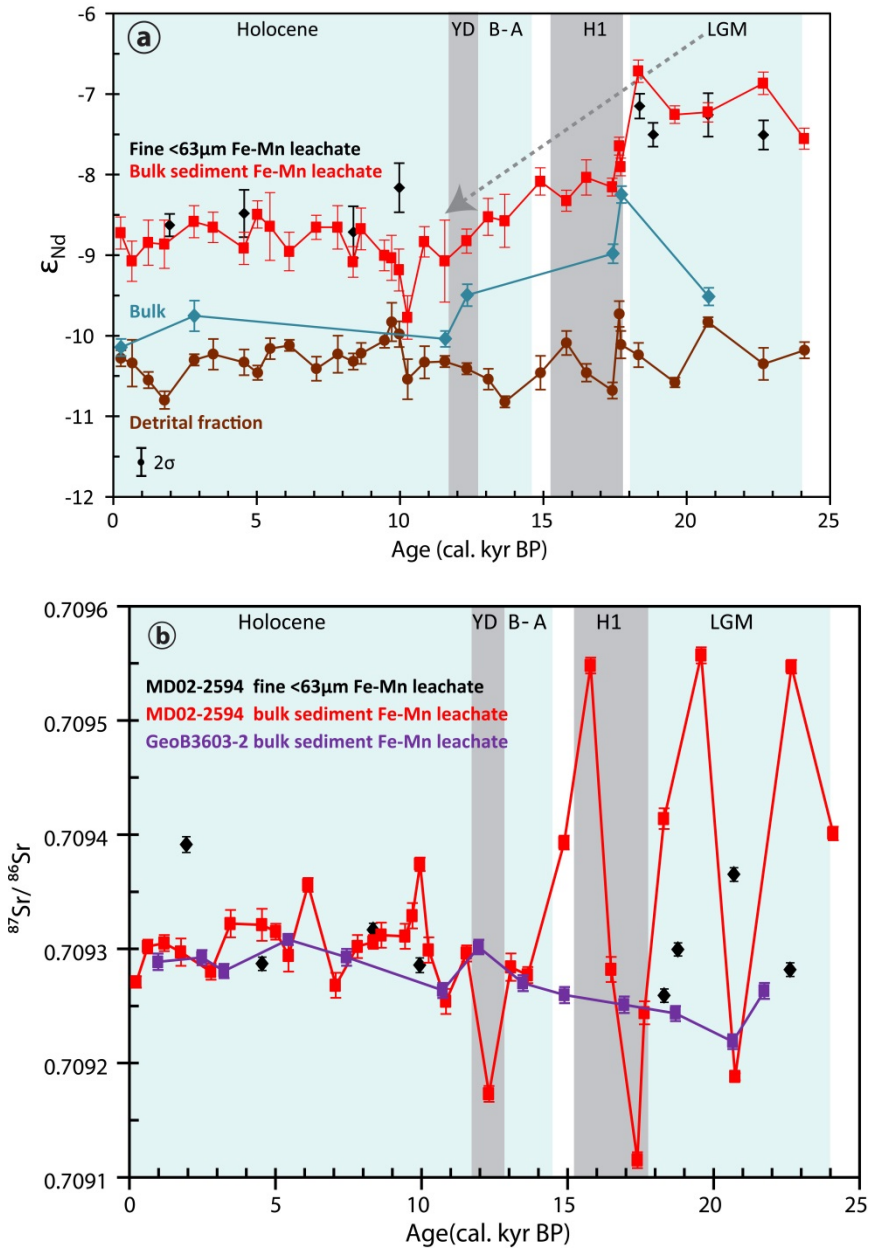

Fig. 2.2 (a) Nd isotope ratios of MD02-2594 Fe-Mn oxide leachates on bulk sediment (red) and on sieved < 63µm fraction (black), detrital fraction (brown), and bulk sediment (blue); (b) Sr isotope ratios of MD02-2594 (red) and GeoB3603-2 (purple) Fe-Mn oxide leachates from bulk sediment and sieved < 63µm fraction (black) in core MD02-2594.

Indeed, our results show that a detrital Nd contribution to the Fe-Mn leachates can be ruled out, since partial dissolution of the detrital fraction, which exhibits ε_{Nd} values of -10 to -11 in both cores, would shift $\varepsilon_{Ndleach}$ towards less radiogenic values, and this is not observed throughout the whole records as seen in Fig. 2.3a. Instead, $\varepsilon_{Ndleach}$ appear to be more radiogenic than the modern composition of NADW (ε_{Nd} = -10.9 ± 1.2 (2SD, N=12)) measured

in the Eastern Atlantic (hereafter ENADW) (Jeandel, 1993; Stichel et al., 2012; Garcia-Solsona et al., 2014) throughout the whole records, and even more so during the LGM (ε_{Nd} = -7.1) than the Holocene (ε_{Nd} = -8.8). Altogether, these results indicate that Nd isotopic variations in the Fe-Mn leachates could be considered as indicative of changes in seawater isotopic compositions over the past 24 kyr.

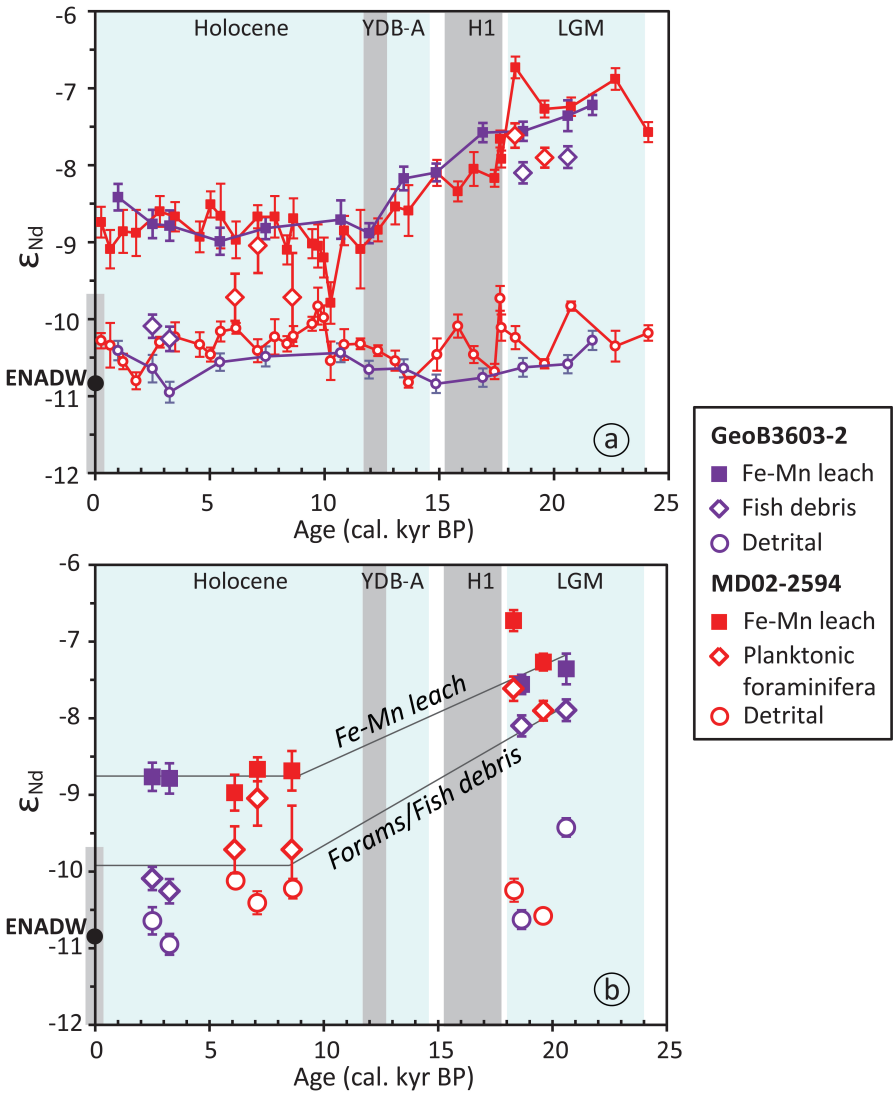

Fig. 2.3 (a) Sedimentary Nd isotope records in core MD02-2594 (34°43'S, 17°20'E, 2,440 m water depth) and GeoB3603-2 (35°08'S, 17°33'E, 2,840 m water depth) in the Cape Basin, South Atlantic. (b) Comparison of ε_{Nd} in Fe-Mn leachates, planktonic foraminifera, fish debris and detrital fractions from the LGM and Holocene sections of the two cores. Note the good agreement between the Fe-Mn leachates and fish debris/foraminifera data for the LGM and the noticeable offset of about 1.2 ε_{Nd}-units for the Holocene data. Holocene: 11.7 kyr BP to present; YD: Younger Dryas (11.7-12.8 kyr BP); B-A: Bølling-Allerød (12.8-14.5 kyr BP); H1: Heinrich Event 1 (~16.8 kyr BP); LGM (18-24 kyr BP).

2.3.2 Nd isotopes in foraminifera and fish debris vs. Fe-Mn leachates.

The use of acid-reductive leaching to extract a reliable seawater ε_{Nd} value from the authigenic fraction (Fe-Mn leachates) of bulk deep-sea sediments has been questioned in some studies (Gutjahr et al., 2007; Wilson et al., 2013). Instead, Nd isotopic measurements in fish debris and mixed planktonic foraminifera species have been shown to retain a "pristine" seawater Nd isotopic signal (Piotrowski et al., 2012) and can thus be used to assess the significance of the Nd isotopic signal recorded by Fe-Mn leachates.

In view of the offset between the Holocene $\varepsilon_{Ndleach}$ in our cores (-8.8) and the contemporaneous seawater ε_{Nd} value (-10.9 ± 1.2), which cannot be explained by a detrital influence (see above), we undertook a few analyses on foraminifera and fish debris to validate that the Nd isotopic signal recorded by the Fe-Mn leachates record changes in seawater composition over the past 24 kyrs.

Figure 2.3b shows a comparison of ε_{Nd} in the mixed planktonic foraminifera species, fish debris and Fe-Mn leachates with those of the corresponding detrital fractions. Both the Fe-Mn leachates and foraminifera and fish debris are offset to higher ε_{Nd} values relative to the detrital fractions, confirming the "authigenic" nature of the Nd isotopic signal they record. Most important is the evidence that the decreasing ε_{Nd} trend exhibited by the Fe-Mn leachates is reproduced by the fish debris and foraminifera data, with an even larger offset between the LGM and Holocene, albeit with less radiogenic values (-9.9 *vs.* -7.9) during the Holocene in the latter. Importantly, these Holocene values fall within the range reported for present-day ENADW, suggesting that the elevated ε_{Nd} in the Holocene Fe-Mn leachates might be the result of Nd released from easily leached volcanogenic material, as has been described elsewhere (Roberts et al., 2010; Elmore et al., 2011; Piotrowski et al., 2012; Osborne et al., 2014).

The evidence that ε_{Nd} values of planktonic foraminifera and fish debris more closely approximate modern deep seawater values than the $\varepsilon_{Ndleach}$ of bulk sediment samples strongly

suggests that foraminifera and fish debris ε_{Nd} are a more reliable proxy for the reconstruction of past deep water changes. Nevertheless, the glacial/deglacial offset is seen in both datasets, despite a difference in the absolute ε_{Nd} values between Fe-Mn leachates and foraminifera-fish debris, confirming that the Fe-Mn leachates Nd isotope record monitor changes in deep water mass source and mixing over the past 24 kyr in the South Atlantic.

2.4 Discussion

2.4.1 Nd isotopic evolution of deep waters in the deep Cape Basin

The evolution from LGM radiogenic ε_{Nd} (~-7.9) to less radiogenic (~-9.9) Holocene values (Fig. 2.3) can be explained as primarily reflecting changes in the contribution and distribution of northerly *vs.* southerly water masses in the Cape Basin in relation with reorganization of the AMOC during the last deglaciation.

According to modern-day oceanographic descriptions, the study sites lay in the southern extension of NADW. However, both the LGM and Holocene ε_{Nd} signatures indicate the presence of a water mass that is isotopically distinct from modern NADW, albeit with a Holocene signature pointing to a greater presence of NADW in the Cape Basin (see Figs. 2.1, 2.3 and 2.4a). The more radiogenic signature seen during the LGM results from an increased influence of SCW in the Cape Basin due to northward expansion of the deep-reaching ACC, in agreement with benthic $\delta^{13}C$ and Cd/Ca records in this region (Oppo and Horowitz, 2000; Martínez-Méndez et al., 2008). By contrast, enhanced contribution of NCW during the Holocene is indicated by a decrease of ε_{Nd} to a value of -9.9, which falls within the range of modern ENADW (ε_{Nd} = -10.9 ± 1.2) (Jeandel, 1993; Stichel et al., 2012; Garcia-Solsona et al., 2014).

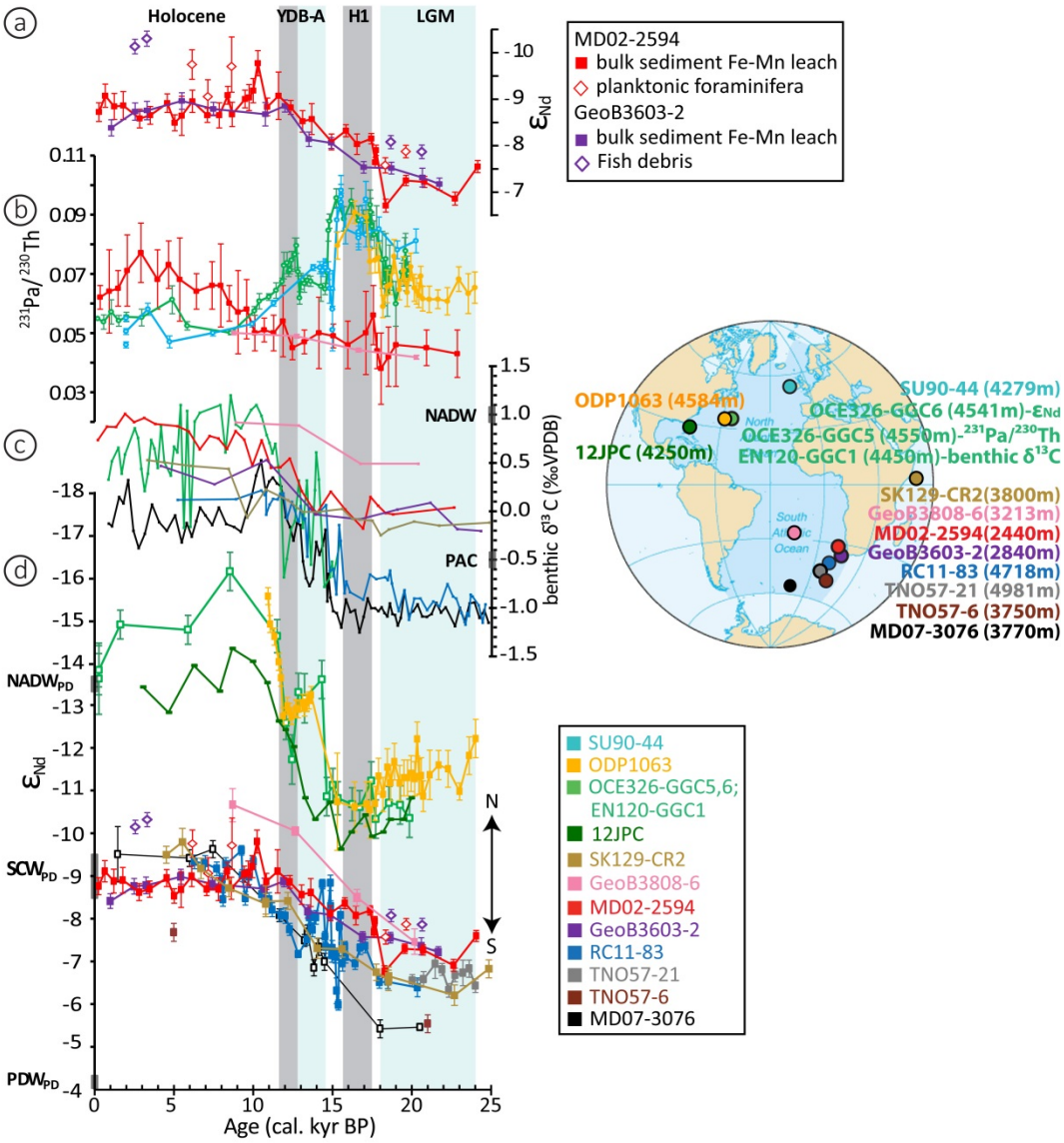

Fig. 2.4 Multi-proxy records of the cores in this study, MD02-2594 and GeoB3603-2 in the Cape Basin, South Atlantic. The records are compared with existing ones from the equatorial Indian Ocean and Atlantic whose location and water depths are reported on the map in the right panel (see also Table 2.4 in Supplementary material for cores locations and data sources). (a) Nd isotope ratios of Fe-Mn leachates, planktonic foraminifera, and fish debris in sediment cores from this study. (b) Sedimentary $^{231}Pa/^{230}Th$ ratios from Cape Basin (MD02-2594), central South Atlantic (GeoB3808-6), eastern North Atlantic (SU90-44), and Northwest Atlantic (OCE326-GGC5 and ODP1063). (c) Benthic foraminiferal $\delta^{13}C$ records of Cape Basin cores MD02-2594, GeoB3603-2 and RC11-83, central South Atlantic (GeoB3808-6), Northwest Atlantic (EN120-GGC1), east Mid-Atlantic Ridge (MD07-3076) and central Indian Ocean (SK129-CR2). (d) Comparison of Nd isotope records of authigenic fractions in sediment cores from the North to South Atlantic, as well as the equatorial Indian Ocean. Composition of present-day (PD) NADW, PAC (Pacific Deep Water) and SCW (Southern Component Water) are indicated with grey bars along y-axes in panels (c) and (d). Note that the scale is reversed for ε_{Nd}. Error bars are 2SE. In the figures, the uncleaned foraminifera Nd isotopic compositions of core OCE326-GGC6 are combined with benthic foraminiferal $\delta^{13}C$ data from nearby core EN120-GGC1 and $^{231}Pa/^{230}Th$ ratios from core OCE326-GGC5.

In Figure 2.4d, our records are compared to published ε_{Nd} records from the Atlantic in an attempt to draw some inferences on past water mass distributions during the transition from the LGM to the Holocene and associated changes of the AMOC. The Nd isotope records show a similar trend at other South Atlantic core sites, where ε_{Nd} values consistently display a more radiogenic signature during the LGM (between -5.5 and -7.9) when compared to Holocene values (between -7.9 and -10.2) (Fig. 2.4d).

The LGM spread of values correlates with the latitudinal position of the cores, with the southerly sites displaying more radiogenic values than the sites further north, thus pointing at a prominent influence of SCW on the more southerly sites. The depth gradient from -5.5 at 44°S (MD07-3076) at 3,770 m water depth, to -6.5 at 41°S (RC11-83 and TN057-21) at 4,718 m and 4,981 m water depth further suggests that bottom waters north of the ACC received some contribution of less radiogenic ε_{Nd} from the north (Fig. 2.4). In the South Atlantic, the further decrease of the mean LGM ε_{Nd} to -7.9 at sites MD02-2594 (34˚43'S) at 2,440 m water depth and GeoB3603-2 (35˚43'S) at 2,840 m water depth supports the indication of a stronger NCW contribution at shallower depths, even though those sites are more distal from the immediate Southern Ocean domain than the bottom water sites referred to above. That domain is best represented by the southernmost sites MD07-3076 and TNO57-6 at 44°S and 43°S, whose ε_{Nd} of -5.5 are the most radiogenic values displayed at the South Atlantic sites. At water depths of 3,750 m and 3,770 m, these two cores are in the southern extension of NADW today and display the largest amplitude change from the LGM to the Holocene (4 ε_{Nd}-units) of all profiles compiled here. Such a feature indicates the isolation of high latitude South Atlantic deep waters from NCW influence, and as a result, a glacial Circumpolar Deep Water (CDW) with the most radiogenic signature (Skinner et al., 2010; Skinner et al., 2013). The most radiogenic LGM values of sites MD07-3076 and TNO57-6 at 44°S and 43°S are clearly distinct from those of the other core sites further north (Fig. 2.5) and confirm the existence of a vertical divide in sense of Martínez-Méndez et al. (2009), separating glacial CDW

circulating in the ACC from deep waters circulating in the South Atlantic subtropical gyre to the north. Our cores MD02-2594 and GeoB3603-2 at about 35˚S, located at 2,440 m and 2,840 m, display the least radiogenic ε_{Nd} values (~ -7.9) of all core sites during the LGM, potentially diagnosing SCW presence with a measurable portion of NCW admixed at these shallow depths. The Nd isotope gradient seen in the South Atlantic records here is similar to the benthic carbon isotope gradient observed along a depth transect in the South Atlantic Ocean (Hodell et al., 2003).

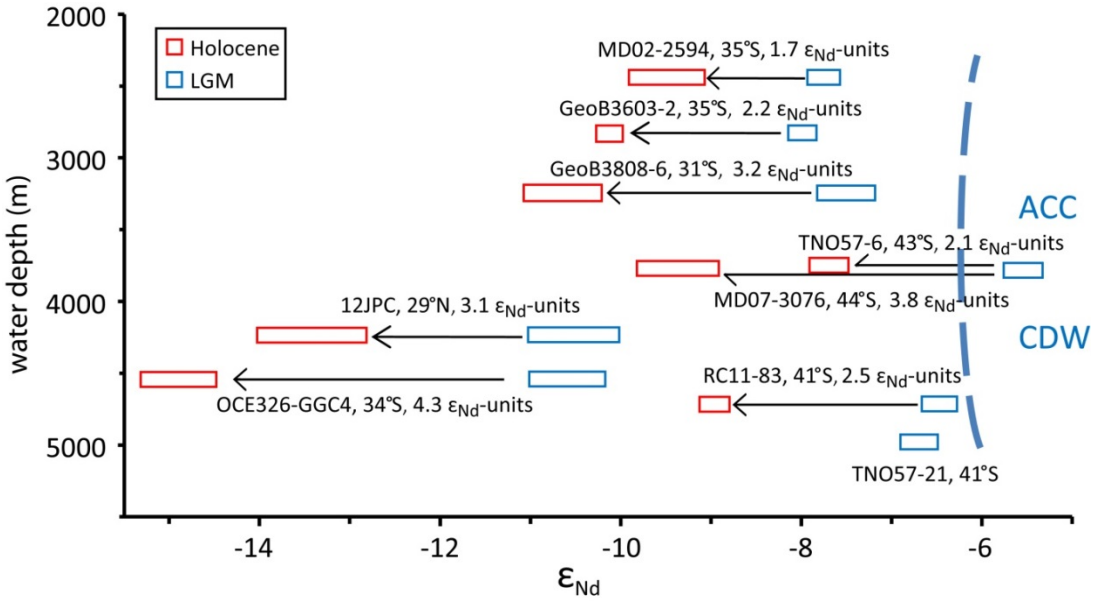

Fig. 2.5 Amplitude of LGM to Holocene ε_{Nd} shifts as a function of water depth. The rectangles correspond to the ε_{Nd} range for each period (same as in Fig. 2.3), labeled with corresponding core name, latitude and the amplitude of LGM to Holocene shift in ε_{Nd} units. Note that ε_{Nd} values refer to the Fe-Mn leachates data, except for core OCE326-GGC6, MD02-2594 and GeoB3603-2 for which the uncleaned foraminifera and fish debris data are plotted. Data sources are listed in Table 2.4 in Supplementary material.

The South Atlantic records display ε_{Nd} decreases to less radiogenic values during the glacial termination by 1.7 to 3.8 ε_{Nd}-units, indicating an increased influence of NADW in the Holocene at all sites, albeit in variable strength (Fig. 2.5). The deglacial ε_{Nd} decrease in the South Atlantic is largest at the southernmost site MD07-3076, demonstrating the hydrographic impact of NADW was strengthening in the Southern Ocean domain, which is consistent with earlier benthic $\delta^{13}C$- and Cd/Ca-based studies (Oppo and Fairbanks, 1987; Charles and

Fairbanks, 1992; Oppo and Rosenthal, 1994; Ninnemann and Charles, 2002; Martínez-Méndez et al., 2009; Waelbroeck et al., 2011). This core site was most efficiently cut-off from NCW during the LGM, hence the larger ε_{Nd} amplitude as the ACC contracted around Antarctica, and NCW started arriving at the core site during the transition into the Holocene. By contrast, the smallest deglacial ε_{Nd} decrease of about 1.7 and 2.2 ε_{Nd}-units occurs at sites MD02-2594 and GeoB3603-2. The ε_{Nd} amplitude of 2.0 ε_{Nd}-units at the bottom-water site OCE326-GGC6 in the North Atlantic reflects the stronger contribution of Labrador Sea Water during the Holocene (Böhm et al., 2015). The intermediate ε_{Nd} decrease of around 3 units (cores GeoB3808-6 and 12JPC), indicates that the deep-water isopycnals at those depths in the North and South Atlantic were ventilated by roughly the same mixture of NCW and SCW. The compilation of ε_{Nd} records (Fig. 2.4) and amplitudes of changes (Fig. 2.5) confirms earlier suggestions that variations of NADW strength impacted most prominently the South Atlantic deep and bottom water layers that were particularly deprived of NCW during the LGM (Oppo and Fairbanks, 1987; Charles and Fairbanks, 1992; Oppo and Rosenthal, 1994). The data compilation also shows that the ε_{Nd} values observed during the Holocene at the South Atlantic core sites remained higher than those at the bottom water reference site 12JPC in the North Atlantic (Gutjahr et al., 2008). This overall pattern is consistent with southward setting NCW continuously affecting the shallow sites MD02-2594 and GeoB3603-2 in the South Atlantic, which display the smallest ε_{Nd} increase during the deglacial.

Glacial-interglacial Nd isotope values of authigenic phases from core SK129-CR2 in the deep equatorial Indian Ocean fall within the range of values observed in the South Atlantic cores (Fig. 2.4d) (Piotrowski et al., 2009; Wilson et al., 2015b). This suggests that the contribution change of NADW reaching the Indian Ocean was roughly the same as in the South Atlantic, and that the associated water mass signal propagated quantitatively from the South Atlantic through the Southern Ocean into the deep Indian Ocean, in agreement with previous studies (Piotrowski et al., 2009). Our new Nd isotope records in the South Atlantic,

along with the other records compiled in Figs. 2.4 and 2.5 corroborate earlier reconstructions of deep water circulation patterns and modelling results which indicated mid-depth ventilation in the North Atlantic during the LGM and a prominent SCW presence and shoaling of the boundary between northern and southern water sources (Boyle and Keigwin, 1987; Sarnthein et al., 1994; Bertram et al., 1995; Curry et al., 1999; Willamowski and Zahn, 2000; Lund et al., 2011). The nearly constant approximately 3 ε_{Nd}-units difference between the North and South Atlantic during the last 24 kyrs can be sustained if deep water export from the North to the South Atlantic persisted, with shallow overturning in the north and stronger convection in the south. Such a scenario is supported by the oceanic budget of ^{231}Pa, which suggests that the export flux of ^{231}Pa from the North Atlantic to the Southern Ocean was not very different during the LGM (Yu et al., 1996).

Altogether, our new Nd isotopic records from the Cape Basin support the concept of continuous southward export of NADW, albeit with a glacial predominance of southern water sources in the South Atlantic.

2.4.2 Contribution changes in northern and southern component waters

Benthic δ^{13}C is commonly used as a nutrient proxy to reconstruct past ocean circulation changes. In order to confirm the NCW influence at MD02-2594 and GeoB3603-2, we compare the benthic δ^{13}C records with those of core RC11-83 from Cape Basin, MD07-3076Q located on the eastern flank of the Mid-Atlantic Ridge, EN120-GGC1 in the North Atlantic and SK129-CR2 in the equatorial Indian Ocean (Fig. 2.4c). The benthic δ^{13}C records show increases from the LGM to the Holocene of between 1.0‰ and 1.5‰ (Boyle and Keigwin, 1987; Charles et al., 1996; Negre et al., 2010), which are substantially in excess of the global mean-ocean δ^{13}C increase of 0.3‰ (Duplessy et al., 1988), hence alluding to shifted deep and bottom water δ^{13}C and ventilation. During the LGM, lower benthic δ^{13}C values around -1.0‰ are recorded at the bottom water sites RC11-83 (Charles et al., 1996)

and EN120-GGC1 (Boyle and Keigwin, 1987) in the South and North Atlantic respectively, indicating a strongly reduced admixture of NCW into SCW and a larger influence of high-nutrient SCW, possibly in combination with an increased flux of phyto-detritus at the southern site and subsequent remineralization in the benthic boundary layer (Mackensen et al., 1993). The higher nutrient concentrations in the deep North Atlantic inferred from benthic Cd/Ca during the LGM are in accordance with the more radiogenic LGM ε_{Nd} values seen in our cores. Glacial-interglacial benthic $\delta^{13}C$ changes in core SK129-CR2 from the central Indian Ocean (Piotrowski et al., 2009) are similar to those observed at deep water sites MD02-2594 and GeoB3603-2 at the South African margin. The three sites consistently display the most positive LGM $\delta^{13}C$ values of the compiled southern sites suggesting an influence of air-sea gas exchange on ambient deep waters that did not reach the deeper sites in the South Atlantic. Altogether, both proxies, $\delta^{13}C$ and ε_{Nd}, show synchronous variations over the last 24 kyrs consistent with northward penetration of SCW and shift in deep water circulation patterns.

Further insights into water mass patterns can be derived from plotting the paired ε_{Nd} and benthic $\delta^{13}C$ data and using a simple binary mixing model to estimate the proportions of the endmember water masses (see Table 2.3) contributing during the Holocene and LGM (Fig. 2.6). Modern seawater Nd isotopic compositions and concentrations were used for the Holocene compositions of NADW (ε_{Nd} = -13.5; [Nd] = 21 pmol/kg) (Piepgras and Wasserburg, 1987; Jeandel, 1993) and PAC (ε_{Nd} = -4, [Nd] = 40 pmol/kg) (Piepgras and Jacobsen, 1988), with corresponding benthic $\delta^{13}C$ of 1.1‰ and 0‰ (Charles and Fairbanks, 1992; Matsumoto and Lynch-Stieglitz, 1999; Matsumoto et al., 2002), respectively. For the LGM, glacial benthic $\delta^{13}C$ of 0.6‰ and -0.5‰ for NCW and PAC (Charles and Fairbanks, 1992; Matsumoto and Lynch-Stieglitz, 1999; Matsumoto et al., 2002), respectively, were considered, while Nd isotopic compositions and concentrations were assumed to be identical to those of the Holocene.

Table 2.3 Water mass end-member compositions for the Holocene and LGM mixing calculation.

period	water mass	curve color	ε_{Nd}	[Nd] (pmol/kg)	dissolved CO_2 (μmol/kg)	$\delta^{13}C$
Holocene	NADW	blue	-13.5 (Piepgras and Wasserburg, 1987)	21 (Jeandel, 1993)	2175 (Kroopnick, 1985)	1.1 (Ninnemann and Charles, 2002; Hodell et al., 2003)
	PAC	blue	-4 (Piepgras and Jacobsen, 1988)	40 (Piepgras and Jacobsen, 1988)	2350 (Kroopnick, 1985)	0 (Matsumoto and Lynch-Stieglitz, 1999; Matsumoto et al., 2002)
LGM	NADW	grey	-13.5 (Piepgras and Wasserburg, 1987)	21 (Jeandel, 1993)	2175 (Kroopnick, 1985)	0.6 (Matsumoto and Lynch-Stieglitz, 1999)
	PAC	grey	-4 (Piepgras and Jacobsen, 1988)	40 (Piepgras and Jacobsen, 1988)	2350 (Kroopnick, 1985)	-0.5 (Matsumoto and Lynch-Stieglitz, 1999; Matsumoto et al., 2002)
LGM	NADW	orange	-10 (Burton and Vance, 2000; Gutjahr et al., 2008)	21 (Jeandel, 1993)	2175 (Kroopnick, 1985)	0.6 (Matsumoto and Lynch-Stieglitz, 1999)
	PAC	orange	-4 (Piepgras and Jacobsen, 1988)	40 (Piepgras and Jacobsen, 1988)	2350 (Kroopnick, 1985)	-0.5 (Matsumoto and Lynch-Stieglitz, 1999; Matsumoto et al., 2002)

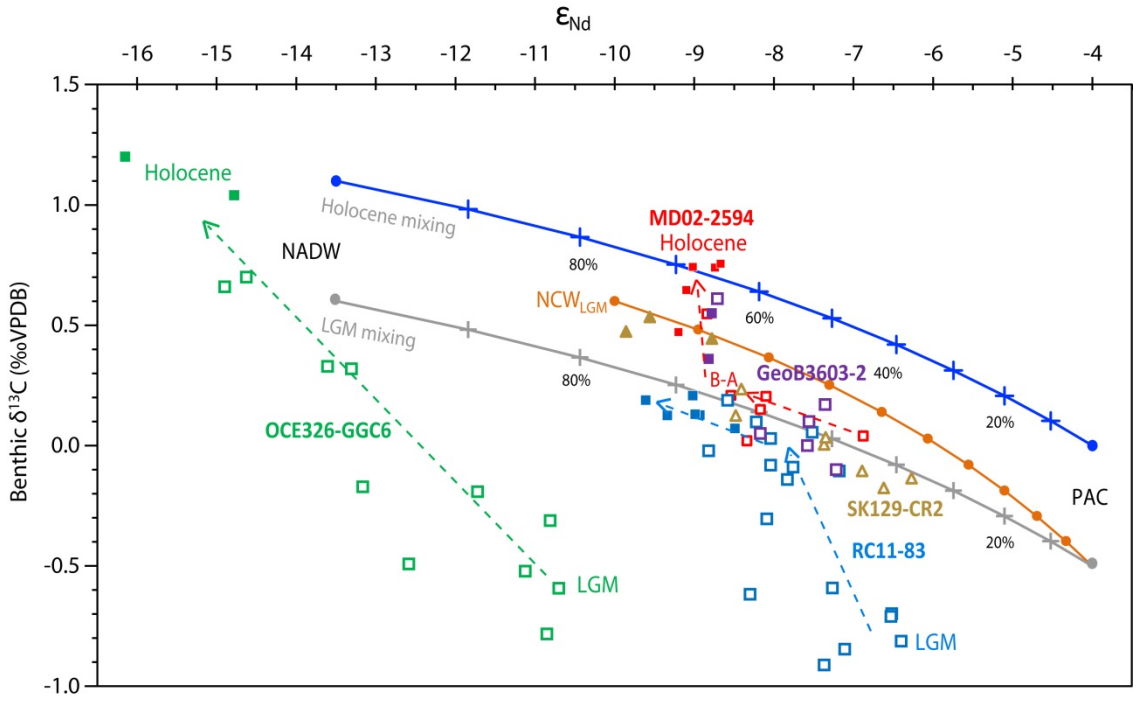

Fig. 2.6 Water mass mixing inferred from the combined ε_{Nd} and benthic foraminiferal $\delta^{13}C$ data for the LGM to Holocene. The data for Indian Ocean (SK129-CR2), South (RC11-83) and North Atlantic (OCE326-GGC6) cores are shown for comparison. Note that ε_{Nd} values refer to the Fe-Mn leachates data, except for core OCE326-GGC6 for which the uncleaned foraminifera data are used. Data sources are listed in Table 2.4 in Supplementary material.

Figure 2.6 shows that the Holocene data of both cores MD02-2594 and GeoB3603-2 cluster along the modern mixing line (blue), while MIS2 data straddle along the LGM mixing line (grey) at lower $\delta^{13}C$ and higher ε_{Nd} values. This transition pattern can be explained by a 20% lesser contribution of NCW during the LGM at the sites of MD02-2594 and GeoB3603-2, in agreement with other estimates (Rutberg et al., 2000; Piotrowski et al., 2005). A similar development of benthic $\delta^{13}C$ and ε_{Nd} is recorded at site SK129-CR2 suggesting the same percentage change of NADW also affected the Indian Ocean. Short-term, millennial-scale variations in a North Atlantic record indicate that glacial NCW might have been more radiogenic, with ε_{Nd} of about -10 as a result of decreased contribution of Labrador Seawater (Gutjahr et al., 2008). Such a scenario (orange line in Fig. 2.6), however, does not appear to be consistent with the LGM to Holocene Nd isotopic shift seen in our records, which imply little changes in the Nd isotopic compositions of the water mass endmember sources during the LGM.

The relationship between ε_{Nd} and benthic $\delta^{13}C$ at upper deep water (MD02-2594) and bottom water depths (RC11-83) in the South Atlantic exhibits a two-stage change from the LGM into the Holocene (Fig. 2.6). For core MD02-2594 at 2,440 m, the LGM to Bølling-Allerød (B-A) ε_{Nd} change is large (1.9 ε_{Nd}-units) with only a minor $\delta^{13}C$ change, while in the second step, ε_{Nd} undergoes only small changes with a large $\delta^{13}C$ increase. The implication is that the first step constitutes a major increase of NCW endmember contribution, consistent with substantial strengthening of NADW formation during the B-A warm period (Sarnthein et al., 1994; Sarnthein et al., 1995), with only a minor change in deep water ventilation. The second step, from the B-A into the Holocene, then constitutes a major increase in deep water ventilation with a modest further increase in NADW endmember contribution. In contrast, the largest $\delta^{13}C$ change at bottom water site RC11-83 at 4,718 m is recorded during the first step from the LGM to the B-A, while the coeval ε_{Nd} change is slightly larger than in MD02-2594, and the second step into the Holocene displays a smaller $\delta^{13}C$ increase but larger ε_{Nd} change

than in MD02-2594. The offset pattern between the two core sites suggests that changes of physical water mass mixing and deep ocean carbon storage were decoupled during the last glacial-interglacial transition, plausibly in conjunction with changing sea ice extension, ocean stratification and physical overturning strength (Piotrowski et al., 2005; Adkins, 2013).

In summary, the glacial feature of more radiogenic ε_{Nd} and low $\delta^{13}C$, consistently seen in records from the North and South Atlantic and the Indian Ocean, indicates that both proxies record shifted deep and bottom water circulation ventilation, with a predominance of SCW during the LGM and reduced contribution from northern water sources.

2.4.3 Implications of sedimentary ε_{Nd}, $^{231}Pa/^{230}Th$ and benthic $\delta^{13}C$ for past AMOC states

To place the interpretation of our ε_{Nd} data into a framework of AMOC changes, we use $^{231}Pa/^{230}Th$ data from core sites in the North (OCE326-GGC6, McManus et al., 2004; ODP1063, Böhm et al., 2015) and South Atlantic (MD02-2594, Negre et al., 2010; GeoB3808-6, Jonkers et al., 2015) as a proxy for deep water flow rate (Fig. 2.7). While nutrient-based proxies and modeling results suggest a reduced ventilation of the deep North Atlantic during the LGM, $^{231}Pa/^{230}Th$ ratios indicate little changes in the AMOC strength (Lippold et al., 2012). On the basis of the sedimentary basin-scale north to south gradient in $^{231}Pa/^{230}Th$, Negre et al. (2010) proposed that the deep water flow was reversed with northward flowing SCW invading the Atlantic basin during the LGM, prior the establishment during the Holocene of the modern circulation pattern with a mainly southward flowing NADW. Although recent seawater data have raised some concern about the applicability of $^{231}Pa/^{230}Th$ ratios as a tracer of changes in deep water turnover rates (Deng et al., 2014), we examine the systematics of three independent proxies, $\delta^{13}C$, ε_{Nd} and $^{231}Pa/^{230}Th$ ratios, to draw some implications on the AMOC pattern during the last 24 kyrs.

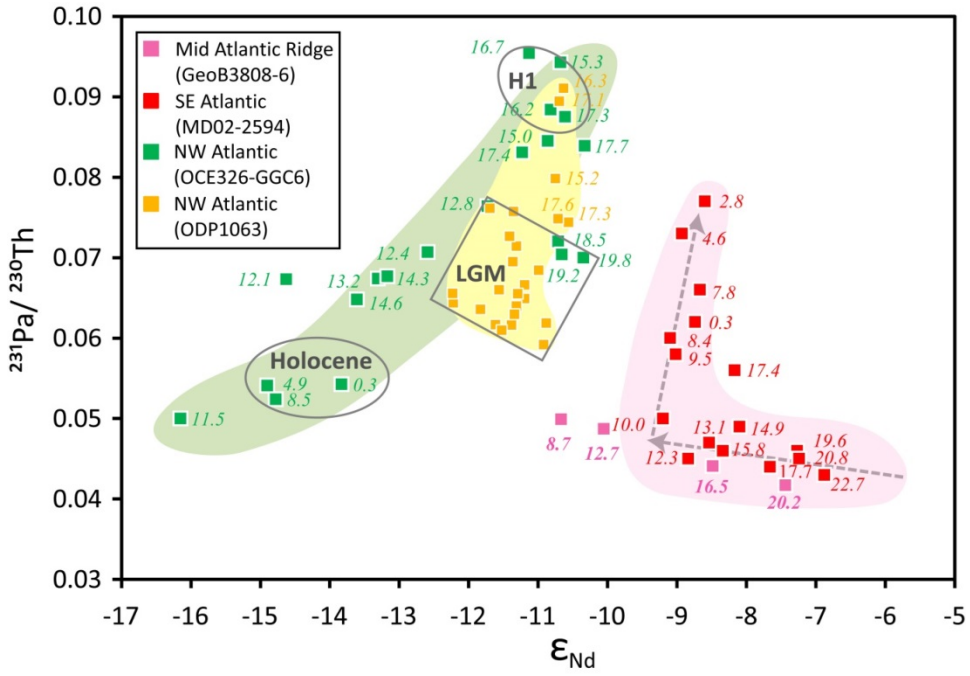

Fig. 2.7 Co-variations of ε_{Nd} and $^{231}Pa/^{230}Th$ relations in the South and North Atlantic core sites. Note that ε_{Nd} values refer to the Fe-Mn leachates data, except for core OCE326-GGC6 for which the uncleaned foraminifera data are used. Values in italic refer to the ages. Data sources are listed in Table 2.4 in Supplementary material.

The ε_{Nd} and $^{231}Pa/^{230}Th$ patterns show contrasted behavior in the North versus South Atlantic cores (Fig. 2.7). In the South African margin core MD02-2594, systematic and time-dependent changes in ε_{Nd} and $^{231}Pa/^{230}Th$ are observed during the LGM and Holocene, with a noticeable change in the slope of the relationship occurring at the climate transition between the LGM and the Holocene. While the LGM association of more radiogenic ε_{Nd} and low $^{231}Pa/^{230}Th$ is consistent with a glacial predominance of SCW in the South Atlantic and export of ^{231}Pa, the increase in $^{231}Pa/^{230}Th$ ratios at nearly constant ε_{Nd} suggests a decoupling between the two systems during the Holocene. A similar development is not seen at mid-Atlantic Ridge core GeoB3808-6, suggesting either that full-interglacial $^{231}Pa/^{230}Th$ values were not obtained in this core due to an incomplete recovery of Holocene sediments; or that some ^{231}Pa is missing from the deep South Atlantic due to boundary scavenging or ^{231}Pa loss to the Southern Ocean (Jonkers et al., 2015). By comparison, the two bottom water sites in the North Atlantic (OCE326-GGC6, ODP1063) display a nearly linear $^{231}Pa/^{230}Th$-ε_{Nd}

relationship from the LGM into the Holocene, which is only interrupted by maximum $^{231}Pa/^{230}Th$ and ε_{Nd} values during H1. This indicates a synchronous and gradual change of the physical circulation and endmember contribution in the deepest North Atlantic that is also expressed in the nearly linear ε_{Nd}: $\delta^{13}C$ development at this location, expressing a gradual increase in chemical ventilation at the same time (Fig. 2.6).

The two-step transition in $^{231}Pa/^{230}Th$ *vs.* ε_{Nd} in core MD02-2594 (Fig. 2.7) is very similar to that observed between benthic $\delta^{13}C$ and ε_{Nd} in the same core (Fig. 2.6). Initially, a small increase of $^{231}Pa/^{230}Th$ ratios (~0.01) associated with a slight increase of benthic $\delta^{13}C$ (less than 0.2‰) from the LGM to the B-A, that remains however below the whole-ocean carbon isotope shift, is paralleled by a significant shift of ε_{Nd} (1.5 ε_{Nd}-units) to less radiogenic values. This is followed by a larger increase of $^{231}Pa/^{230}Th$ ratios (by ~0.03) but a small increase of benthic $\delta^{13}C$ values (by ~0.3‰) which remains within the global carbon isotope shift and is accompanied by a comparatively small change in ε_{Nd} (0.3 ε_{Nd}-units) from the B-A into the Holocene. In the North Atlantic, the profiles of core OCE326-GGC6 show a continuous decrease of $^{231}Pa/^{230}Th$ ratios from the LGM to the beginning of the Holocene that is associated with a ca. 4 ε_{Nd}-units decrease to less radiogenic values. During the Holocene, the $^{231}Pa/^{230}Th$ remains constant and is coupled to a shift by one ε_{Nd}-unit towards the present-day value of -13.5.

To visualize the direction and magnitude of the changes in the North versus the South Atlantic, a cross-plot between the mean values of benthic $\delta^{13}C$ and $^{231}Pa/^{230}Th$ with the average ε_{Nd} indicated for each time slice is shown in Figure 2.8. The progressive glacial-interglacial transition to higher values of benthic $\delta^{13}C$ and $^{231}Pa/^{230}Th$ in core MD02-2594, is also recorded in the lower resolution core GeoB3808-6 near the mid-Atlantic Ridge (Jonkers et al., 2015). In the North Atlantic, the $\delta^{13}C$ and $^{231}Pa/^{230}Th$ changes are anti-correlated, with a clear disruption by iceberg discharges during H1 when the AMOC was substantially weakened below the moderate overturning during the LGM and Younger Dryas (YD)

(McManus et al., 2004). These features of relative high-nutrient/low $\delta^{13}C$ waters (SCW) during the LGM and low-nutrient/high $\delta^{13}C$ waters (NCW) during the Holocene are consistent with the general decreasing trend of mean ε_{Nd} in each core site.

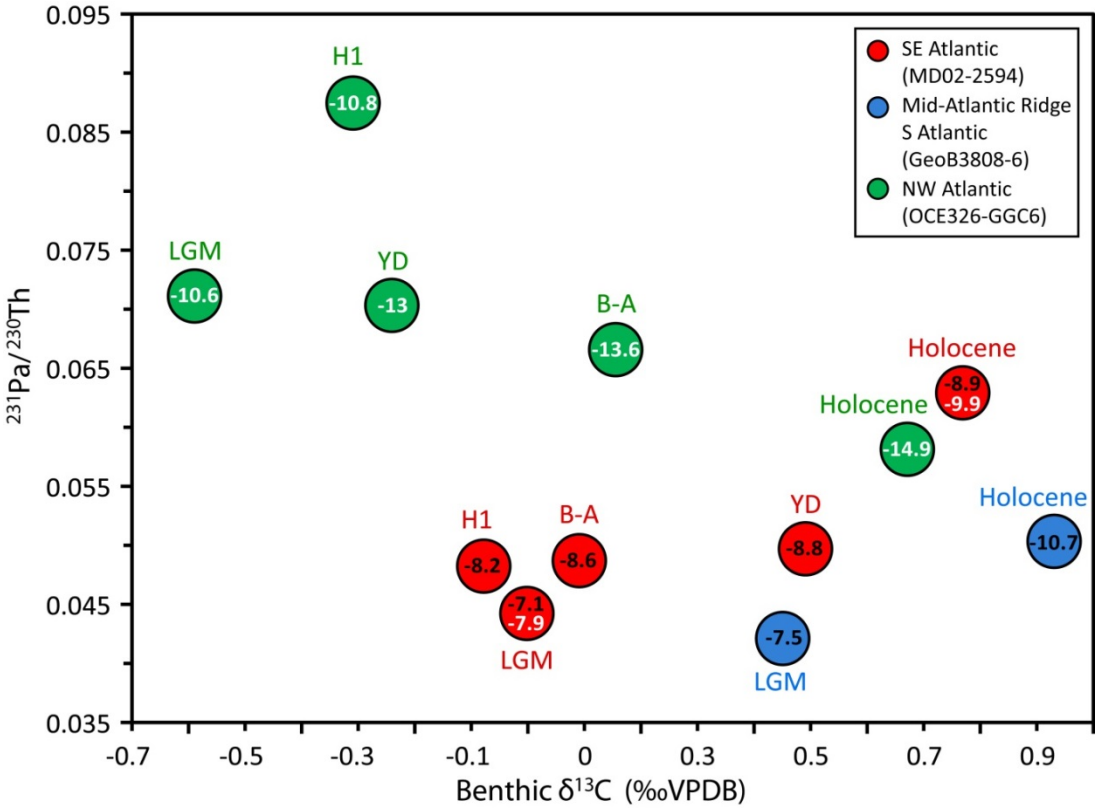

Fig. 2.8 Relationships between benthic foraminiferal $\delta^{13}C$ and sedimentary $^{231}Pa/^{230}Th$ ratios at South and North Atlantic core sites. Circles correspond to the average $^{231}Pa/^{230}Th$ and $\delta^{13}C$ values for each period, with the mean ε_{Nd} value for the authigenic fractions (white: uncleaned planktonic foraminifera; black: Fe-Mn leachates). Data sources are listed in Table 2.4 in Supplementary material.

The fact that changes in three independent proxies occur simultaneously at these two locations suggests that these are largely controlled by the basin-scale abyssal circulation of the Atlantic Ocean. The evidence for a synchronous decrease in ε_{Nd} of similar magnitude in both the North and South Atlantic records is consistent with a progressively increasing influence of NCW flowing southward and concomitant decrease of northward inflow of SCW from the LGM to the beginning of the Holocene. This contrasts with the small increases of $^{231}Pa/^{230}Th$ and benthic $\delta^{13}C$ which reveal a moderately reinvigorated, but not yet fully recovered AMOC compared to the present configuration. The subsequent large increases of $^{231}Pa/^{230}Th$ ratios

and benthic $\delta^{13}C$ would suggest that the AMOC reorganized to full strength during the Holocene, while the subtle ε_{Nd} decrease towards less radiogenic values hints at continuous incorporation into NCW of SCW from the south and an overall relatively stable circulation pattern in the Cape Basin region.

The different patterns of variations of $^{231}Pa/^{230}Th$:ε_{Nd} in the North Atlantic and Cape Basin cores, as well as the different slopes in the same time segments (Fig. 2.7) can thus be interpreted in terms of different overturning and water mass histories at upper mid-depth isopycnals in the South Atlantic (MD02-2594) versus bottom water isopycnals in the North Atlantic (OCE326-GGC6, ODP1063). The North Atlantic $^{231}Pa/^{230}Th$ at >4,000 m water depth shows that the AMOC was significantly weakened and water renewal was much slower with unchanged water mass source through the transition from the LGM to H1. This was followed by a dramatically weakened deep water circulation at H1 due to fresh water perturbation and a subsequent transition to full-strength AMOC with a progressively increased proportion of NCW relative to SCW during the Holocene (McManus et al., 2004; Gherardi et al., 2009; Lippold et al., 2009; Roberts et al., 2010). The Nd isotope evidence for a decreased influence of SCW and increased contribution of NCW in the Cape Basin, along with $^{231}Pa/^{230}Th$ decrease in the North Atlantic but increase in the South Atlantic, suggests continuous 'loss' of ^{231}Pa in the North during the Holocene, reflecting faster deep water flow rates and thus enhanced export of ^{231}Pa to the South Atlantic and Southern Ocean. This is in contrast with the glacial pattern of variation whereby northward penetration of southern waters resulted in greater export of ^{231}Pa from the South leading to the lower glacial $^{231}Pa/^{230}Th$ ratios seen in the South Atlantic records (Negre et al., 2010; Jonkers et al., 2015). Such a scenario does not preclude nor exclude the possibility of minor boundary scavenging near the African margin (Lippold et al., 2012) that may have contributed to the $^{231}Pa/^{230}Th$ increase observed during the Holocene at our site. Nevertheless, the overall agreement between the pattern of variations of three independent proxies – ε_{Nd}, $\delta^{13}C$ and $^{231}Pa/^{230}Th$ – in the Cape Basin records, along

with similar findings in a comparable lower resolution record from the central South Atlantic (Jonkers et al., 2015), provide support for the reversed deep water flow model of Negre et al. (2010) based on the spatial distribution of $^{231}Pa/^{230}Th$ alone in the Atlantic.

2.5 Conclusions

We report two new Nd isotope records from cores MD02-2594 and GeoB3603-2 in the Cape Basin combined with $^{231}Pa/^{230}Th$ and benthic $\delta^{13}C$ records to reconstruct past variation of deep water circulation in the southeast Atlantic during the past 24 kyrs. The Nd isotope records from the Fe-Mn leachates show a decreasing LGM to Holocene trend which is confirmed by Nd isotopes of planktonic foraminifera/fish debris, indicating that the Nd isotopic variations in the Fe-Mn leachates reliably monitor changes in deep water mass sources and mixing. Systematic and synchronous changes in ε_{Nd} and published $^{231}Pa/^{230}Th$ and benthic $\delta^{13}C$ at both sites highlight significant shifts in deep water circulation and endmember contributions during the last glacial-interglacial transition. Some of these changes appear to have also propagated into the Indian Ocean. The overall pattern of variations of these proxies is consistent with a northward invasion of SCW during the LGM and weakened influence of NCW at abyssal depths in the Atlantic basin, albeit with little changes in the Nd isotopic composition of southern and northern water sources.

Our results, along with a compilation of other published Atlantic sedimentary records, further reveal the existence of a depth gradient and a latitudinal control on Nd isotopes reflected by increasingly unradiogenic ε_{Nd} northwards in the South Atlantic. The combined Nd isotopes, $^{231}Pa/^{230}Th$ ratios and benthic $\delta^{13}C$ globally sustain continuous export of deep water with a glacial shallow overturning in the north, and stronger convection in the south with increased northward flow of SCW.

The nearly constant signature found in several South Atlantic records during the Holocene indicates an overall remarkable stability of the deep water circulation pattern and the establishment of a reinvigorated AMOC to full strength.

Acknowledgments

We thank I. Hall for providing aliquots of MD02-2594 sieved fractions, T. Bickert for sampling core GeoB3603-2 from the GeoB Core Repository at MARUM – Center for Marine Environmental Sciences, University of Bremen, and H. Feldman for his help in the lab. R.W was funded by the China Scholarschip Council. WA acknowledges support from the DFG through the Leibniz Prize Award to Klaus Mezger, and from the UnivEarths Labex program at Sorbonne Paris Cité (ANR-10-LABX-0023 and ANR-11-IDEX-0005-02). PM was supported in part by a Gledden Visiting Fellowship awarded by the Institute of Advanced Studies at The University of Western Australia. RZ and PM acknowledge the support of the Generalitat de Catalunya through MERS (2014 SGR 1356) and the Ministerio de Economía y Competitividad through grant CTM2012-38889. This is IPGP contribution 3696.

Supplementary Material

S1. Detailed methodology

The bulk and fine fraction samples were weighed on clean aluminium foil with a microbalance to ±0.01 mg. The bulk sediment (~50 mg) was leached to remove sequentially the Fe-Mn oxide component using procedures described in previous studies (Chester and Hughes, 1967; Rutberg et al., 2000; Bayon et al., 2002). The calcium carbonate fraction was first removed using a sodium acetate buffered acetic-acid solution (pH=5) by shaking for 2 hours. The leaching step was repeated to assure that the samples were carbonate-free. Following several rinses with ultrapure MilliQ water, the Fe-Mn oxide component was subsequently isolated by leaching the remaining sediment with 0.02 M hydroxylamine hydrochloride in 25% glacial acetic acid by shaking for 4 hours. The supernatant was dried down and converted to a chloride salt. The residual material, left after removal of the carbonate and Fe-Mn oxide, corresponds to the detrital component and was dissolved using a mixture of hot concentrated HNO_3 and HF.

Mixed planktonic foraminifera were hand-picked from the sieved-fraction (>70 μm) of four samples (2 LGM and 2 Holocene) in MD02-2594. The samples were weighed-in (1.5 to 4mg) and then gently crushed between two glass plates. Following on, the samples were sonicated several times in methanol and then, repeatedly in MilliQ water to remove any fine particles. After a final rinse in MilliQ water, samples were screened under the microscope for remaining fines, in which case the last step was repeated until the sample was considered particles-free. Following on, the samples were left to dissolve in hot 2 N HNO_3.

Fossil fish debris (bones and teeth) found in core GeoB3603-2 were hand-picked on the >70 μm sieved fraction and cleaned following the same procedure described above for the foraminifera, with an additional mild leach in dilute HNO_3. The particle-free samples were dissolved in hot 2N HNO_3.

The samples were processed through ion exchange columns following standard procedures to separate Sr and Nd. Samples were re-dissolved in 6 N of HCl and loaded onto glass columns containing a cation-exchange resin (Biorad AG50W-X8, 200-400 mesh) to separate Sr and the Rare Earth Element fraction from the other elements. Nd was separated from the other REE on a secondary cation-exchange column (AG50W-X2, 200-400 mesh) using 0.15M alpha-hydroxy isobutyric acid (α-HIBA) solution buffered at pH = 4.5. Both duplicate analyses and full leaching procedures replicates were performed on a few samples and the data reported in Table 2.3.

S2. Bulk sediment and fine fraction leachates isotopic compositions

The ε_{Nd} values (Fig. 2.2a) of the bulk sediment are clearly distinct from those of the Fe-Mn leachates and detrital fractions, demonstrating that the "seawater" and "terrigenous" isotope signals have been successfully and efficiently separated during leaching.

The temporal Nd isotopic variation in the bulk sediments generally mirrors that of the Fe-Mn leachates with more radiogenic ε_{Nd} found during cold periods and less radiogenic values similar to those of the detrital fraction during the Holocene. These differences could reflect variable proportions of the detrital and authigenic fractions contributing to the bulk sediment Nd isotopic composition and/or a change in sources of water and particles to the Cape Basin during the last 24 kyrs.

The leachates on the fine sieved (<63 μm) fraction of the sediment exhibit Nd isotopic compositions in agreement with those of the bulk sediment leachates with a similar pattern of variations throughout the 24 kyrs record. This result demonstrates that the leaching procedure yields reproducible results and that grain-size does not affect the Nd isotopic compositions of the Fe-Mn leachates.

Table 2.4 Location of sediment cores and data sources discussed in this paper.

Core	SU90-44	ODP1063	OCE326-GGC6	OCE326-GGC5	EN120-GGC1
Color	light blue	orange	green	green	green
Latitude	50°01'N	33°41'N	33°42'N	33°42'N	33°40'N
Longitude	17°06'W	57°37'W	57°35'W	57°35'W	57°37'W
Depth	4279 m	4584 m	4541 m	4550 m	4450 m
Bulk sediment leachate ε_{Nd}		(Böhm et al., 2015)			
Uncleaned foraminifera ε_{Nd}			(Roberts et al., 2010)		
$^{231}Pa/^{230}Th$	(Gherardi et al., 2009)	(Böhm et al., 2015)		(McManus et al., 2004)	
Benthic foraminiferal $\delta^{13}C$					(Boyle and Keigwin, 1987)

Core	12JPC	SK129-CR2	GeoB3808-6	MD02-2594	GeoB3603-2
Color	dark green	olive	pink	red	purple
Latitude	29°05'N	3°N	30°48'S	34°43'S	35°08'S
Longitude	72°54'W	76°E	14°42'W	17°20'E	17°33'E
Depth	4250 m	3800 m	3213 m	2440 m	2840 m
Bulk sediment leachate ε_{Nd}	(Gutjahr et al., 2008)	(Piotrowski et al., 2009)	(Jonkers et al., 2015)	this study	this study
Uncleaned foraminifera ε_{Nd}				this study	
Fish debri ε_{Nd}					this study
$^{231}Pa/^{230}Th$		(Piotrowski et al., 2009)	(Jonkers et al., 2015)	(Negre et al., 2010)	
Benthic foraminiferal $\delta^{13}C$	12JPC	SK129-CR2	(Jonkers et al., 2015)	(Negre et al., 2010)	(Caley et al., 2014)

Core	RC11-83	TNO57-21	TNO57-6	MD07-3076
Color	blue	grey	brown	black
Latitude	42°04'S	41°08'S	42°55'S	44°09'S
Longitude	10°43'E	7°49'E	8°53'E	14°14'W
Depth	4718 m	4981 m	3750 m	3770 m
Bulk sediment leachate ε_{Nd}	(Rutberg et al., 2000; Piotrowski et al., 2004, 2005)	(Piotrowski et al., 2005)	(Piotrowski et al., 2004)	
Uncleaned foraminifera ε_{Nd}				
Fish debri ε_{Nd}				(Skinner et al., 2013)
$^{231}Pa/^{230}Th$				
Benthic foraminiferal $\delta^{13}C$	(Charles et al., 1996)			(Waelbroeck et al., 2011)

References

Abouchami, et al. (1997), Secular changes of lead and neodymium in central Pacific seawater recorded by a Fe-Mn crust, *Geochimica et Cosmochimica Acta*, *61*(18), 3957-3974.

Adkins (2013), The role of deep ocean circulation in setting glacial climates, *Paleoceanography*, *28*(3), 539-561.

Asahara, et al. (1999), Provenance of the north Pacific sediments and process of source material transport as derived from Rb–Sr isotopic systematics, *Chemical Geology*, *158*(3–4), 271-291.

Bayon, et al. (2004), Sedimentary Fe–Mn oxyhydroxides as paleoceanographic archives and the role of aeolian flux in regulating oceanic dissolved REE, *Earth and Planetary Science Letters*, *224*(3–4), 477-492.

Bayon, et al. (2002), An improved method for extracting marine sediment fractions and its application to Sr and Nd isotopic analysis, *Chemical Geology*, *187*(3–4), 179-199.

Beal, et al. (2011), On the role of the Agulhas system in ocean circulation and climate, *Nature*, *472*(7344), 429-436.

Bertram, et al. (1995), Cadmium/calcium and carbon isotope reconstructions of the glacial northeast Atlantic Ocean, *Paleoceanography*, *10*(3), 563-578.

Biscaye, and Dasch (1971), The rubidium, strontium, strontium-isotope system in deep-sea sediments: Argentine Basin, *Journal of Geophysical Research*, *76*(21), 5087-5096.

Boyle, and Keigwin (1987), North Atlantic thermohaline circulation during the past 20,000 years linked to high-latitude surface temperature, *Nature*, *330*(6143), 35-40.

Broecker, and Denton (1990), The role of ocean-atmosphere reorganizations in glacial cycles, *Quaternary Science Reviews*, *9*(4), 305-341.

Broecker, and Maier-Reimer (1992), The influence of air and sea exchange on the carbon isotope distribution in the sea, *Global Biogeochemical Cycles*, *6*(3), 315-320.

Burton, and Vance (2000), Glacial–interglacial variations in the neodymium isotope composition of seawater in the Bay of Bengal recorded by planktonic foraminifera, *Earth and Planetary Science Letters*, *176*(3–4), 425-441.

Böhm, et al. (2015), Strong and deep Atlantic meridional overturning circulation during the last glacial cycle, *Nature*, *517*(7532), 73-76.

Caley, et al. (2014), Quantitative estimate of the paleo-Agulhas leakage, *Geophysical Research Letters*, *41*(4), 2014GL059278.

Charles, and Fairbanks (1992), Evidence from Southern Ocean sediments for the effect of North Atlantic deep-water flux on climate, *Nature*, *355*(6359), 416-419.

Charles, et al. (1996), Climate connections between the hemisphere revealed by deep sea sediment core/ice core correlations, *Earth and Planetary Science Letters*, *142*(1–2), 19-27.

Charles, et al. (2010), Millennial scale evolution of the Southern Ocean chemical divide, *Quaternary Science Reviews*, *29*(3–4), 399-409.

Chester, and Hughes (1967), A chemical technique for the separation of ferro-manganese minerals, carbonate minerals and adsorbed trace elements from pelagic sediments, *Chemical Geology*, *2*(0), 249-262.

Curry, and Oppo (2005), Glacial water mass geometry and the distribution of $\delta^{13}C$ of ΣCO_2 in the western Atlantic Ocean, *Paleoceanography*, *20*(1), PA1017.

Curry, et al. (1999), Millennial-scale changes in ventilation of the thermocline, intermediate, and deep waters of the glacial North Atlantic, in *Mechanisms of Global Climate Change at Millennial Time Scales*, pp. 59-76, American Geophysical Union.

Deng, et al. (2014), Controls on seawater ^{231}Pa, ^{230}Th and ^{232}Th concentrations along the flow paths of deep waters in the Southwest Atlantic, *Earth and Planetary Science Letters*, *390*(0), 93-102.

Dickson, and Brown (1994), The production of North Atlantic Deep Water: sources, rates, and pathways, *Journal of Geophysical Research*, *99*(C6), 12319-12341.
Duplessy, et al. (1988), Deepwater source variations during the last climatic cycle and their impact on the global deepwater circulation, *Paleoceanography*, *3*(3), 343-360.
Dyez, et al. (2014), Multicentennial Agulhas leakage variability and links to North Atlantic climate during the past 80,000 years, *Paleoceanography*, *29*(12), 1238-1248.
Elderfield, et al. (1988), The oceanic chemistry of the rare-earth elements, *Philosophical Transactions of the Royal Society of London. Series A, Mathematical and Physical Sciences*, *325*(1583), 105-126.
Elliot, et al. (2002), Changes in North Atlantic deep-water formation associated with the Dansgaard–Oeschger temperature oscillations (60–10 ka), *Quaternary Science Reviews*, *21*(10), 1153-1165.
Elmore, et al. (2011), Testing the extraction of past seawater Nd isotopic composition from North Atlantic deep sea sediments and foraminifera, *Geochemistry, Geophysics, Geosystems*, *12*(9).
Esper, et al. (2004), A palynological reconstruction of the Agulhas Retroflection (South Atlantic Ocean) during the Late Quaternary, *Global and Planetary Change*, *41*(1), 31-62.
Foster, et al. (2007), No change in the neodymium isotope composition of deep water exported from the North Atlantic on glacial-interglacial time scales, *Geology*, *35*(1), 37-40.
Garcia-Solsona, et al. (2014), Rare earth elements and Nd isotopes tracing water mass mixing and particle-seawater interactions in the SE Atlantic, *Geochimica et Cosmochimica Acta*, *125*(0), 351-372.
Gebbie (2014), How much did Glacial North Atlantic Water shoal?, *Paleoceanography*, *29*(3), 190-209.
Gherardi, et al. (2009), Glacial-interglacial circulation changes inferred from $^{231}Pa/^{230}Th$ sedimentary record in the North Atlantic region, *Paleoceanography*, *24*(2), PA2204.
Goldstein, and Hemming (2003), Long-lived isotopic tracers in oceanography, paleoceanography, and ice-sheet dynamics, in *Treatise on Geochemistry*, edited by Turekian, pp. 453-489, Elsevier, Oxford.
Gordon (1986), Interocean exchange of thermocline water, *Journal Geophysical Research*, *91*(C4), 5037-5046.
Gordon, et al. (1992), Thermocline and Intermediate Water communication between the South Atlantic and Indian Oceans, *Journal Geophysical Research*, *97*(C5), 7223-7240.
Gutjahr, et al. (2008), Tracing the Nd isotope evolution of North Atlantic Deep and Intermediate Waters in the western North Atlantic since the Last Glacial Maximum from Blake Ridge sediments, *Earth and Planetary Science Letters*, *266*(1–2), 61-77.
Gutjahr, et al. (2007), Reliable extraction of a deepwater trace metal isotope signal from Fe–Mn oxyhydroxide coatings of marine sediments, *Chemical Geology*, *242*(3–4), 351-370.
Hemming, et al. (1998), Provenance of Heinrich layers in core V28-82, northeastern Atlantic: $^{40}Ar/^{39}Ar$ ages of ice-rafted hornblende, Pb isotopes in feldspar grains, and Nd–Sr–Pb isotopes in the fine sediment fraction, *Earth and Planetary Science Letters*, *164*(1–2), 317-333.
Hesse, et al. (2011), A model-data comparison of $\delta^{13}C$ in the glacial Atlantic Ocean, *Paleoceanography*, *26*(3), PA3220.
Hirschi, et al. (2003), A monitoring design for the Atlantic meridional overturning circulation, *Geophysical Research Letters*, *30*(7), 1413.
Hodell, et al. (1990), Variation in the strontium isotopic composition of seawater (8 Ma to present) : Implications for chemical weathering rates and dissolved fluxes to the oceans, *Chemical Geology: Isotope Geoscience section*, *80*(4), 291-307.
Hodell, et al. (2003), Pleistocene vertical carbon isotope and carbonate gradients in the South Atlantic sector of the Southern Ocean, *Geochemitry, Geophysics, Geosystems*, *4*(1), 1004.

Jeandel (1993), Concentration and isotopic composition of Nd in the South Atlantic Ocean, *Earth and Planetary Science Letters*, *117*(3–4), 581-591.
Jonkers, et al. (2015), Deep circulation changes in the central South Atlantic during the past 145 kyrs reflected in a combined $^{231}Pa/^{230}Th$, neodymium isotope and benthic $\delta^{13}C$ record, *Earth and Planetary Science Letters*, *419*(0), 14-21.
Kasper, et al. (2014), Salinity changes in the Agulhas leakage area recorded by stable hydrogen isotopes of C_{37} alkenones during Termination I and II, *Climate of Past*, *10*(1), 251-260.
Koutsodendris, et al. (2014), Exceptional Agulhas leakage prolonged interglacial warmth during MIS 11c in Europe, *Paleoceanography*, *29*(11), 2014PA002665.
Kuhlbrodt, et al. (2007), On the driving processes of the Atlantic meridional overturning circulation, *Reviews of Geophysics*, *45*(2), RG2001.
Lacan, and Jeandel (2005), Neodymium isotopes as a new tool for quantifying exchange fluxes at the continent–ocean interface, *Earth and Planetary Science Letters*, *232*(3–4), 245-257.
Lippold, et al. (2009), Does sedimentary $^{231}Pa/^{230}Th$ from the Bermuda Rise monitor past Atlantic meridional overturning circulation?, *Geophysical Research Letters*, *36*(12), L12601.
Lippold, et al. (2012), Boundary scavenging at the East Atlantic margin does not negate use of $^{231}Pa/^{230}Th$ to trace Atlantic overturning, *Earth and Planetary Science Letters*, *333–334*(0), 317-331.
Lund, et al. (2011), Abyssal Atlantic circulation during the Last Glacial Maximum: Constraining the ratio between transport and vertical mixing, *Paleoceanography*, *26*(1).
Lynch-Stieglitz, et al. (2007), Atlantic meridional overturning circulation during the Last Glacial Maximum, *Science*, *316*(5821), 66-69.
Mackensen, and Licari (2004), Carbon isotopes of live benthic foraminifera from the South Atlantic: sensitivity to bottom water carbonate saturation state and organic matter rain rates, in *The South Atlantic in the Late Quaternary*, edited by Wefer, Mulitza and Ratmeyer, pp. 623-644, Springer Berlin Heidelberg.
Mackensen, et al. (1993), The $\delta^{13}C$ in benthic foraminiferal tests of Fontbotia wuellerstorfi (Schwager) Relative to the $\delta^{13}C$ of dissolved inorganic carbon in Southern Ocean Deep Water: Implications for glacial ocean circulation models, *Paleoceanography*, *8*(5), 587-610.
Marchitto, and Broecker (2006), Deep water mass geometry in the glacial Atlantic Ocean: a review of constraints from the paleonutrient proxy Cd/Ca, *Geochemistry Geophysics Geosystems*, *7*(12).
Martin, and Scher (2004), Preservation of seawater Sr and Nd isotopes in fossil fish teeth: bad news and good news, *Earth and Planetary Science Letters*, *220*(1–2), 25-39.
Martínez-Méndez, et al. (2009), Variable water column structure of the South Atlantic on glacial–interglacial time scales, *Quaternary Science Reviews*, *28*(27–28), 3379-3387.
Martínez-Méndez, et al. (2008), 345,000-year-long multi-proxy records off South Africa document variable contributions of Northern versus Southern Component Water to the deep South Atlantic, *Earth and Planetary Science Letters*, *267*(1–2), 309-321.
Martínez-Méndez, et al. (2010), Contrasting multiproxy reconstructions of surface ocean hydrography in the Agulhas Corridor and implications for the Agulhas Leakage during the last 345,000 years, *Paleoceanography*, *25*(4), PA4227.
Matsumoto, and Lynch-Stieglitz (1999), Similar Glacial and Holocene deep water circulation inferred from Southeast Pacific benthic foraminiferal carbon isotope composition, *Paleoceanography*, *14*(2), 149-163.
Matsumoto, et al. (2002), Interior hydrography and circulation of the glacial Pacific Ocean, *Quaternary Science Reviews*, *21*(14–15), 1693-1704.

McManus, et al. (2004), Collapse and rapid resumption of Atlantic meridional circulation linked to deglacial climate changes, *Nature*, *428*(6985), 834-837.
Mejía, et al. (2014), Effects of midlatitude westerlies on the paleoproductivity at the Agulhas Bank slope during the penultimate glacial cycle: Evidence from coccolith Sr/Ca ratios, *Paleoceanography*, *29*(7), 2013PA002589.
Munk, and Wunsch (1998), Abyssal recipes II: energetics of tidal and wind mixing, *Deep Sea Research Part I: Oceanographic Research Papers*, *45*(12), 1977-2010.
Nakai, et al. (1993), Provenance of dust in the Pacific Ocean, *Earth and Planetary Science Letters*, *119*(1–2), 143-157.
Negre, et al. (2010), Reversed flow of Atlantic deep water during the Last Glacial Maximum, *Nature*, *468*(7320), 84-88.
Ninnemann, and Charles (2002), Changes in the mode of Southern Ocean circulation over the last glacial cycle revealed by foraminiferal stable isotopic variability, *Earth and Planetary Science Letters*, *201*(2), 383-396.
Oppo, and Fairbanks (1987), Variability in the deep and intermediate water circulation of the Atlantic Ocean during the past 25,000 years: Northern Hemisphere modulation of the Southern Ocean, *Earth and Planetary Science Letters*, *86*(1), 1-15.
Oppo, and Rosenthal (1994), Cd/Ca changes in a Deep Cape Basin Core over the past 730,000 years: Response of circumpolar deepwater variability to northern hemisphere ice sheet melting?, *Paleoceanography*, *9*(5), 661-675.
Oppo, and Horowitz (2000), Glacial deep water geometry: South Atlantic benthic foraminiferal Cd/Ca and $\delta^{13}C$ evidence, *Paleoceanography*, *15*(2), 147-160.
Oppo, and Curry (2012), Deep Atlantic circulation during the Last Glacial Maximum and deglaciation, *Nature Education Knowledge*, *3*(10), 1.
Osborne, et al. (2014), The seawater neodymium and lead isotope record of the final stages of Central American Seaway closure, *Paleoceanography*, *29*(7), 715-729.
Palmer, and Elderfield (1985), Sr isotope composition of sea water over the past 75 Myr, *Nature*, *314*(6011), 526-528.
Peeters, et al. (2004), Vigorous exchange between the Indian and Atlantic oceans at the end of the past five glacial periods, *Nature*, *430*(7000), 661-665.
Piepgras, and Wasserburg (1980), Neodymium isotopic variations in seawater, *Earth and Planetary Science Letters*, *50*(1), 128-138.
Piepgras, and Wasserburg (1987), Rare earth element transport in the western North Atlantic inferred from Nd isotopic observations, *Geochimica et Cosmochimica Acta*, *51*(5), 1257-1271.
Piepgras, and Jacobsen (1988), The isotopic composition of neodymium in the North Pacific, *Geochimica et Cosmochimica Acta*, *52*(6), 1373-1381.
Piepgras, et al. (1979), The isotopic composition of Nd in different ocean masses, *Earth and Planetary Science Letters*, *45*(2), 223-236.
Piotrowski, et al. (2004), Intensification and variability of ocean thermohaline circulation through the last deglaciation, *Earth and Planetary Science Letters*, *225*(1–2), 205-220.
Piotrowski, et al. (2005), Temporal relationships of carbon cycling and ocean circulation at glacial boundaries, *Science*, *307*(5717), 1933-1938.
Piotrowski, et al. (2009), Indian Ocean circulation and productivity during the last glacial cycle, *Earth and Planetary Science Letters*, *285*(1–2), 179-189.
Piotrowski, et al. (2012), Reconstructing deglacial North and South Atlantic deep water sourcing using foraminiferal Nd isotopes, *Earth and Planetary Science Letters*, *357–358*(0), 289-297.
Rahmstorf (2002), Ocean circulation and climate during the past 120,000 years, *Nature*, *419*(6903), 207-214.

Raymo, et al. (2004), Stability of North Atlantic water masses in face of pronounced climate variability during the Pleistocene, *Paleoceanography*, *19*(2), PA2008.
Revel, et al. (1996), Grain-size and Sr-Nd isotopes as tracer of paleo-bottom current strength, Northeast Atlantic Ocean, *Marine Geology*, *131*(3–4), 233-249.
Roberts, et al. (2010), Synchronous deglacial overturning and water mass source changes, *Science*, *327*(5961), 75-78.
Rutberg, et al. (2000), Reduced North Atlantic Deep Water flux to the glacial Southern Ocean inferred from neodymium isotope ratios, *Nature*, *405*(6789), 935-938.
Sarnthein, et al. (1994), Changes in East Atlantic deepwater circulation over the last 30,000 years: eight time slice reconstructions, *Paleoceanography*, *9*(2), 209-267.
Sarnthein, et al. (1995), Variations in Atlantic surface ocean paleoceanography, 50°-80°N: A time-slice record of the last 30,000 years, *Paleoceanography*, *10*(6), 1063-1094.
Schlitzer (2014), Ocean Data View, http://odv.awi.de.
Scussolini, et al. (2015), Saline Indian Ocean waters invaded the South Atlantic thermocline during glacial termination II, *Geology*.
Siddall, et al. (2008), Towards explaining the Nd paradox using reversible scavenging in an ocean general circulation model, *Earth and Planetary Science Letters*, *274*(3–4), 448-461.
Skinner, et al. (2010), Ventilation of the deep Southern Ocean and deglacial CO_2 rise, *Science*, *328*(5982), 1147-1151.
Skinner, et al. (2013), North Atlantic versus Southern Ocean contributions to a deglacial surge in deep ocean ventilation, *Geology*, *41*(6), 667-670.
Stichel, et al. (2012), The hafnium and neodymium isotope composition of seawater in the Atlantic sector of the Southern Ocean, *Earth and Planetary Science Letters*, *317–318*(0), 282-294.
Tachikawa, et al. (1999), A new approach to the Nd residence time in the ocean: the role of atmospheric inputs, *Earth and Planetary Science Letters*, *170*(4), 433-446.
van de Flierdt, et al. (2006), Temporal stability of the neodymium isotope signature of the Holocene to glacial North Atlantic, *Paleoceanography*, *21*(4), PA4102.
Waelbroeck, et al. (2011), The timing of deglacial circulation changes in the Atlantic, *Paleoceanography*, *26*(3), PA3213.
Walter, et al. (2000), Provenance and transport of terrigenous sediment in the south Atlantic Ocean and their relations to glacial and interglacial cycles: Nd and Sr isotopic evidence, *Geochimica et Cosmochimica Acta*, *64*(22), 3813-3827.
Willamowski, and Zahn (2000), Upper ocean circulation in the glacial North Atlantic from benthic foraminiferal isotope and trace element fingerprinting, *Paleoceanography*, *15*(5), 515-527.
Wilson, et al. (2013), Reactivity of neodymium carriers in deep sea sediments: Implications for boundary exchange and paleoceanography, *Geochimica et Cosmochimica Acta*, *109*, 197-221.
Wilson, et al. (2015), Interhemispheric controls on deep ocean circulation and carbon chemistry during the last two glacial cycles, *Paleoceanography*, *30*(6), 621-641.
Yu, et al. (1996), Similar rates of modern and last-glacial ocean thermohaline circulation inferred from radiochemical data, *Nature*, *379*(6567), 689-694.
Yu, et al. (2008), Seawater carbonate ion-$\delta^{13}C$ systematics and application to glacial–interglacial North Atlantic ocean circulation, *Earth and Planetary Science Letters*, *271*(1–4), 209-220.
Zahn, and Keir (1994), Tracer-nutrient correlations in the upper ocean: observational and box model constraints on the use of benthic foraminiferal $\delta^{13}C$ and Cd/Ca as paleo-proxies for the intermediate-depth ocean, in *Carbon Cycling in the Glacial Ocean: Constraints on the Ocean's Role in Global Change*, edited by Zahn, Pedersen, Kaminski and Labeyrie, pp. 195-221, Springer Berlin Heidelberg.

Chapter 3

Sourcing North African dust inputs into the eastern Equatorial Atlantic and their long-term response to climate using radiogenic isotopes

Ran Wei[1], Stephen J.G. Galer[1], Wafa Abouchami[2], Meinrat O. Andreae[1]

[1]Max Planck Institute for Chemistry, Biogeochemistry and Climate Geochemistry Departments, P.O. Box 3060, 55020 Mainz, Germany

[2]Institut de Physique du Globe de Paris, 1 Rue Jussieu, 75005 Paris, France

Corresponding author: ran.wei@mpic.de

Abstract

Mineral dust deposited in the Northeastern Tropical Atlantic Ocean over time provides an important archive of sources of dust and paleoclimate prevailing in the Sahara and Sahel regions of North Africa. Radiogenic isotopes are arguably the most definitive means of characterizing dust emission sources from this region, but only a single sedimentary record exists of how dust sources evolved through time. Here, we have undertaken a Pb, Nd and Sr isotope study on the detrital fraction of sediment core GeoB2910-1 (4°50'N, 21°03'W, 2,703 m) located on the Sierra Leone Rise (SLR), which consists solely of eolian dust transported westwards from the African continent. Our 180-kyr record improves our understanding of the provenance and mixture of dust from potential source areas (PSA) on the adjacent African continent and transport pathways to the Sierra Leone Rise; variations in the record are driven by climate (aridity/humidity) and the prevailing wind regimes over West Africa. Our study shows that two principle source end-members in the Sahara-Sahel region are contributing to GeoB2910-1 in about equal proportions, and are located in the Bodélé Depression (PSA-5) and Northern Mali/Southern Algeria (PSA-3). Dust is delivered to the SLR mainly during the boreal winter, based upon published models, associated with a southward shift of the intertropical convergence zone (ITCZ); the ITCZ migrates northward during the summer monsoon months and blocks dust transport. The radiogenic isotope compositions do not vary significantly over glacial-interglacial cycles, indicating that emission sources remained relatively stable in this region, despite greatly enhanced dust loading in the atmosphere globally during glacial periods.

Nevertheless, Pb isotopes exhibit a systematic shift to more radiogenic compositions during African Humid Periods (AHP), with a good correlation with North African Humidity Index, while Sr and Nd isotopes appear unaffected. This illustrated that during AHP, changes in vegetation and filling of once dry lake beds - especially Lake Megachad in the Bodélé Depression - influenced at a local, but not regional scale, the location of dust emission sources.

Keywords: Africa dust, Sr-Nd-Pb isotopes, Provenance, African Humid Periods, Sierra Leone Rise

Highlights

- We found a previous unreported interaction between Pb isotope in terrigenous fraction of sediment core and relative North African humidity
- Sierra Leone Rise (SLR) mainly receives dust during the boreal winter over the last 180 kyrs from Mauritania, Northern Mali/Southern Algeria and the Bodélé Depression
- During boreal summer, migrated northward ITCZ blocks dust transport from Africa to the SLR
- More Western Mauritania contribution leads to systematic changes in Pb isotopes during African Humid Periods (AHP)
- Dust provenance changes during AHP reflect increased spread of vegetation and lakes

3.1 Introduction

North Africa is demonstrably the Earth's largest source of mineral dust to the atmosphere (Prospero et al., 2002; Washington et al., 2003). The emission of dust affects the precipitation in southern West Africa (Huang et al., 2009; Touré et al., 2012), causes Atlantic sea surface and subsurface temperature anomalies (Evan et al., 2012), and modulates the formation of cyclones and hurricanes over the Atlantic Ocean (Sun et al., 2008). Dust delivered by wind also provides huge quantities of nutrients to the ocean surface (more than 90% of the ocean's vital iron), controlling patterns of primary productivity and carbon cycling throughout the oceans (Jickells et al., 2005; Conway and John, 2014). Thus, Saharan dust input is especially important in the oligotrophic tropical Atlantic.

Sources of North African dust, have been subdivided into six potential source areas (PSA) - see Fig. 3.1 - which are regions exhibiting pronounced emission of dust (Scheuvens et al., 2013). The Bodélé Depression, located just northeast of Lake Chad, in a dried-up lakebed composed of fine-grained diatomite and is the most active dust emission source in North Africa, designated as PSA-5. Other major source areas in North Africa are: PSA-3, that stretches from Northern Mali to Southern Algeria, PSA-2 in Mauritania near the western coast, sources at the Algerian–Tunisian boundary (PSA-1), plus central Libya (PSA-4) and northern Sudan in the east (PSA-6). These PSA have been identified by studies of satellite imagery from which one can derive the Total Ozone Mapping Spectrometer aerosol absorption index (Prospero et al., 2002; Koren et al., 2006; Ginoux et al., 2012; Ashpole and Washington, 2013).

Local- and long-range dust transport from Africa is governed by the prevailing atmospheric wind circulation over the African continent. The Intertropical Convergence Zone (ITCZ) separates the northern and southern Hadley cells and is the location where the northeastern and southeastern Trade Winds meet (Schneider et al., 2014). In seasonal migrations of the ITCZ, the mean position of the ITCZ shifts towards the differentially

warming hemisphere in response to changes in cross-equatorial temperature gradients; this divides the global air circulation into two mirror images, north and south, of the climate "equator" (Schneider et al., 2014).

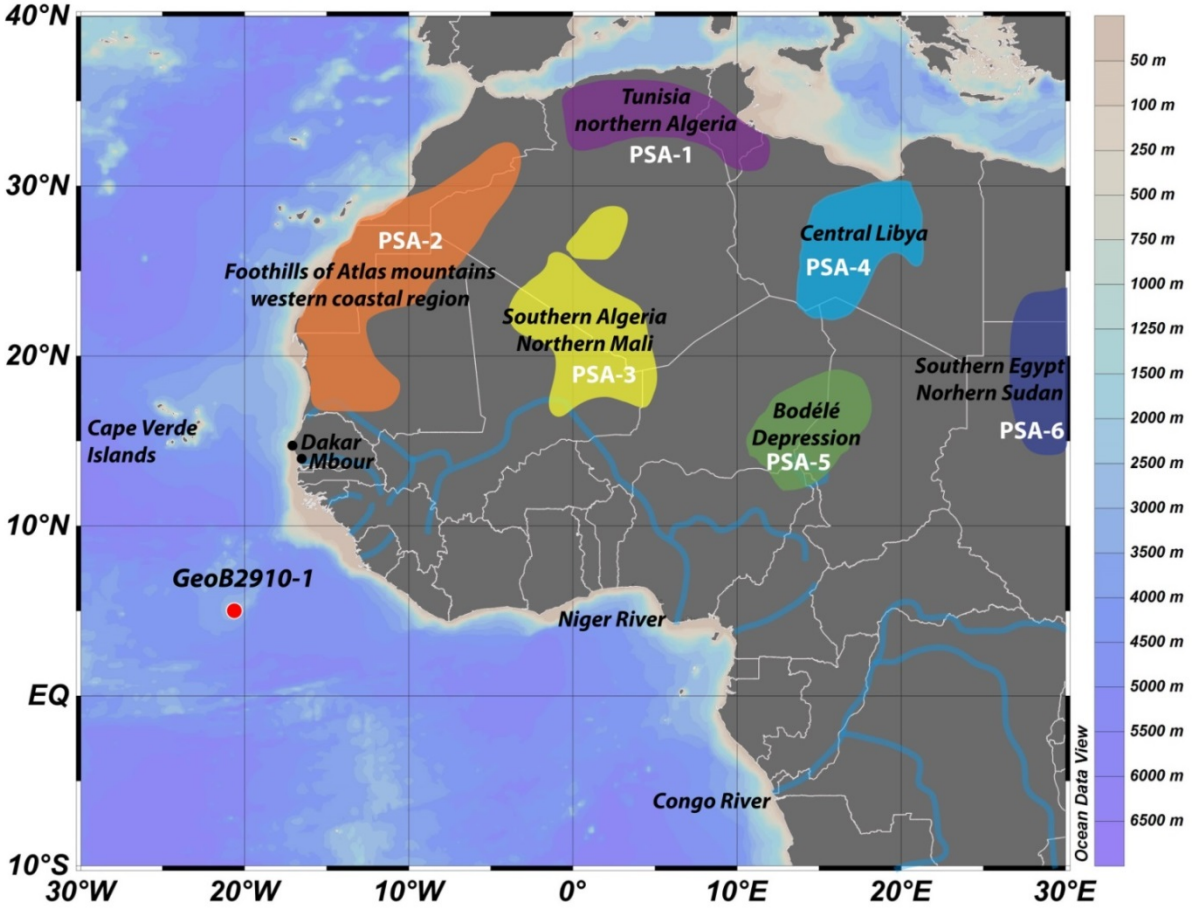

Fig. 3.1 Map of northwest Africa showing the locaiton of core GeoB2910-1. Scheuvens et al. (2013) proposed major potential source areas have been marked in different colors. Figure prepared using Ocean Data View software (Schlitzer, 2014).

An important point to note is that it is the position of the ITCZ that controls deflation and export of dust from Africa to other regions (Bou Karam et al., 2008). The ITCZ is the boundary where the warm and dry SAL (north) is undercut by the denser wet tropical monsoon air masses (south) (Bou Karam et al., 2008; Sunnu et al., 2008). It behaves as a barrier, over which dust plumes can be lofted to high altitude for long-range transport (Bou Karam et al., 2008; Lyngsie et al., 2013). When the ITCZ arrives its most northerly position at ~15 °N to 23°N during boreal summers, the dust plume is mainly derived from the western

and central Sahara at ~5 °N to 10°N. This dust is then lofted into the Saharan Air Layer (SAL) mid-tropospheric levels, in which it is transported westward out of Africa across the Atlantic to the Caribbean (Koren et al., 2006; Tsamalis et al., 2013). During boreal winters, the Harmattan northeast Trade Winds deliver huge amounts of nutrient-rich dust in low-level jets from the Bodélé Depression, some of which ultimately is transported over the Atlantic Ocean as far as South America (Stuut et al., 2005; Tsamalis et al., 2013).

There are two principal gross changes in climate that North Africa has undergone in the Quaternary. First, there are the oscillations, globally, between "cold" and "warm" periods associated with glacial-interglacial cycles. Second, so-called African Humid Periods (AHP) occur irregularly over time.

During AHP, the Saharan desert region changed from arid/hyperarid conditions to a nearly completely vegetated landscape with numerous lakes - for example, the Bodélé Depression was a gigantic lake, named Lake Megachad (Cole et al., 2009; Tierney et al., 2011). These periods are characterized by enhanced rainfall, weakened atmospheric circulation over North Africa, and are in directly result of northern hemisphere insolation maxima with a much-enhanced northward penetrating African monsoon system (Rossignol-Strick et al., 1982; Kutzbach and Liu, 1997; Meyer et al., 2011; deMenocal and Tierney, 2012). Various studies document that the onset of AHP is rapid and that climate can remain stable in either "dry Sahara" or "green Sahara" states. The three main humid phases during last 180 kyr occured at 5-10, 90-100 and 130-140 kyr BP (Zouari et al., 1998; deMenocal et al., 2000b). DeMenocal et al. (2000a) have suggested that African dust emission was nearly 50% less during AHP due to loss of potential sources from extensive vegetation and filling of lakes.

Radiogenic isotope systems are among the most robust tracers of the provenance of terrigenous materials. This is so, since Pb, Nd and Sr isotopic compositions vary considerably on continental surfaces, largely in response to the age of the bedrock, and this is inherited by

the dusts emitted. On the other hand, as discussed in reviews by Formenti et al. (2011) and Scheuvens (2013), bulk composition and minerology are often poor or ambiguous indicators of provenance. The use of radiogenic isotopes to trace dust movement in marine sediments was pioneered by Biscaye et al. (1974).

The purpose of this study is to investigate how dust sources in Northern Africa responded to climate change during glacial-interglacial cycles and AHP. We present down-core Sr, Nd and Pb isotope records on the carbonate-free terrigenous fraction of core GeoB2910-1 (4°50'N, 21°03'W, 2,703 m) situated on the Sierra Leone Rise (SLR) recovered in the eastern equatorial Atlantic, located on the main trajectory of the wintertime Harmattan wind system and the summertime African easterly wind system. Previous studies of this core have determined that the terrigenous fluxes are dominanted by eolian rather than riverine material; similarly, there was an increased Saharan dust contribution during glaciations as a result of changes in African wind patterns and aridity (Zabel et al., 1999; Abouchami and Zabel, 2003; Funk et al., 2004). The combined Pb-Sr-Nd isotope dataset on the terrigenous fraction is arguably the best method for distinguishing the contribution of different PSA. The temporal changes in the isotopic compositions are thus expected to provide valuable insights into variations in the sources of Saharan dust exported to the eastern tropical North Atlantic and not simply dust fluxes.

3.2 Methods

First, the terrigenous, detrital sediment fraction was obtained from portions of the bulk sediment from core GeoB2910-1. All steps were performed under clean room conditions. About 50 mg of bulk sediment was processed using procedures similar to those of previous studies (Chester and Hughes, 1967; Rutberg et al., 2000; Bayon et al., 2002). We removed the calcium carbonate fraction by reacting with an ammonium acetate-acetic acid buffer solution (pH=5) and shaking for 2 hours, and repeating a second time. The carbonate-free residues

were then rinsed several times with ultrapure MilliQ water. Authigenic ferromanganese oxide phases were then removed using 0.02 M hydroxylamine hydrochloride in 25% glacial acetic acid, shaking for 4 hours, followed by decanting and washing with MilliQ water. The remaining material left after these procedures is the terrigeneous detrital component in the marine sedimentary core.

This residue was dissolved completely using a mixture of concentrated HF and HNO_3 acids. Chemical separation of the Pb, Nd and Sr for analysis followed standard methods described previously (Abouchami et al., 2013; Kumar et al., 2014). Total procedural blanks (Sr = 24 pg; Nd = 3 pg; Pb ≤ 30 pg) are negligible compared to the amount of the respective elements processed.

All isotopic measurements were performed by thermal ionization mass spectrometry (ThermoFisher, TRITON) operating in static multi-collection mode. Pb was loaded onto single rhenium filaments along with a colloidal silica gel-H_3PO_4 activator solution. Pb isotopic compositions were corrected for instrumental mass bias using the well-established Pb triple-spike technique (Galer, 1999). Strontium was loaded onto single tungsten filaments along with a TaF_5 activator. Sr isotopic compositions were corrected for instrumental fractionation by normalizing to $^{86}Sr/^{88}Sr = 0.1194$. Samples of Nd were loaded onto single tungsten filaments along with TaF_5 solution, and measured as the NdO^+ ion. Multiple measurements of NIST SRM981 yielded $^{206}Pb/^{204}Pb = 16.9427 \pm 37$, $^{207}Pb/^{204}Pb = 15.4998 \pm 31$ and $^{208}Pb/^{204}Pb = 36.7269 \pm 81$ (2SD, N=39), respectively. Replicate measurements of NIST SRM 987 and 5 ng loads of the La Jolla Nd standard yielded 0.710259 ± 13 (2SD, N = 22) and 0.511842 ± 11 (2SD, N = 18) during the period of analysis. Nd isotopic compositions are expressed as parts per 10^4 deviations from that of bulk Earth CHUR (Jacobsen and Wasserburg, 1980) as follows:

$$\varepsilon_{Nd} = \left(\frac{^{143}Nd/^{144}Nd_{sample}}{^{143}Nd/^{144}Nd_{CHUR}} - 1\right)\times 10^4, \text{ where } {}^{143}Nd/{}^{144}Nd_{CHUR}=0.512638.$$

The age model for core GeoB2910-1 was obtained from adjacent core GIK13519 (5°40'N, 19°51'W, 2862 m) based upon a positive correlation of the two carbonate records; the age model of GIK13519 was obtained from measured $\delta^{18}O$ values by comparison with SPECMAP $\delta^{18}O$ chronology (Zabel et al., 1999).

3.3 Results

Pb, Sr and Nd isotopic compositions of the terrigenous sediment fractions of GeoB2910-1 from the last six Marine Isotope Stages (MIS) - around 180 kyr - are reported in Table 1 and Fig. 3.2. The Pb isotope ratios lie within a narrow range ($^{206}Pb/^{204}Pb$ = 18.87 to 18.96, $^{207}Pb/^{204}Pb$ = 15.71 to 15.72, $^{208}Pb/^{204}Pb$ = 39.15 to 39.24). The data exhibit similar values and show the same trends over time as the Pb isotope dataset obtained previously on bulk sediment samples (Abouchami and Zabel, 2003). Nevertheless, compared to the bulk sediment, the detrital fractions have less radiogenic $^{206}Pb/^{204}Pb$, roughly equal $^{207}Pb/^{204}Pb$ and more radiogenic $^{208}Pb/^{204}Pb$. These small offsets can probably be ascribed to the authigenic phases and carbonate fractions present in the bulk sediment (Fig. 3.2).

Sr and Nd isotopes are anti-correlated and display general similar trends over the past 180 kyr. $^{87}Sr/^{86}Sr$ ratios vary between 0.719 and 0.722, while ε_{Nd} values lie between -11.0 and -12.6, within the range of Nd and Sr isotope data available for North African PSA of dust (Abouchami et al., 2013; Scheuvens et al., 2013). Sr isotopic records exhibit an increasing trend, becoming more radiogenic from the early- to mid-Holocene and during MIS5, while the lowest ratios are observed during MIS2 and MIS4. By contrast, during MIS6, $^{87}Sr/^{86}Sr$ is at a maximum value while ε_{Nd} almost reaches the Holocene value.

Table 3.1 Pb, Sr and Nd isotopic composition of terrigenous fraction on core GeoB2910-1.

Depth in core (m)	Age (cal-kyr BP)	$^{206}Pb/^{204}Pb$ (2σ)	$^{207}Pb/^{204}Pb$ (2σ)	$^{208}Pb/^{204}Pb$ (2σ)	$^{87}Sr/^{86}Sr$ (2σ)	$^{143}Nd/^{144}Nd$ (2σ)	ε_{Nd} (2σ)	Al/Ti*
0.020	3.6	18.9493 (31)	15.7235 (38)	39.2365 (125)	0.721597 (7)	0.511993 (6)	-12.58 ± 0.11	15.22
0.125	8.8	18.9581 (19)	15.7215 (23)	39.2245 (76)	0.720113 (7)	0.512020 (4)	-12.06 ± 0.09	13.41
0.145	9.8	18.9226 (22)	15.7116 (27)	39.1745 (89)	0.719918 (7)	0.512056 (4)	-11.35 ± 0.09	13.05
0.185	14.1	18.9054 (26)	15.7117 (32)	39.1736 (106)	0.720110 (7)	0.512069 (4)	-11.10 ± 0.08	12.86
0.300	30.1	18.8790 (18)	15.7074 (23)	39.1594 (76)	0.718997 (6)	0.512055 (4)	-11.37 ± 0.06	14.00
0.530	50.9	18.8962 (18)	15.7130 (22)	39.1942 (72)	0.719876 (6)	0.512011 (4)	-12.23 ± 0.08	14.13
0.615	60.0	18.8907 (16)	15.7121 (20)	39.1847 (66)	0.719097 (9)	0.512060 (4)	-11.27 ± 0.06	12.90
0.635	63.0	18.8698 (31)	15.7072 (38)	39.1597 (127)	0.719307 (6)	0.512057 (2)	-11.34 ± 0.06	12.60
0.750	74.1	18.8757 (27)	15.7114 (34)	39.1754 (113)	0.721410 (6)	0.511998 (8)	-12.48 ± 0.14	14.08
0.950	85.5	18.8884 (32)	15.7200 (40)	39.2017 (134)	0.720949 (7)	0.512021 (4)	-12.05 ± 0.09	13.61
1.160	101.3	18.9274 (28)	15.7224 (34)	39.2117 (115)	0.720275 (6)	0.512028 (4)	-11.90 ± 0.07	14.64
1.360	119.7	18.8874 (29)	15.7129 (36)	39.1538 (119)	0.719986 (6)	0.512016 (4)	-12.12 ± 0.09	16.73
1.810	150.8	18.8767 (20)	15.7084 (25)	39.1773 (81)	0.720323 (6)	0.512054 (4)	-11.39 ± 0.08	12.72
2.050	166.2	18.8781 (25)	15.7128 (32)	39.1851 (105)	0.721636 (7)	0.512034 (4)	-11.79 ± 0.09	14.80
2.250	178.5	18.8981 (26)	15.7159 (32)	39.1983 (106)	0.721578 (7)	0.512018 (6)	-12.09 ± 0.12	13.38

(*) from Zabel et al. (1999)

The SLR ε_{Nd} isotope record exhibits only minor variability of 1.5 ε_{Nd} unit over the last 180 kyr BP, which implies that there was no general change in the source area of sediments or changes in mixing proportions among North African PSA. The high-resolution reconstructions of dust deposition by Meyer et al. (2011) inferred from ε_{Nd} variability of a meridional transect of deep-sea sediment cores and atmospheric dust samples - recovered offshore of northwest Africa between 15°N and 29°N - do not exhibit any resolvable temporal variations, implying that the provenance of the sediment has remained constant over the entire Holocene. Marine sediment core ODP 658 C offshore of Mauritania shows minor variability of < 0.9 ε_{Nd} unit throughout the last glacial-interglacial cycle, also indicating that the contributing geological terranes have not changed appreciably (Cole et al., 2009), to the extent that this is resolvable using Nd isotopes.

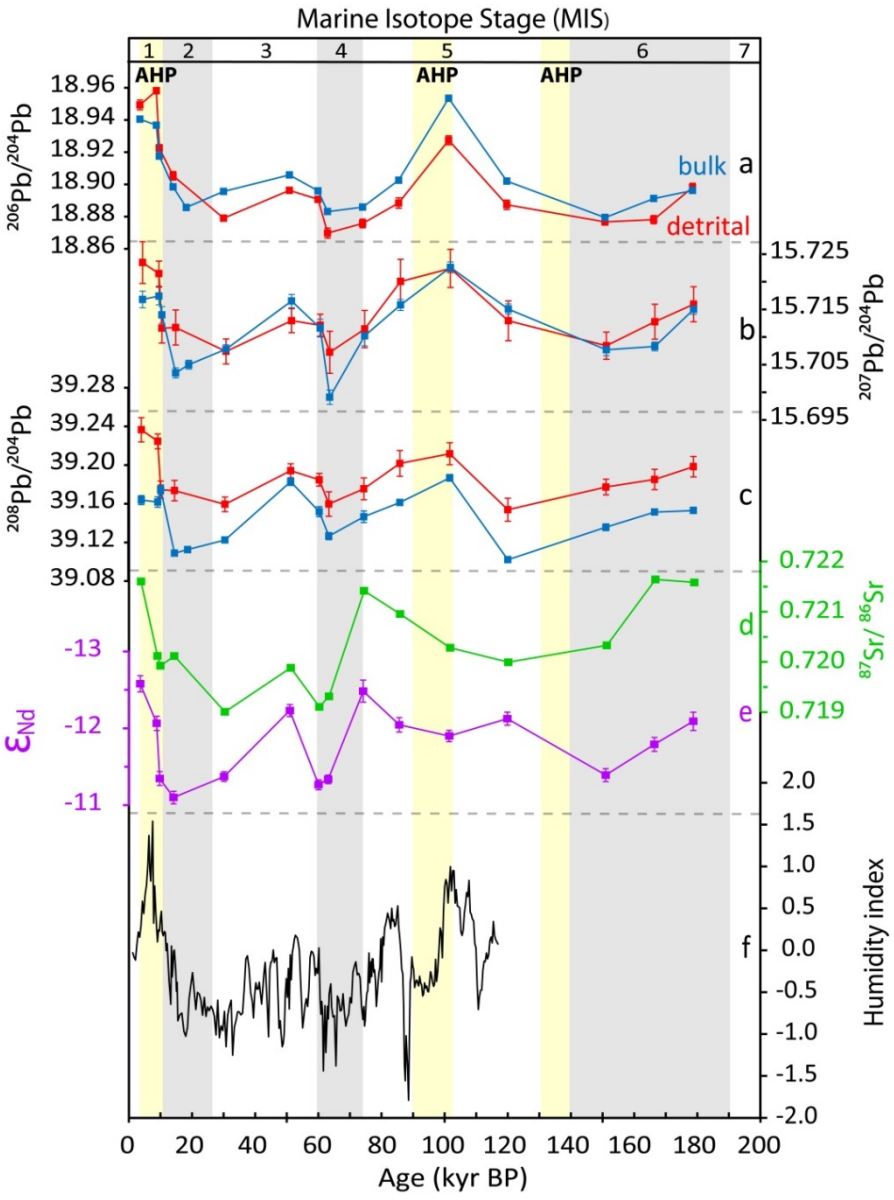

Fig. 3.2 Downcore isotopic records of terrigenous fraction (this study, red) and bulk sediment (Abouchami and Zabel, 2003, blue) from GeoB2910-1 (4°50'N, 21°03'W, 2,703 m) located in the Sierra Leone Rise, and continental humidity index of northwest Africa (Tjallingii et al., 2008). Note that the ε_{Nd} scale has been reversed in (e).

Suspended and dissolved loads delivered to the Atlantic Ocean by the main rivers draining western equatorial Africa are characterized by unradiogenic values lower than -15, such as ε_{Nd} of the Congo (around -16) and Ntem (around -28), while those of the Niger, Sanaga, Nyong lie between -11 to -14 (Allègre et al., 1996; Grousset and Biscaye, 2005; Weldeab et al., 2011). The terrigenous fraction (≤63 μm) of marine sediment core MD03-2707 displays low ε_{Nd} (-17 to -24), which indicates that this sediment core, lying adjacent to

major river outflows off the west African coast, receives a mixture of the material carried by the Sanaga, Nyong and Ntem rivers (Weldeab et al., 2011). Hence, if any significant fluvial supply of terrigenous sediment took place to the SLR, one would expect an unradiogenic ε_{Nd} signature to be delivered by the freshwater riverine plumes. Our measured Nd isotopic compositions at the SLR are wholly inconsistent with such an idea, however. Rather, the supply of terrestrial material to the SLR site is dominantly eolian, while wet deposition over the Atlantic is the principle mode of delivery (Prospero and Carlson, 1972; Bloemendal et al., 1988; Schepanski et al., 2009).

3.4 Discussion

3.4.1 Variability during glacial-interglacials and AHP

Abouchami and Zabel (2003) measured Pb isotopes in bulk sediment from the same samples from core GeoB2910-1 which predominantly reflects Saharan dust input. Their data were taken to show more unradiogenic sources of Pb during glacial times and a more radiogenic Pb source during interglacial periods in response to latitudinal migration of the ITCZ. However, our isotopic records on this core do not show any clear change between glacial and interglacial periods. Rather, the variability observed in the Pb isotopic compositions of our detrital fractions are better subdivided according to African wet phases with more radiogenic Pb and unradiogenic Pb isotopes during drier periods (Figs. 3.2 and 3.3). This suggests a connection between Pb isotopic fluctuations and climate alternations during AHP instead of glacial-interglacial transitions.

A further observation is that none of the Pb-Sr-Nd isotopic compositions we measured correlates in any systematic way with precession nor 30°N June insolation (figures not shown; orbital data from Berger and Loutre, 1991). Similarly, no correlations are apparent between detrital fraction Al/Ti ratio in GeoB2910-1 (Zabel et al., 1999) and radiogenic isotopic compositions (not shown).

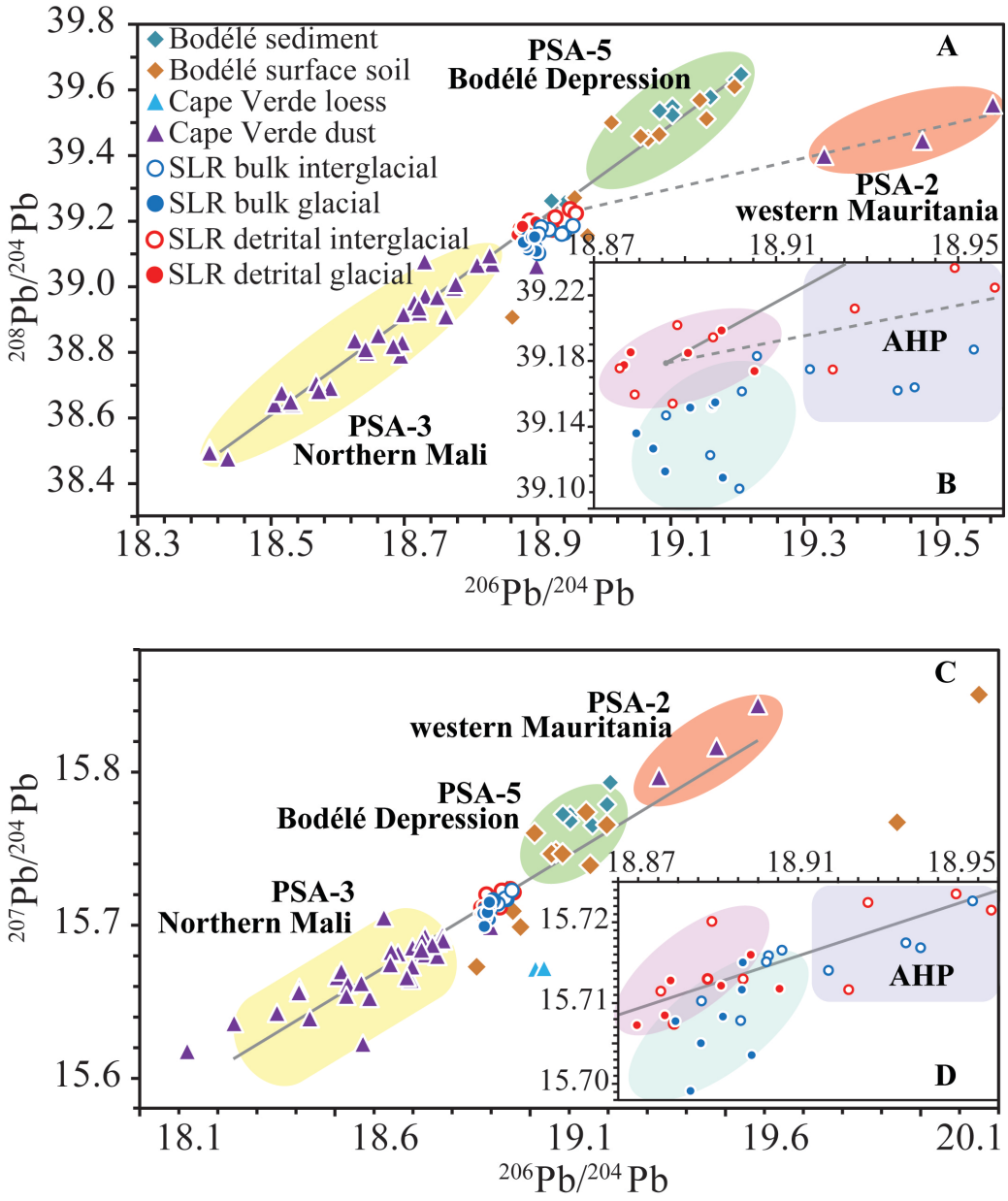

Fig. 3.3 Sr-Nd-Pb isotope cross plots. (a) $^{208}Pb/^{204}Pb$ vs. $^{206}Pb/^{204}Pb$ and (c) $^{207}Pb/^{204}Pb$ vs. $^{206}Pb/^{204}Pb$. The thick line represents a mixing line. (a) linear regression fits with r^2=0.97 between two endmembers, with the Bodélé Depression (Abouchami et al., 2013) representing the Saharan endmember, and Northern Mali endmembers based on data from (Kumar et al., 2014). (c) linear regression fits with r^2=0.87 among three endmembers: Bodélé Depression, Northern Mali and Western Mauritania. (e) ε_{Nd} vs. $^{206}Pb/^{204}Pb$, and (g) $^{87}Sr/^{86}Sr$ vs. $^{206}Pb/^{204}Pb$. (b), (d), (f), (h) are the zoom in isotope data of core GeoB2910-1. Symbols present the data during the interglacial (open) and glacial (closed) periods. Literature data of Bodélé Depression from (Abouchami et al., 2013), Cape Verde from (Kumar et al., 2014) and bulk sediment data of GeoB2910-1 from (Abouchami and Zabel, 2003).

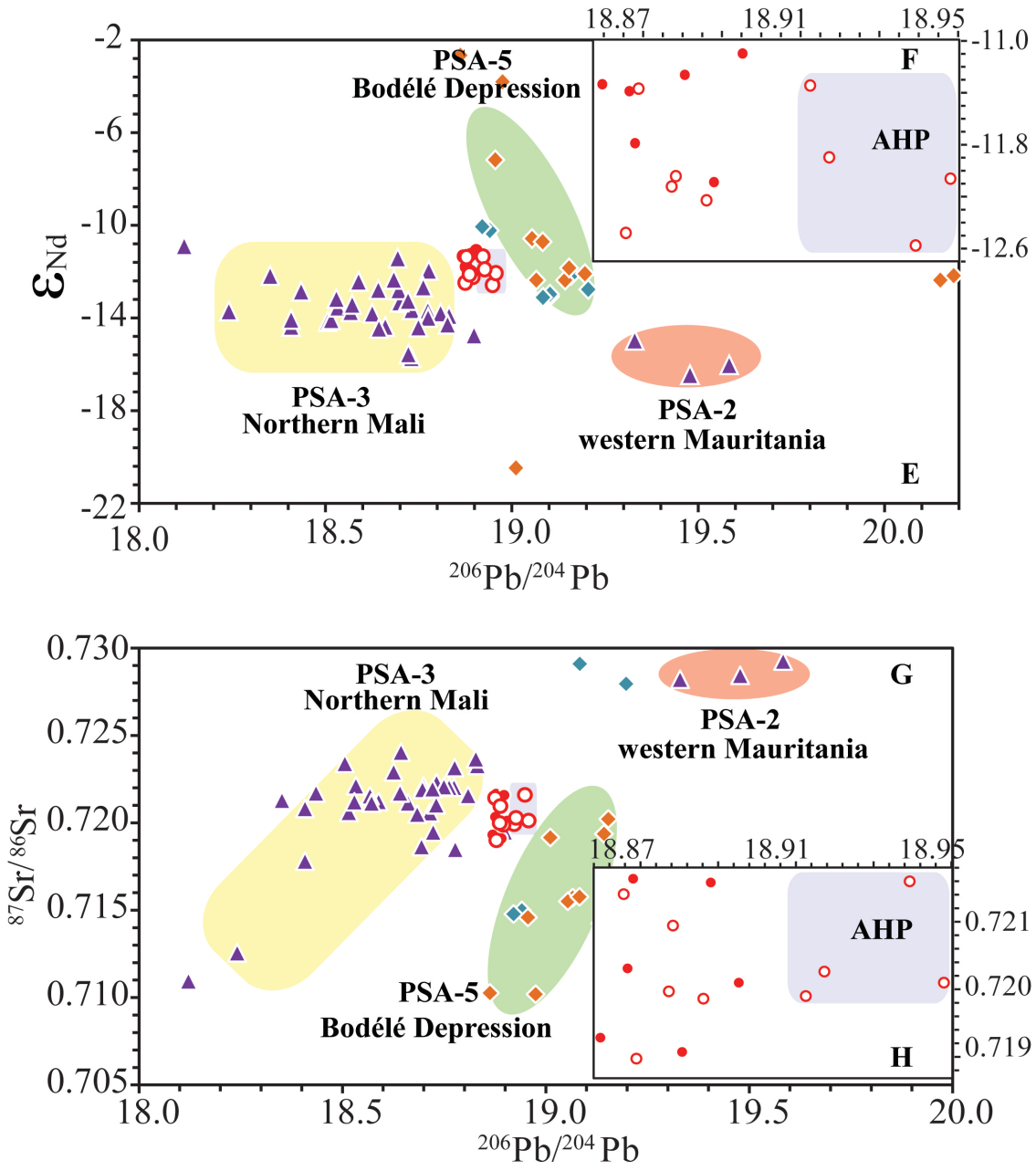

Continued **Fig. 3.3**

Overall, this emphasizes that the main control on the Pb-Sr-Nd isotopic compositions of the dusts delivered to the SLR – and therefore their North African source regions – appears to be whether the climate was wetter, as during AHP, or drier as today.

3.4.2 Climate control in dust delivery

Core GeoB2910-1 is located at 5°N on the Sierra Leone Rise just off the western coast of North Africa. Since the core is on a rise on the ocean floor, terrigenous material cannot be supplied via turbidity currents on the West African continental shelf. Similarly, fluvial sources – such as from the Senegal and Niger Rivers – can be ignored based upon the lack of any detectable fresh water plume at this site (Abouchami and Zabel, 2003). Therefore, the residual detrital fraction measured in GeoB2910-1 reflects solely dust emissions from North African sources areas.

Many factors could ultimately affect dust delivery to the core GeoB2910-1 site on the Sierra Leone Rise. These include changes in seasonal wind intensity and direction, physical grain-size sorting on transport, chemical weathering intensity in the PSA, the drying out and filling of lake sources, as well as vegetation cover (Cole et al., 2009). Below we use the radiogenic isotopic compositions of the dust in the core to try and identify the PSA responsible for emissions, assess the mixing proportions of them, and then examine how these were affected by the climate changes occurring in Northern Africa over the past 180 kyr.

3.4.3 African PSA contribution at the Sierra Leone Rise

In order to pin-point where the dust at the SLR comes from would appear simple: one compares the radiogenic isotopic compositions measured in GeoB2910-1 with those of known dust-emitting regions in Northern Africa. Unfortunately, characterization of African dust sources for radiogenic isotopes is still incomplete, at present.

The potential source areas (PSA) – regions responsible for most of African dust emissions – are well delimited by satellite imagery, as summarized in reviews by Formenti et al. (2011) and Scheuvens et al. (2013), and are shown in Fig. 3.1. Contour maps of North African $^{87}Sr/^{86}Sr$ and ε_{Nd} have been presented in Scheuvens et al. (2013) based largely on data collected by Grousset and co-workers on dusts, soils and marine core-top sediments (e.g.

Grousset et al., 1998). However, these maps are rudimentary and only allow crude estimates of the PSA Sr and Nd isotopic compositions to be made; Pb isotope data are lacking entirely. Here, we will assess the Pb, Nd and Sr isotopic compositions of the PSA using three more recently available datasets generated at MPIC from Abouchami et al. (2013), Kumar et al. (2013) and Singh et al. (2015).

As can be seen in Fig. 3.1, dust at the GeoB2910-1 site at 5°N may potentially come from PSA-2 (Mauritania), PSA-3 (Northern Mali/Southern Algeria) and PSA-5 (Bodélé Depression); contributions from PSA-1, PSA-4 and PSA-6 can safely be ignored.

The Bodélé Depression (PSA-5) has to be considered potentially the most important source because it is the "dustiest place in Earth" (Bristow et al., 2010). Dusts originated from this region traverse and provide large amounts of nutrients to the oligotrophic eastern equatorial Atlantic (Prospero et al., 2002; Washington et al., 2006; Schepanski et al., 2009; Scheuvens et al., 2013). Abouchami et al. (2013) have measured surface dry-lake sediment samples collected directly from the Bodélé Depression, chemically subdivided as 'Ca-rich', 'Si-rich' and 'Fe-rich' whose chemistry and isotopic compositions differ. The Pb, Sr and Nd isotopic compositions of Bodélé Depression sediments fall in the ranges: $\varepsilon_{Nd} = -10$ to -13; $^{87}Sr/^{86}Sr = 0.715$ to 0.730; $^{206}Pb/^{204}Pb = 18.92$ to 19.21, $^{207}Pb/^{204}Pb = 15.72$ to 15.79, and $^{208}Pb/^{204}Pb = 39.26$ to 39.65. These ranges are consistent with data on soils from the lake Chad region (Singh et al., 2015) and additional, unpublished data from the Bodélé region.

Kumar et al. (2013) measured radiogenic isotopes in a summer and winter time series of dusts collected on the Cape Verde Islands. Modelling by Schepanski et al. (2009) suggest that the predominant source of dusts under normal meteorological conditions at ~15°N is the Northern Mali/Southern Algeria area (PSA-3), and this was confirmed by back-trajectory analysis and satellite imagery for the times of sampling. Thus, this dataset characterizes PSA-3.

A large dust outbreak caught in the Kumar et al. (2013) time series, which partly activated a region in Western Mauritania at ~20°N, provides our assessment of the composition of PSA-2. The more radiogenic Pb found in Western Mauritania is consistent with the presence of old, cratonic continental crust in that region. Our best estimate of the radiogenic isotopic compositions, and ranges for the North African dust sources PSA-2, PSA-3 and PSA-5 is summarized in Fig. 3.3, and are in general agreement with the $^{87}Sr/^{86}Sr$ and ε_{Nd} maps for Northern Africa summarized by Schenvens et al. (2013).

The Pb isotopic compositions of dust from the SLR core fall in between the fields defining PSA-3 (Northern Mali) and PSA-5 (Bodélé Depression) (see Fig. 3.3). Mass balance dictates each source is contributing approximately half of the load and presumably half of the dust, assuming similar Pb concentrations in these sources. On the fact that at the SLR site at 5°N mixing PSA-3 and PSA-5 material in roughly equal proportions is entirely consistent with the North African dust emission and transport model of Schepanski et al. (2009).

It should be emphasized that this mixture of PSA at the SLR reflects a long-term average, probably integrating over 500-1000 years given the sedimentation rate of GeoB2910-1 and the size of samples. It is for this reason that the isotopic fields for the SLR core are highly constrained compared to those of the PSA.

During the AHP one sees in Fig. 3.3 a slight shift in $^{206}Pb/^{204}Pb$ with only a modest change to $^{208}Pb/^{204}Pb$. This shift suggests the appearance of dust from PSA-2 (Western Mauritania) at the SLR site in AHP, though the amount of dust is probably less than 10%. This is consistent with the development of extensive lakes and vegetation cover during the AHP, which triggered the reactivation of a large paleoriver system – the Tamanrasett – on the Mauritanian coast, and contributed terrigenous material from this region to the Tropical Atlantic Margin, even though no major river exists in the area today (Skonieczny et al., 2015).

Therefore, the isotope signatures in the SLR core support the interpretation that the PSA-3 and PSA-5 regions are always supplying most of the dust while during AHP PSA-2

sources originating in Senegal and Mauritania made a contribution as well. Overall, our data are in agreement with the known potential dust source regions in western North Africa proposed by Prospero et al. (2002): the Bodélé Depression, the basins east and south of the Ahaggar Mountains (Hoggar Massif), the base of the Tibesti Mountains and the western coasts of Mauritania and Western Sahara.

3.4.4 Saharan dust westward transport and deposition

Several studies have documented the transportation and deposition of Saharan dust at the Cape Verde Islands, along the West African margin and apparently even crossing the Atlantic Ocean to the Caribbean Islands and South America (Prospero et al., 2002; Stuut et al., 2005; Koren et al., 2006; Abouchami et al., 2013; Kumar et al., 2014). The isotopic compositions of the SLR detrital fraction are tightly clustered and indistinguishable for glacial and interglacial periods. This implies that the Mali (PSA-3) and Bodélé (PSA-5) sources, and their relative proportions, remained nearly unaltered over 180 kyr, even though latitude shifts in the ITCZ are known to have taken place.

Our Pb isotope data can also be subdivided into wetter AHP and drier periods in order to evaluate temporal and seasonal features of atmospheric transport. Dramatic changes in dust emission from North Africa have been demonstrated to be closely related to drought patterns, rather than to changes in atmospheric circulation, as inferred from a ^{4}He dust load record from the Cape Verde Islands (Mukhopadhyay and Kreycik, 2008). A previous study has proposed that around half of the dust from Palaeolake Megachad falls into the tropical Atlantic Ocean (Bristow et al., 2010). The Bodélé depression as a dust source will be enhanced or switched off by subtle variations in wind patterns and precipitation in the Chad region (Washington et al., 2009). During the early to middle Holocene, the potential dust source of the Lake Chad basin would have been limited due to the expanses of a larger lake area than today, which would have lead to sustained humidity, further influencing the regional climate pattern.

Drake and Bristow (2006) investigated the history of paleolake Megachad desiccation/flooding in detail because of its association with climate change in North Africa generally. They recognized that the basin was occupied by a greatly expanded lake area, producing highstand shorelines during the early-mid Holocene, while the highest lake-level, with the largest area, appeared at around 6 kyr BP (~372 m and 837,000 km^2). Decreased dust input into the Atlantic Ocean and enhanced in West African monsoon precipitation are associated with a northward shift of the ITCZ during AHP (McGee et al., 2013).

After 4 kyr BP, lake Megachad split into separate water bodies until, finally, the Bodélé Depression dried up completely, as inferred from an abrupt fall of lake level. During this process, within the dried-up Bodélé depression, extensive erodible diatomites were exposed, leading to dramatically enhanced dust emission from this region. The long-term reconstructed dust flux record in northeastern Nigeria roughly agrees with variations of the exposed area of the Lake Chad Basin (Cockerton et al., 2014).

The ^{230}Th-normalized flux of sediments along the northwest African margin also shows an abrupt rise in dust input at the end of the AHP, followed by a gradual increase in dust inputs over the remainder of the Late Holocene (McGee et al., 2013); this would be consistent with the our down-core radiogenic Pb isotopic compositions at the SLR. An intense increase (at least 17%) in cumulative rainfall in parts of Africa following the last ice age, lasting almost 10 kyr, caused enhanced wet deposition of aerosols (Kutzbach and Liu, 1997; Mahowald et al., 2014), due to moist convection over the Atlantic within the ITCZ (Schepanski et al., 2009).

During the dry season (boreal winter), when the ITCZ migrates to the southernmost position (~ 5°S), huge amounts of aeolian dust from the central Sahara (e.g. Bodélé Depression) are transported out of Africa to the SLR area as dust outbreaks. These outbreaks are enhanced by the increased southwesterly low-level jet Harmattan wind system, the lack of surface vegetation cover and due to local topographic control of low-level winds (Stuut et al.,

2005; Washington et al., 2006). This “Harmattan” dust plume, is raised from near ground level to higher altitudes (below 1.5 km) due to the south-tilted structure of the ITCZ, making the dust available for long-range transport, consistent with air-parcel trajectory analysis (Stuut et al., 2005; Washington et al., 2009; Lyngsie et al., 2013). This dust layer often extends down to the surface, which enhances dry depositioned fluxes by turbulent mixing processes with high mean AOT (aerosol optical thickeness). Wet deposition of dust, on the other hand, is very low over the North African domain in winter due to very little or no precipitation, arising from the southerly position of the ITCZ. Wet deposition occurs mainly over the Eastern Atlantic, and is related to moist convection within the ITCZ and low pressure disturbances further north (Schepanski et al., 2009).

The Pb isotope record in the SLR indicates that the relative mixing proportions of dust originating from PSA-5 (the Bodélé Depression) and PSA-3 (Northern Mali/Southern Algeria) is roughly one to one, with minor contributions from PSA-2 (Senegal and Mauritania). A modelling study of zonal dust export supports this interpretation of a circa 50% contribution of Bodélé Depression dust at 20°W and 5°N (the location of the SLR) relative to dust emissions from the rest of North Africa (Schepanski et al., 2009).

During the wet season (boreal summer), the SAL is active and it carries finer-grained dust at mid-tropospheric levels (3-5 km), which is ultimately transported westward to as far as the Caribbean, when the ITCZ shifts to the northernmost position and the ITCZ lies slightly north of the Bodélé Depression (near 18°N). Lyngsie et al. (2013) proposed the idea that the ITCZ uplifts Harmattan winds to higher altitudes and functions as a barrier which prevents long-range transported Harmattan dust originating from the Sahara-Sahel region to settle south and below the ITCZ. Uplifting of air masses from near ground to higher altitudes is seen from trajectory analysis of the median annual cycle from the Bodélé and over Ghana computed by the NOAA HYSPLIT model (Washington et al., 2009; Lyngsie et al., 2013). Overall, this means that the majority of dust transport from West Africa is blocked during

summertime, and atmospheric disturbances near to the sea surface are main dust contributors to the SLR. However, minor amounts of wind-blown dust deposited at the SLR are likely to also occur due to gravitational settling, and cannot be ruled out.

These generalized ideas on dust transport mechanisms are supported by many modelling studies. The AOT and aerosol optical depth (AOD) output patterns of the model simulations agree in general that there is maximum mean AOT/AOD values over the Bodélé Depression (PSA-5) during southwesterly transportation in boreal winter; in contrast, significant dust emission from Mauritania (PSA-2), and from Northern Mali/Southern Algeria (PSA-3) occurs during boreal summer (Schepanski et al., 2009; Lyngsie et al., 2013; Scheuvens et al., 2013). HY-SPLIT backward trajectory analysis along the West African margin (1° N to 7° N, 7° E to 13° W) by Stuut et al. (2005) suggests that the high-level, wind-blown dust originates from the central Sahara/Chad region, while surface winds all point to an oceanward origin which are clearly unable to carry any African-derived dust at all to the SLR. But, it should be borne in wind that back-trajectory analysis is typically utilized to estimate the origin of air masses and is not necessarily definitive in identifying the provenance of the dust emission (Stuut et al., 2005).

Washington et al. (2009) have computed average transport pathways out of the Bodélé Depression for years of actual meteorological data on wind patterns. They argue that when dust emission from the Bodélé is greatly reduced during the boreal summer, the transport pathway can take Bodélé dust over West Africa carried in the Sahara Air Layer. Attenuated material derived from the Bodélé augments other key dust source areas over Mali and Mauritania during the summer time. Vertical dust emission and transport modelling agrees with this view that dust export westwards at 20°W is within the lower tropospheric level within the Trade Wind layer during boreal winter (Schepanski et al., 2009).

Although latitude shifts in the ITCZ during glacial-interglacial periods have been observed in several studies, our SLR dataset appears to have little bearing on seasonal and

global migration of the ITCZ changing the African monsoon (Schepanski et al., 2009). This is because the principal Bodélé emissions occur in the winter when the ITCZ is at its most southerly extent, while the monsoon takes place when the ITCZ is farthest north in the summer.

3.4.5 Changes in continental humidity and the termination of AHP

North African Humid Periods are caused by enhanced transport of moist maritime air from the Atlantic Ocean into western and central Africa in response to increased solar insolation in the North African subtropics during the boreal summer season. This scenario appears to be supported by modeling of the insolation-forced increase in sea surface temperatures, and associated changes in atmospheric circulation (Kutzbach and Liu, 1997). Similarly, rainy conditions and greater contribution of rain from the Atlantic during AHP can be inferred from low δD_{wax} in offshore records (Tierney et al., 2011).

Continent-wide reconstructions of past lake-level, collated in the Oxford Lake-Level Database, indicate numerous large and small paleolakes during the early Holocene that extended from the far northern Sahara to as far south at 10°S in East Africa; the lakes formed as a result of moisture supply exceeding evaporation during the African wet phases (Tierney et al., 2011). Enhanced rainfall in the AHP leads to less dust emission from the Bodélé Depression (PSA-5), when this region was extensively covered with vegetation and lakes, and thus contributed less dust to the SLR core as well.

During the AHP, the African rainbelt had a more northern position than today. Hooghiemstra (1988) illustrates the African rainbelt shifted northward by about 700 km during AHP while an equatorward retreat of the monsoonal rainfall front took place during glacial times, as a result of the influence of the North Atlantic climate system. A northward shift or expansion of the African rainbelt and the monsoon winds during the mid-Holocene can be inferred from isotopic records along the African margin, and are in agreement with this

finding (Meyer et al., 2011). Increased summer insolation and an intensified monsoon circulation linked to a northward shift of the African rainbelt over northwest Africa caused more humid conditions and increased vegetation cover. This supported a positive biogeophysical feedback between rainfall and vegetation, as can be seen in AOV-IC simulation of the precipitation (Tjallingii et al., 2008).

Climate instability in the northern high latitudes exerts a dominant role on the West African monsoon through an atmospheric linkage (Weldeab et al., 2007). When precessional forcing is weak during glacial periods, expansion of the Northern Hemisphere ice caps suppress the African monsoonal system in the Sahara-Sahel region, resulting in a colder and drier climate, such as in MIS4 and MIS2 (Tjallingii et al., 2008).

The North African Humidity Index is defined by Tjallingii et al. (2008) as the log ratio of the non-aeolian (hemi-pelagic mud) and the aeolian material (coarse and fine aeolian dust) present in marine sediment core GeoB7920-2 off the coast of Mauritania; this was used as a proxy to indicate relative changes in continental humidity and vegetation cover. The idea of the index is that an increased value reflects enhanced riverine discharge or decreased aeolian input due to expansion of the continental vegetation cover.

Variations of rainfall and humidity are clearly present in the Pb isotope ratios of the down-core record at the SLR, as three Pb isotope ratios correlate strongly with the North African Humidity Index of Tjallingii et al. (2008) (see Fig. 3.4). High humidity during the AHP results in the Pb isotopes becoming systematically more radiogenic while Sr and Nd isotopic compositions show no clear-cut response (Fig. 3.2). This fact can be expected mainly because stronger wet deposition during these heavy rain events leads to more dust emitted from higher latitude regions.

Orbital precession greatly influences North African climate because it controls the strength and northward penetration of the monsoonal rains and moisture transport from the eastern equatorial Atlantic to the West Africa (Kutzbach, 1981). In the early Holocene,

orbital-forced strengthening of African monsoon penetrated much further north resulting in a much more northward rainbelt, large amount of precipitation and high relative humidity. This caused extreme environmental change to occur: extensive grass-covered savannah with numerous lakes are present during the AHP while arid desert exists at present in the Sahara/Sahel region (deMenocal et al., 2000a; Tjallingii et al., 2008; Collins et al., 2011). During MIS5, the expansion of Saharan vegetation cover was comparable to that of the Holocene AHP, which is attributed to latitudinal displacement of the ITCZ and, consequently, the West African monsoon precipitation (Weldeab et al., 2007; Tjallingii et al., 2008; Collins et al., 2011). Collins et al. (2013) have evaluated the position of the Sahara-Sahel boundary over time using the chemistry of marine cores off west Africa and proposed that this is strongly influenced by the Atlantic Meridional Overturning Circulation (AMOC).

Here, we suggest that the Pb isotope composition of the terrigenous fraction of sediment cores such as GeoB2910-1 on the SLR may be used as proxies of relative humidity, as relative high North African humidity is associated with more radiogenic isotopic compositions, corresponding to warmer conditions, and vice versa. Our records provide evidence as that increased rainfall leads to higher levels of vegetation and fillings of lakes as the Sahara-Sahel boundary expands northward during the AHP. Our Pb isotope data from GeoB2910-1 also support the case for termination of the Holocene AHP after 4.0 kyr BP in northwest Africa, since there exists a clear shift to higher ratios during the last deglaciation (4 – 10 kyr BP) and at 101 kyr BP (Fig. 3.2).

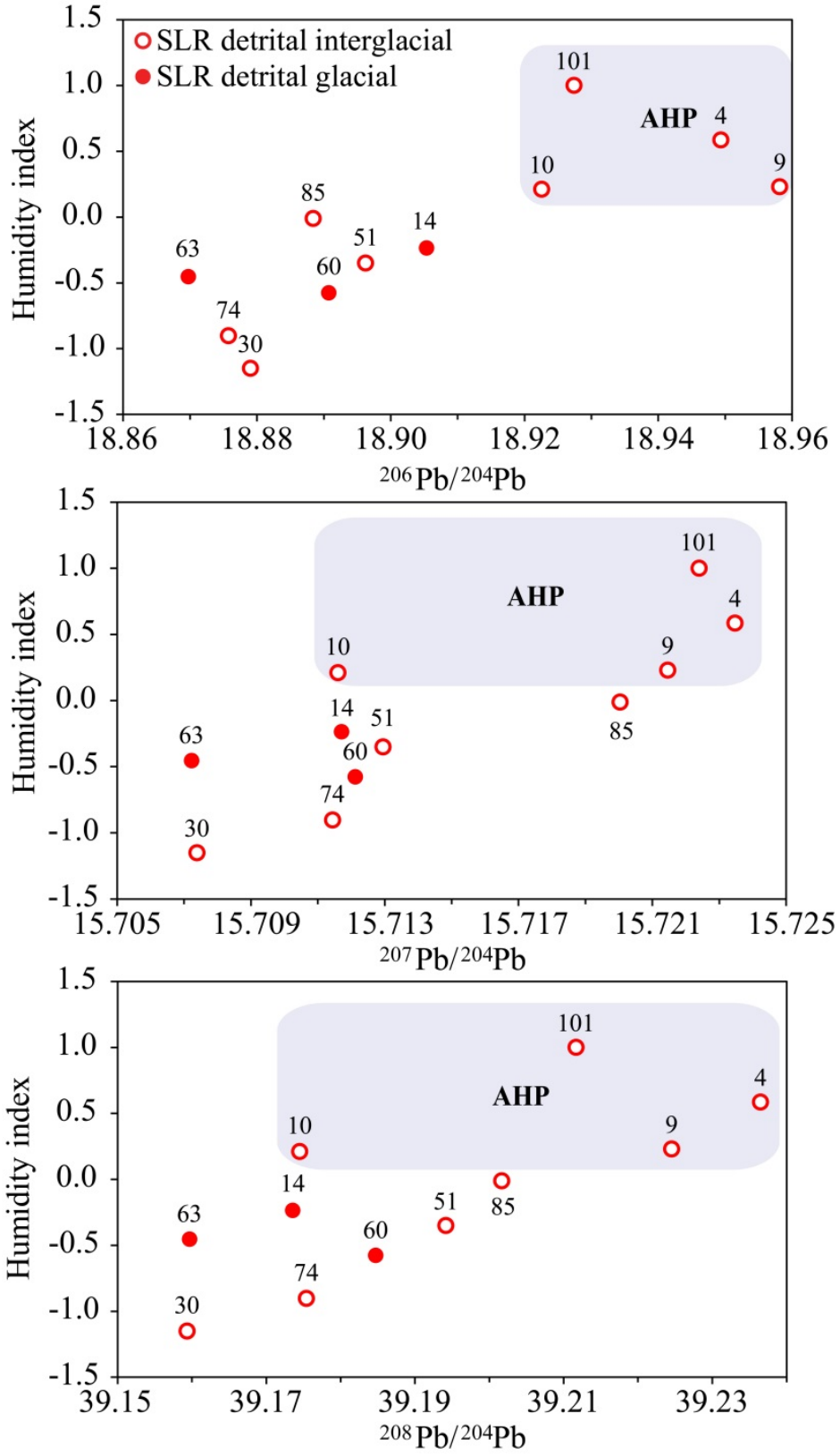

Fig. 3.4 Relationship between Pb isotopic ratios and northwest Africa humidity index. Records of northwest Africa humidity index are from (Tjallingii et al., 2008). Symbols along age lables present the data during the interglacial (open) and glacial (closed) periods.

Evidence for wetter conditions during the early and mid-Holocene has been found in many records throughout northwest Africa. Ritchie et al. (1985) reported that the last AHP occurred roughly between ~9 and ~6 kyr BP. However, there has been an increase in dust deposits/flux seen in high-resolution marine sediment cores offshore of West Africa downwind from the Sahara since 5.5 kyr BP, which points to drier conditions towards the end of Holocene (deMenocal et al., 2000a; Adkins et al., 2006). The salinity of riverine outflow plumes can yeild a measure of discharge – and thus catchment rainfall – and can be inferred from $\delta^{18}O_{seawater}$ in the outflow (Weldeab et al., 2005). These authors found low salinity in the Niger River plume between 11.5 and 5.0 kyr BP indicative of greater discharge. This is in agreement with a δD_{wax} record from Lake Tanganyika (Tierney et al., 2011) and abrupt increases in dust emission at a mean-transition age of 4.9 ± 0.2 kyr BP (McGee et al., 2013).

Paleoenviromental reconstruction from northern Chad shows a strong reduction in tropical vegetation cover resulting in large-scale dust mobilization after 4.3 kyr BP and gradual establishment of a desert system by 2.7 kyr BP, pointing to a progressive termination of the AHP (Kröpelin et al., 2008). However, a rapid fresh-to-hypersaline transition in paleolake salinity happened only after 4.0 kyr BP based upon fossil chironomids and diatoms. Recently, Shanahan et al. (2015) used hydrologic changes across North Africa to show that the termination of the AHP occurred later over much of subtropical-to-tropical West and Central Africa (< 15° N; 2.5 – 4.0 BP) than at sites north of the modern-day monsoon system limit (>15° N; 5.0 – 6.0 BP). Shorelines in the Sahara indicate the retreat and desiccation of lake Megachad started at around 4 kyr BP and later split into two separate lakes (Drake and Bristow, 2006). Our SLR records support a termination of the last AHP after 4 kyr BP, although the timing is not very precise because our isotopic record has low-resolution and due to the low sedimentation rate of the GeoB2910-1 core. In the future, higher-resolution records will hopefully help to improve estimates of the timing of the termination of the last AHP.

3.5 Conclusions

Sr, Nd and Pb isotopes were obtained on the detrital fraction of sediment core GeoB2910-1 (4°50'N, 21°03'W, 2,703 m) located on the Sierra Leone Rise off West Africa. This 180-kyr archive helps us to reconstruct the coupled marine-terrestrial climate in the eastern equatorial Atlantic and changes in sources of North African dust emission.

Our study shows that there are three major dust source end-members present at the SLR originating in the Sahara-Sahel region. The predominant contributors are: the Bodélé Depression (PSA-5) and Northern Mali (PSA-3), with a minor, transient contribution from Western Mauritania (PSA-2). Sr-Nd-Pb isotopic compositions show little variability throughout the 180-kyr interval when the climate was arid, indicating that the contributing sources on average did not change much. Nevertheless, during AHP there is a shift in Pb isotope compositions of the terrigenous fraction towards PSA-2, as well as a good correlation with indicators of North African Humidity. This minor contribution from Western Mauritania during AHP was probably deposited by westward transport in the Sahara Air Layer, while less dust was emitted from the Bodélé Depression region due to its filling-up as lake Megachad and general enhanced vegetation cover. By contrast, Sr and Nd isotopic compositions show no clear response to African wet phases. Variations in the proportions of PSA contributions, inferred from the isotopic variability, do not appear to be affected by seasonal and global migration of ITCZ, nor glacial-interglacial cycling.

Our radiogenic isotope record of eolian dust in SLR core GeoB2910-1 illustrates the importance of measuring Pb isotopes in order to delimit the dust source contributions over time. The fact that we can resolve changes in PSA that are clearly related to climatic, oceanographic and meteorological shifts in the North African region during AHP is promising. It suggests that future such studies in cores along the western African margin will likely help greatly in evaluating latitudinal migrations of the Sahara-Sahel boundary over time.

Acknowledgments

R.W. was funded by the State Scholarship Study Abroad Program for Graduate Studies and a Max Planck Society Research fellowship. We thank H. Feldmann, S. Herrmann and R. Jotter for their help in the lab.

References

Abouchami, W., Näthe, K., Kumar, A., Galer, S.J.G., Jochum, K.P., Williams, E., Horbe, A.M.C., Rosa, J.W.C., Balsam, W., Adams, D., Mezger, K., Andreae, M.O., 2013. Geochemical and isotopic characterization of the Bodélé Depression dust source and implications for transatlantic dust transport to the Amazon Basin. Earth and Planetary Science Letters 380, 112-123.

Abouchami, W., Zabel, M., 2003. Climate forcing of the Pb isotope record of terrigenous input into the Equatorial Atlantic. Earth and Planetary Science Letters 213, 221-234.

Adkins, J., deMenocal, P., Eshel, G., 2006. The "African humid period" and the record of marine upwelling from excess ^{230}Th in Ocean Drilling Program Hole 658C. Paleoceanography 21, PA4203.

Allègre, C.J., Dupré, B., Négrel, P., Gaillardet, J., 1996. Sr-Nd-Pb isotope systematics in Amazon and Congo River systems: constraints about erosion processes. Chemical Geology 131, 93-112.

Ashpole, I., Washington, R., 2013. A new high-resolution central and western Saharan summertime dust source map from automated satellite dust plume tracking. Journal of Geophysical Research: Atmospheres 118, 6981-6995.

Bayon, G., German, C.R., Boella, R.M., Milton, J.A., Taylor, R.N., Nesbitt, R.W., 2002. An improved method for extracting marine sediment fractions and its application to Sr and Nd isotopic analysis. Chemical Geology 187, 179-199.

Berger, A., Loutre, M.F., 1991. Insolation values for the climate of the last 10 million years. Quaternary Science Reviews 10, 297-317.

Biscaye, P.E., Chesselet, R., Prospero, J.M., 1974. Rb-Sr, ^{87}Sr/^{86}Sr isotope system as an index of provenance of continental dusts in the open Atlantic ocean. Journal de Recherches Atmospheriques 8, 819-829.

Bloemendal, J., Lamb, B., King, J., 1988. Paleoenvironmental implications of rock-magnetic properties of Late Quaternary sediment cores from the eastern equatorial Atlantic. Paleoceanography 3, 61-87.

Bou Karam, D., Flamant, C., Knippertz, P., Reitebuch, O., Pelon, J., Chong, M., Dabas, A., 2008. Dust emissions over the Sahel associated with the West African monsoon intertropical discontinuity region: A representative case-study. Quarterly Journal of the Royal Meteorological Society 134, 621-634.

Bristow, C.S., Hudson-Edwards, K.A., Chappell, A., 2010. Fertilizing the Amazon and equatorial Atlantic with West African dust. Geophysical Research Letters 37, L14807.

Chester, R., Hughes, M.J., 1967. A chemical technique for the separation of ferro-manganese minerals, carbonate minerals and adsorbed trace elements from pelagic sediments. Chemical Geology 2, 249-262.

Cockerton, H.E., Holmes, J.A., Street-Perrott, F.A., Ficken, K.J., 2014. Holocene dust records from the West African Sahel and their implications for changes in climate and land surface conditions. Journal of Geophysical Research: Atmospheres 119, 8684-8694.

Cole, J.M., Goldstein, S.L., deMenocal, P.B., Hemming, S.R., Grousset, F.E., 2009. Contrasting compositions of Saharan dust in the eastern Atlantic Ocean during the last deglaciation and African Humid Period. Earth and Planetary Science Letters 278, 257-266.

Collins, J.A., Schefusz, E., Heslop, D., Mulitza, S., Prange, M., Zabel, M., Tjallingii, R., Dokken, T.M., Huang, E., Mackensen, A., Schulz, M., Tian, J., Zarriess, M., Wefer, G., 2011. Interhemispheric symmetry of the tropical African rainbelt over the past 23,000 years. Nature Geosci 4, 42-45.

Conway, T.M., John, S.G., 2014. Quantification of dissolved iron sources to the North Atlantic Ocean. Nature 511, 212-215.

deMenocal, P., Ortiz, J., Guilderson, T., Adkins, J., Sarnthein, M., Baker, L., Yarusinsky, M., 2000a. Abrupt onset and termination of the African Humid Period: rapid climate responses to gradual insolation forcing. Quaternary Science Reviews 19, 347-361.

deMenocal, P., Ortiz, J., Guilderson, T., Sarnthein, M., 2000b. Coherent high- and low-latitude climate variability during the Holocene warm period. Science 288, 2198-2202.

deMenocal, P.B., Tierney, J.E., 2012. Green Sahara: African Humid Periods paced by Earth's orbital changes. Nature Education Knowledge 3, 12.

Drake, N., Bristow, C., 2006. Shorelines in the Sahara: geomorphological evidence for an enhanced monsoon from palaeolake Megachad. The Holocene 16, 901-911.

Evan, A.T., Foltz, G.R., Zhang, D., 2012. Physical response of the tropical–subtropical North Atlantic Ocean to decadal–multidecadal forcing by African Dust. Journal of Climate 25, 5817-5829.

Formenti, P., Schütz, L., Balkanski, Y., Desboeufs, K., Ebert, M., Kandler, K., Petzold, A., Scheuvens, D., Weinbruch, S., Zhang, D., 2011. Recent progress in understanding physical and chemical properties of African and Asian mineral dust. Atmos. Chem. Phys. 11, 8231-8256.

Funk, J.A., von Dobeneck, T., Wagner, T., Kasten, S., 2004. Late Quaternary sedimentation and early diagenesis in the Equatorial Atlantic Ocean: Patterns, trends and processes deduced from rock magnetic and geochemical records, in: Wefer, G., Mulitza, S., Ratmeyer, V. (Eds.), The South Atlantic in the Late Quaternary. Springer Berlin Heidelberg, pp. 461-497.

Galer, S.J.G., 1999. Optimal double and triple spiking for high precision lead isotopic measurement. Chemical Geology 157, 255-274.

Ginoux, P., Prospero, J.M., Gill, T.E., Hsu, N.C., Zhao, M., 2012. Global-scale attribution of anthropogenic and natural dust sources and their emission rates based on MODIS Deep Blue aerosol products. Reviews of Geophysics 50, RG3005.

Grousset, F.E., Biscaye, P.E., 2005. Tracing dust sources and transport patterns using Sr, Nd and Pb isotopes. Chemical Geology 222, 149-167.

Grousset, F.E., Parra, M., Bory, A., Martinez, P., Bertrand, P., Shimmield, G., Ellam, R.M., 1998. Saharan wind regimes traced by the Sr-Nd isotopic composition of subtropical Atlantic sediments: Last Glacial Maximum vs today. Quaternary Science Reviews 17, 395-409.

Hooghiemstra, H., 1988. Changes of major wind belts and vegetation zones in NW Africa 20,000–5000 yr B.P., as deduced from a marine pollen record near cap blanc. Review of Palaeobotany and Palynology 55, 101-140.

Huang, J., Zhang, C., Prospero, J.M., 2009. African aerosol and large-scale precipitation variability over West Africa. Environmental Research Letters 4, 015006.

Jacobsen, S.B., Wasserburg, G.J., 1980. Sm-Nd isotopic evolution of chondrites. Earth and Planetary Science Letters 50, 139-155.

Jickells, T.D., An, Z.S., Andersen, K.K., Baker, A.R., Bergametti, G., Brooks, N., Cao, J.J., Boyd, P.W., Duce, R.A., Hunter, K.A., Kawahata, H., Kubilay, N., laRoche, J., Liss, P.S., Mahowald, N., Prospero, J.M., Ridgwell, A.J., Tegen, I., Torres, R., 2005. Global iron connections between desert dust, ocean biogeochemistry, and climate. Science 308, 67-71.

Koren, I., Kaufman, J.Y., Washington, R., Todd, C.M., Rudich, Y., Martins, J.V., Rosenfeld, D., 2006. The Bodélé depression: a single spot in the Sahara that provides most of the mineral dust to the Amazon forest. Environmental Research Letters 1, 014005.

Kröpelin, S., Verschuren, D., Lézine, A.-M., Eggermont, H., Cocquyt, C., Francus, P., Cazet, J.-P., Fagot, M., Rumes, B., Russell, J.M., Darius, F., Conley, D.J., Schuster, M., von Suchodoletz, H., Engstrom, D.R., 2008. Climate-driven ecosystem succession in the Sahara: The past 6000 years. Science 320, 765-768.

Kumar, A., Abouchami, W., Galer, S.J.G., Fomba, K., Andreae, M.O., 2013. Isotopic characterization of winter time aeolian dust over Cape Verde. Mineralogical Magazine 77, 1523.

Kumar, A., Abouchami, W., Galer, S.J.G., Garrison, V.H., Williams, E., Andreae, M.O., 2014. A radiogenic isotope tracer study of transatlantic dust transport from Africa to the Caribbean. Atmospheric Environment 82, 130-143.

Kutzbach, J.E., 1981. Monsoon climate of the Early Holocene: Climate experiment with the Earth's orbital parameters for 9000 years ago. Science 214, 59-61.

Kutzbach, J.E., Liu, Z., 1997. Response of the African Monsoon to orbital forcing and ocean feedbacks in the middle Holocene. Science 278, 440-443.

Lyngsie, G., Olsen, J.L., Awadzi, T.W., Fensholt, R., Breuning-Madsen, H., 2013. Influence of the inter tropical discontinuity on Harmattan dust deposition in Ghana. Geochemistry, Geophysics, Geosystems 14, 3425-3435.

Mahowald, N., Albani, S., Kok, J.F., Engelstaeder, S., Scanza, R., Ward, D.S., Flanner, M.G., 2014. The size distribution of desert dust aerosols and its impact on the Earth system. Aeolian Research 15, 53-71.

McGee, D., deMenocal, P.B., Winckler, G., Stuut, J.B.W., Bradtmiller, L.I., 2013. The magnitude, timing and abruptness of changes in North African dust deposition over the last 20,000 yr. Earth and Planetary Science Letters 371–372, 163-176.

Meyer, I., Davies, G.R., Stuut, J.-B.W., 2011. Grain size control on Sr-Nd isotope provenance studies and impact on paleoclimate reconstructions: An example from deep-sea sediments offshore NW Africa. Geochemistry, Geophysics, Geosystems 12, Q03005.

Mukhopadhyay, S., Kreycik, P., 2008. Dust generation and drought patterns in Africa from helium-4 in a modern Cape Verde coral. Geophysical Research Letters 35, L20820.

Prospero, J.M., Carlson, T.N., 1972. Vertical and areal distribution of Saharan dust over the western equatorial north Atlantic Ocean. Journal of Geophysical Research 77, 5255-5265.

Prospero, J.M., Ginoux, P., Torres, O., Nicholson, S.E., Gill, T.E., 2002. Environmental characterization of global sources of atmospheric soil dust identified with the Nimbus 7 Total Ozone Mapping Spectrometer (TOMS) absorbing aerosol product. Reviews of Geophysics 40, 1002.

Ritchie, J.C., Eyles, C.H., Haynes, C.V., 1985. Sediment and pollen evidence for an early to mid-Holocene humid period in the eastern Sahara. Nature 314, 352-355.

Rossignol-Strick, M., Nesteroff, W., Olive, P., Vergnaud-Grazzini, C., 1982. After the deluge: Mediterranean stagnation and sapropel formation. Nature 295, 105-110.

Rutberg, R.L., Hemming, S.R., Goldstein, S.L., 2000. Reduced North Atlantic Deep Water flux to the glacial Southern Ocean inferred from neodymium isotope ratios. Nature 405, 935-938.

Schepanski, K., Tegen, I., Macke, A., 2009. Saharan dust transport and deposition towards the tropical northern Atlantic. Atmos. Chem. Phys. 9, 1173-1189.

Scheuvens, D., Schütz, L., Kandler, K., Ebert, M., Weinbruch, S., 2013. Bulk composition of northern African dust and its source sediments — A compilation. Earth-Science Reviews 116, 170-194.

Schlitzer, R., 2014. Ocean Data View. *http://odv.awi.de*.

Schneider, T., Bischoff, T., Haug, G.H., 2014. Migrations and dynamics of the intertropical convergence zone. Nature 513, 45-53.

Shanahan, T.M., McKay, N.P., Hughen, K.A., Overpeck, J.T., Otto-Bliesner, B., Heil, C.W., King, J., Scholz, C.A., Peck, J., 2015. The time-transgressive termination of the African Humid Period. Nature Geosci 8, 140-144.

Singh, S., Galer, S.J.G., Kandler, K., Abouchami, W., Jotter, R., Andreae, M.O., 2015. Radiogenic Sr, Nd and Pb Isotopes in deflatable soil phases from North Africa. Goldschmidt Abstracts, 2904.

Skonieczny, C., Paillou, P., Bory, A., Bayon, G., Biscara, L., Crosta, X., Eynaud, F., Malaize, B., Revel, M., Aleman, N., Barusseau, J.P., Vernet, R., Lopez, S., Grousset, F., 2015. African humid periods triggered the reactivation of a large river system in Western Sahara. Nature Communications 6.

Stuut, J.-B., Zabel, M., Ratmeyer, V., Helmke, P., Schefuß, E., Lavik, G., Schneider, R., 2005. Provenance of present-day eolian dust collected off NW Africa. Journal of Geophysical Research: Atmospheres 110, D04202.

Sun, D., Lau, K.M., Kafatos, M., 2008. Contrasting the 2007 and 2005 hurricane seasons: Evidence of possible impacts of Saharan dry air and dust on tropical cyclone activity in the Atlantic basin. Geophysical Research Letters 35, L15405.

Sunnu, A., Afeti, G., Resch, F., 2008. A long-term experimental study of the Saharan dust presence in West Africa. Atmospheric Research 87, 13-26.

Tierney, J.E., Lewis, S.C., Cook, B.I., LeGrande, A.N., Schmidt, G.A., 2011. Model, proxy and isotopic perspectives on the East African Humid Period. Earth and Planetary Science Letters 307, 103-112.

Tjallingii, R., Claussen, M., Stuut, J.-B.W., Fohlmeister, J., Jahn, A., Bickert, T., Lamy, F., Rohl, U., 2008. Coherent high- and low-latitude control of the northwest African hydrological balance. Nature Geosci 1, 670-675.

Touré, N.D.E., Konar, A., Siélé, S., 2012. Intercontinental transport and climatic impact of Saharan and Sahelian dust. Advances in Meteorology 2012, 14.

Tsamalis, C., Chédin, A., Pelon, J., Capelle, V., 2013. The seasonal vertical distribution of the Saharan Air Layer and its modulation by the wind. Atmos. Chem. Phys. 13, 11235-11257.

Washington, R., Bouet, C., Cautenet, G., Mackenzie, E., Ashpole, I., Engelstaedter, S., Lizcano, G., Henderson, G.M., Schepanski, K., Tegen, I., 2009. Dust as a tipping element: The Bodélé Depression, Chad. Proceedings of the National Academy of Sciences 106, 20564-20571.

Washington, R., Todd, M., Middleton, N.J., Goudie, A.S., 2003. Dust-storm source areas determined by the Total Ozone Monitoring Spectrometer and surface observations. Annals of the Association of American Geographers 93, 297-313.

Washington, R., Todd, M.C., Engelstaedter, S., Mbainayel, S., Mitchell, F., 2006. Dust and the low-level circulation over the Bodélé Depression, Chad: Observations from BoDEx 2005. Journal of Geophysical Research: Atmospheres 111, L09401.

Weldeab, S., Frank, M., Stichel, T., Haley, B., Sangen, M., 2011. Spatio-temporal evolution of the West African monsoon during the last deglaciation. Geophysical Research Letters 38, L13703.

Weldeab, S., Lea, D.W., Schneider, R.R., Andersen, N., 2007. 155,000 years of West African monsoon and ocean thermal evolution. Science 316, 1303-1307.

Weldeab, S., Schneider, R.R., Kölling, M., Wefer, G., 2005. Holocene African droughts relate to eastern equatorial Atlantic cooling. Geology 33, 981-984.

Zabel, M., Bickert, T., Dittert, L., Haese, R.R., 1999. Significance of the sedimentary Al:Ti ratio as an indicator for variations in the circulation patterns of the equatorial North Atlantic. Paleoceanography 14, 789-799.

Zouari, K., Gibert, E., Causse, C., 1998. Radiocarbon and Th/U chronologies of humid episodes of late quaternary from Sahara: selected sites of Palhydaf programme. Orstom editions, France.

Chapter 4

Climate control on sediment delivery by the Amazon River system: a radiogenic isotope provenance study

Ran Wei[1], Stephen J.G. Galer[1], Wafa Abouchami[2], Meinrat O. Andreae[1]

[1]Max Planck Institute for Chemistry, Biogeochemistry and Climate Geochemistry Departments, P.O. Box 3060, 55020 Mainz, Germany

[2]Institut de Physique du Globe de Paris, Sorbonne Paris Cité, Université Paris Diderot, UMR 7154 CNRS, 75238 Paris, France

*Corresponding author. Tel: +49 (6131) 305 6601: Email: ran.wei@mpic.de

Abstract

The provenance of hemipelagic sediments in the western Atlantic during the last 205 kyr was studied through the temporal variations in radiogenic Sr-Nd-Pb isotopic compositions of terrigenous detrital fractions in sediment core GeoB1523-1 located on the Ceara Rise. This record reflects the fine-grained suspended load of the Amazon River plume that is delivered to the Ceara Rise via the North Brazil Current retroflection over time. The radiogenic isotope data on the detrital fractions are interpreted as a mixture of sediments originating from young "highland" sources (Andes) and old "lowland" cratons (e.g. Guiana Shield) within the Amazon catchment. This shows that there was an increased contribution from highland Andean regions during glacials versus interglacials. The isotopic evidence suggests that changes in terrigenous supply mirror global sea level and, to some extent, high-latitude summer insolation. The balance between main highland (Andes) and lowland (Shield) sources of sediment gradually changed between glacial and interglacial periods, as the climate altered in the Amazon Basin and are in phase with changes of sea level, equatorial Atlantic circulation variation and shelf topography, as well as 65°N summer insolation. The amount of sediment from the South American continent transported to the Ceara Rise is greater during glacial phases, due to an enhanced eastward North Brazil Current retroflection compared to interglacial periods.

Keywords: Amazon Basin, Ceara Rise, radiogenic isotopes, sediment provenance, sea level change, Glaciation, Insolation, Andes, Guiana Shield

Highlights

- Pb, Nd and Sr isotopic compositions of terrigeneous fractions from sediment core on the Ceara Rise, Western Atlantic.
- A 205-kyr record of the Amazon suspended load.
- The proportions of highland (Andes) versus lowland (cratonic) regions affect the isotopic compositions of the Amazon suspended load.
- Isotopic compositional variation implies an increased proportion of material derived from the highland Andean regions during glacial periods.
- Changes in suspended load composition are in phase with variations in the global sea level curve.
- Global climate changes modulate rainfall patterns within the Amazon basin and the sedimentary load of the Amazon River.
- Suspended load is greater in glacials and is transported to the Ceara Rise via an enhanced North Brazil Current retroflection.

4.1 Introduction

River systems deliver a vast plume of fresh water and dissolved and suspended load into the oceans, playing a huge role in supplying elements to the oceans (Dobson et al., 2001; Milliman, 2015). The Amazon is the largest river in the world, accounting for approximately 20% of total fresh water discharge and transporting about 7 % of global suspended sediment load (Gibbs, 1973, 1974; Milliman and Meade, 1983; Milliman, 2015). The Amazon Basin drains much of the northern South American continent, which stretches from the highland Andes, across the Guiana and Brazilian Precambrian Shields to the Atlantic Ocean (Fig. 4.1). This suspended load is deposited at the Amazon River mouth as deltaic and estuarine sediments. Further transportation of fine-grained suspended load is controlled by physical oceanographic processes in the high-energy environment produced by the longshore current, the North Brazil current (NBC), that carries the sediment northwestward along the coast (Gibbs, 1973, 1974; Rühlemann et al., 2001). Studies of Amazon Fan sediments indicate that the Andes is the dominant source of sediment, even though only a small proportion of rivers runs through this region, providing more than 80% of suspended load to the Amazon River (Fig. 4.2) (Parra and Pujos, 1998; Rimington, 1999); contributions from the lowland Guiana Shield to the Amazon are far less (Gibbs, 1967; Meade et al., 1985; McDaniel et al., 1997; Parra and Pujos, 1998).

Moisture availability within the Amazon Basin plays an essential role in the river outflow budget drained by the Amazon River system, which exhibits a strong seasonal pattern in precipitation. This responds to changes in the South American monsoon intensity and the seasonal position of the Intertropical Convergence Zone (ITCZ) over the oceans and continents (Maslin and Burns, 2000; Maslin et al., 2011).

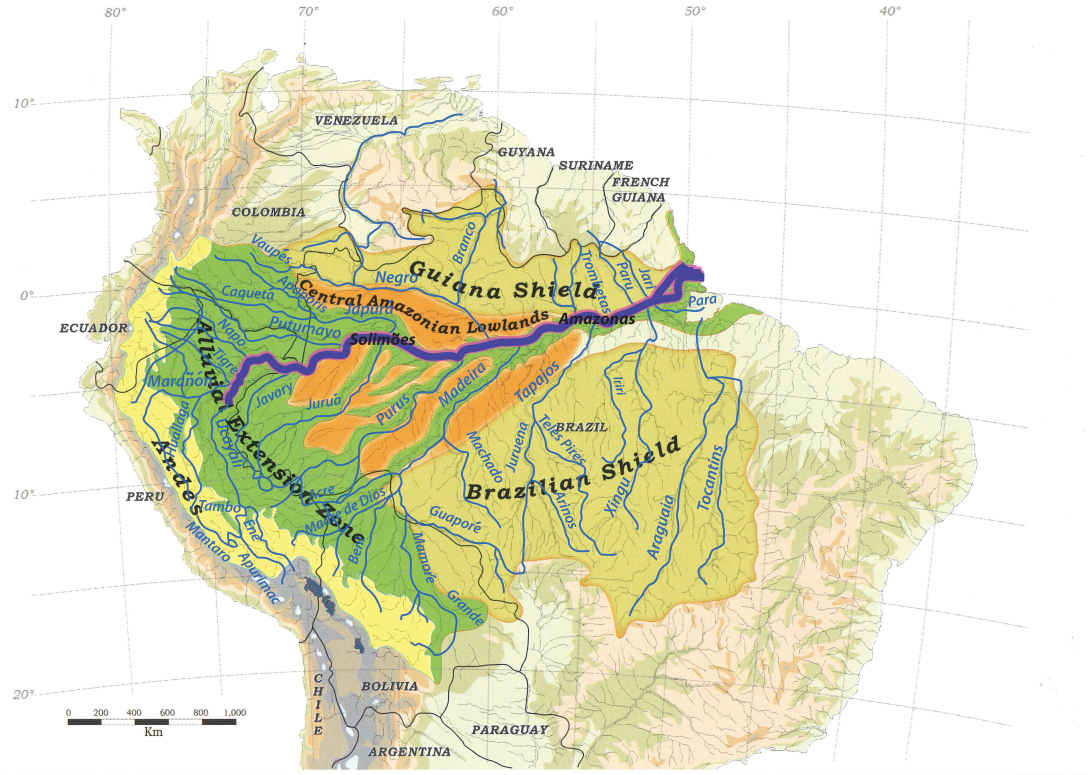

Fig. 4.1 River system and geologic zones of the Amazon Basin (Goulding et al., 2003).

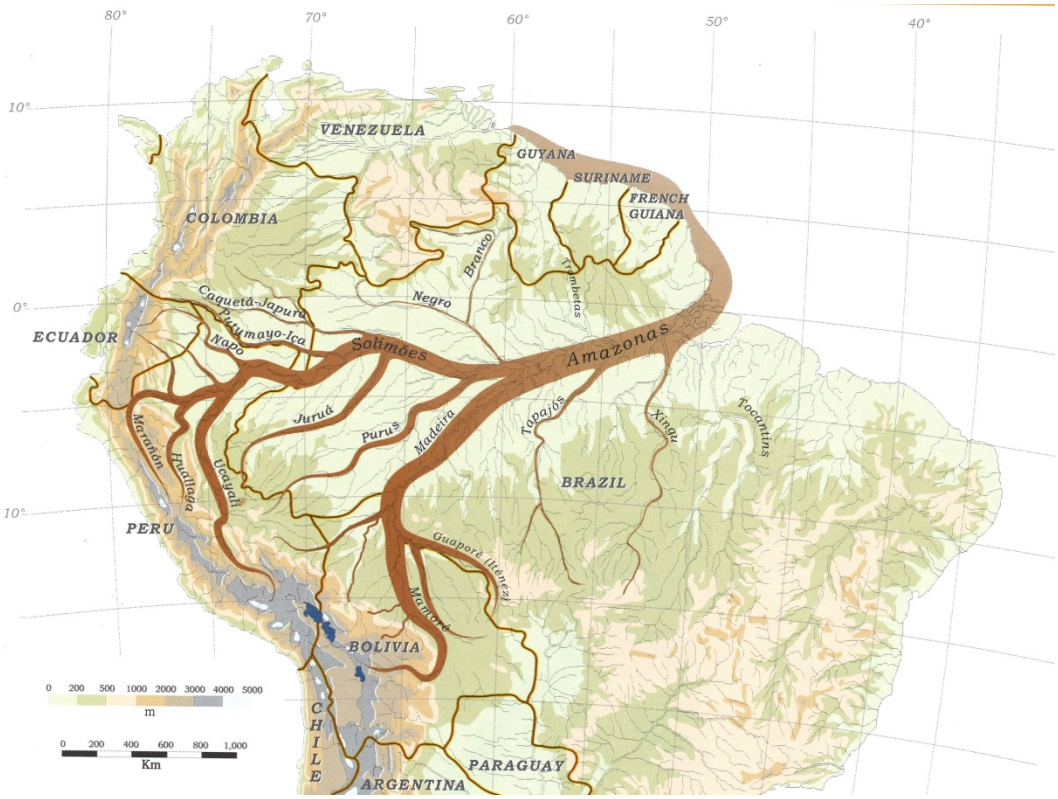

Fig. 4.2 Amazon sediment transport (Goulding et al., 2003).

Lake level records, determined via preserved paleoshorelines, lake sediments and carbonate deposits, provide an overview of South American climate evolution (Harris and Mix, 1999; Sylvestre et al., 1999; Baker et al., 2001a; Fritz et al., 2004; Placzek et al., 2006; Fritz et al., 2012). In the highland Amazonian Andes, lake levels were likely higher during glacial periods due to increased precipitation, which has been linked to orbital- and millennial-scale changes in moisture convectivity (Abbott et al., 1997; Baker et al., 2001a; Fritz et al., 2004; Fritz et al., 2012). By contrast, lowland lakes were fuller in interglacial periods caused by enhanced rainfall and riverine discharge, while the glacial Amazon lowlands are widely believed to have been much drier than at present (Leyden et al., 1993; Colinvaux et al., 1996; Harris and Mix, 1999; Peterson et al., 2000).

These contrasting rainfall regimes in the Amazonia highlands and lowlands can be accounted for by the seasonal migration of the ITCZ, which is ultimately modulated by Northern Hemisphere temperature changes. This fits in well with the "east-west anti-phased climate in South America" hypothesis put forward by Cruz et al. (2005; 2009); their idea is that this results from shifts in the southern and northern boundaries of the South American summer monsoon (SASM) in the western Amazon Basin, while in the eastern Amazon Basin this is mainly affected by the tropical Easterlies and southern position of SASM. Despite the complex mechanism, this means that insolation variations in both hemispheres lead to changes in SASM strength, and its southern and northern boundaries, which then further influence the regional precipitation-evaporation balance and moisture availability in the Amazon Basin (Abbott et al., 1997; Clement et al., 2004; Wang et al., 2006; Wang et al., 2007; Kutzbach et al., 2008; Maslin et al., 2011).

Research on deep-sea sediments provides important evidence for the geological history on land and sea. The various provenances of marine sediment come down to two major categories. One of these is biogenic and authigenic precipitates derived directly from sea water; the second is terrigenous material from the continents, including volcanic ash, dust,

eroded and weathered material produced from land and transported to the ocean by rivers, wind and glacial movement. This fraction is closely related to the composition of parent rocks on the continents. Climatic-forced weathering in the source region and grain-size distribution (sorting effects) during the transport process are the primary factors influencing the terrestrial-sourced component composition.

Existing major element chemistry records in cores from the Cariaco Basin along the northern Venezuela coast and northeastern Brazilian continental margin have documented an increased supply of terrigenous material and higher biological productivity during interstadial times (Arz et al., 1999; Peterson et al., 2000). Govin et al. (2014) used high-resolution geochemical records in such cores to investigate Amazonian climate changes in so far as this affected the terrigenous input from northern South America. That study indicated that at sites from 5°N and 9°N, sediments were derived mainly from the Amazon River, while there was negligible supply from small rivers and African eolian dust (Gibbs, 1974; Dobson et al., 2001; Govin et al., 2014).

There are many geochemical approaches to analyzing the terrigenous fraction in sediments to obtain provenance information. However, radiogenic isotopes are arguably the most robust tool available. Previous work has shown that radiogenic isotopes can be used to distinguish different continental provenances and for reconstructing the weathering history of these regions (Abouchami and Zabel, 2003; Franzese et al., 2006; Franzese et al., 2009; Meyer et al., 2011; Li et al., 2015). Here, we focus on reconstructing source provenance in pelagic sediments from the western equatorial Atlantic, looking for variation that can be linked to glacial-interglacial climate forcing. We present a down-core sedimentary Nd-Sr-Pb isotope record for the last 205 kyr of the detrital fraction in core GeoB1523-1 (3°49'N, 41°37'W, water depth 3292 m) on the Ceara Rise, located off northeastern Brazil. The Ceara Rise is an aseismic ridge, that ranges between 3000 and 4500 m in water depth and its

northern and southern boundaries are formed by fracture zones at 8 °N and 4 °N (Fig. 4.3) (Kumar and Embley, 1977).

Many varied studies have been undertaken on this core site at the Ceara Rise. Stable isotopic compositions – $\delta^{18}O$ and $\delta^{13}C$ - and boron isotopes in planktonic foraminifera have been used to estimate past variations on sea water salinity, sea surface temperature, relative water body stratification and past atmospheric CO_2 concentrations (Dürkoop et al., 1997; Mulitza et al., 1998; Henehan et al., 2013). Magnetic analysis has provided additional information on terrigenous material originating from South American and African sources (Bleil and von Dobeneck, 2004). Other studies have focused on the determination of organic carbon, carbonate accumulation, illit/smectite ratios and other proxies in order to reconstruct changes in the western Equatorial surface circulation and Amazonian climate (Rühlemann et al., 1996; Rühlemann et al., 1999; Kinkel et al., 2000; Rühlemann et al., 2001; Vink et al., 2002). Productivity studies indicate that the Ceara Rise region maintained a low productivity during the last 180 kyr, while vertical expansion of acidic Southern Component Water resulted in carbonate dissolution during cold periods, supporting a reduced contribution of Northern Component Water at this time (Rühlemann et al., 1996; Rutberg et al., 2000).

The Ceara Rise is located southeast of the Amazon Fan and its relative position to South America has kept roughly unchanged throughout the Cenozoic period (Curry et al., 1995), making it a very useful location for reconstructing the long-term changes in sediment supply. Available bulk sediment studies at ODP sites 925/926 in the Ceara Rise provide a record of tectonism and erosion on the northern South American continent for the Cenozoie (Dobson et al., 2001).

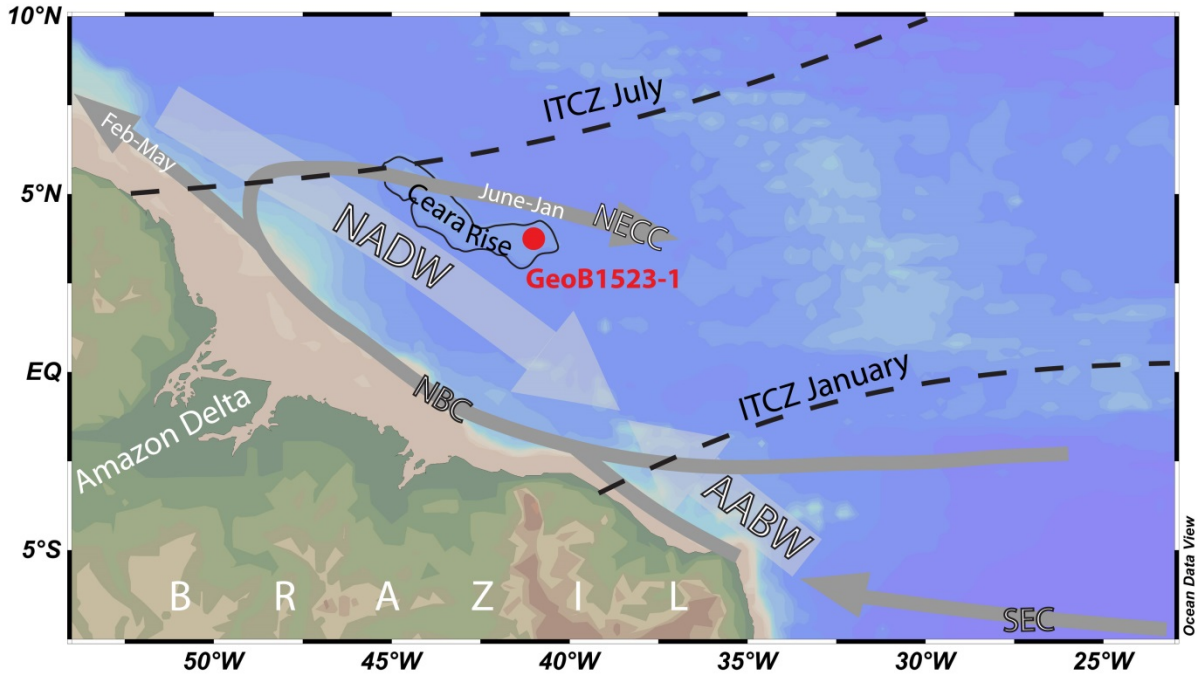

Fig. 4.3 Location of gravity core GeoB1523-1 on the northeastern flanks of the Ceara Rise, regional surface (grey arrow) and deep (white arrow) currents in the study area, and seasonal positions of the Intertropical Convergence Zone (ITCZ). The retroflection of the North Brazil Current (NBC) into the North Equatorial Counter Current (NECC) persists from June to January (Muller-Karger et al., 1988). North Atlantic Deep Water (NADW) flows directly over the Ceara Rise, while Antarctic Bottom Water (AABW) passes around the structural high. Figure prepared using Ocean Data View software (Schlitzer, 2014).SEC presents South Equatorial Current.

The highland Andes and lowlands are the two main geographic regions in the Amazon Basin that provide suspended sediment, while the Andes are the predominant source found at the Ceara Rise, with lower contributions from the lowland Shields (Gibbs, 1967; Meade et al., 1985; McDaniel et al., 1997; Parra and Pujos, 1998; Zabel et al., 1999; Abouchami and Zabel, 2003; Govin et al., 2012). African wind-blown eolian dust is not a significant component at the Ceara Rise, as shown by measured downcore Al/Ti ratios from GeoB1523-1 (Zabel et al., 1999). The terrigenous material ultimately ending up deposited on the Ceara Rise is modulated by relative sea level change, equatorial Atlantic circulation variation and shelf topography, and shows evidence of a 100-kyr cyclicity of wet-dry alternation in Amazonian climate (Rühlemann et al., 1996; Rühlemann et al., 2001).

4.2 Methods

Measurements were made on the terrigenous (detrital) sediment fraction of GeoB1523-1. About 50 mg of bulk sediment samples were processed using procedures similar to those of previous studies (Chester and Hughes, 1967; Rutberg et al., 2000; Bayon et al., 2002). We removed the calcium carbonate fraction using an ammonium acetate-buffered acetic-acid solution (pH=5) by shaking for 2 hours twice, to make sure the samples were completely carbonate-free. After several rinses with ultrapure MilliQ water, ferromanganese oxides were removed using 0.02 M hydroxylamine hydrochloride in 25% glacial acetic acid by shaking for 4 hours. The remaining material left after these procedures corresponds to the detrital component; it was washed with MilliQ water and then dissolved completely using a mixture of concentrated HF and HNO_3 acids. Following dissolution on a hotplate, chemical separation of the elements was performed under clean laboratory conditions followed methods described previously (Abouchami et al., 2013; Kumar et al., 2014). The total procedural blanks (Sr = 24 pg; Nd = 3 pg; Pb ≤ 30 pg) are negligible compared to the amount of these elements isolated from the samples and processed through the chemistry.

All isotopic measurements were performed by thermal ionization mass spectrometry (ThermoFisher, TRITON) in static multi-collection mode. Pb was loaded with a colloidal silica gel-H_3PO_4 activator solution on single rhenium filaments and the isotope ratios were corrected for instrumental mass fractionation bias using the Pb triple-spike technique (Galer, 1999). Strontium was loaded onto single tungsten filaments along with TaF_5 activator and oxidized in air. The $^{87}Sr/^{86}Sr$ ratios were corrected for instrumental fractionation by normalizing to $^{86}Sr/^{88}Sr = 0.1194$. Neodymium samples were sandwich-loaded onto single tungsten filaments with 1 µl of Ta_2F_5 solution, and measured as the NdO^+ species. Multiple measurements of NIST SRM981 yielded $^{206}Pb/^{204}Pb = 16.9427 \pm 37$, $^{207}Pb/^{204}Pb = 15.4998 \pm 31$ and $^{208}Pb/^{204}Pb = 36.7269 \pm 81$ (2SD, N = 39), respectively. Replicate measurements of NIST SRM 987 and 5 ng loads of the La Jolla Nd standard resulted values of 0.710259 ± 13

(2SD, N = 22) and 0.511842 ± 11 (2SD, N = 18) during the period of analysis. The Nd isotope ratios in this paper are expressed as parts per 10^4 deviations from bulk Earth values:

$$\varepsilon_{Nd} = \left(\frac{^{143}Nd/^{144}Nd_{sample}}{^{143}Nd/^{144}Nd_{CHUR}} - 1\right)\times 10^4,$$

where $^{143}Nd/^{144}Nd_{CHUR}$=0.512638 is the Chondrite Uniform Reservoir (CHUR) (Jacobsen and Wasserburg, 1980).

The age model for core GeoB1523-1 was obtained by graphic correlation of characteristic isotopic events in the the oxygen isotope record of Globigerinoides sacculifer to the SPECMAP oxygen isotope stacked record of Imbrie et al. (1984) (see Rühlemann et al., 1996).

4.3 Results

Pb, Sr and Nd isotope measurements on the terrigenous sediment fraction of GeoB1523-1 over the last six Marine Isotope Stage (MIS) are reported in Table 4.1 and in Fig. 4.4. The Pb isotopic compositions scatter within a narrow range of values ($^{206}Pb/^{204}Pb$ = 18.96 to 19.11, $^{207}Pb/^{204}Pb$ = 15.71 to 15.74, $^{208}Pb/^{204}Pb$ = 39.10 to 39.26), while Sr and Nd isotopic compositions vary between 0.722 to 0.726 and -11.3 to -12.9. $^{87}Sr/^{86}Sr$ ratios are strongly negatively correlated with ε_{Nd} and positively correlated with $^{206}Pb/^{204}Pb$, $^{207}Pb/^{204}Pb$ and $^{208}Pb/^{204}Pb$.

Our radiogenic isotopic records show a systematic glacial-interglacial variation over the past 205 kyr. During glacial periods, $^{87}Sr/^{86}Sr$ exhibits relatively unradiogenic values of about 0.723, with the lowest ratio of 0.722 found at the last glacial maximum. Correspondingly, Pb isotopes are relatively unradiogenic with ranges of $^{206}Pb/^{204}Pb$ = 18.96 to 19.09, $^{207}Pb/^{204}Pb$ = 15.71 to 15.74, and $^{208}Pb/^{204}Pb$ = 39.10 to 39.25; the most radiogenic values occur at around 170 kyr BP. ε_{Nd} ratios are relatively radiogenic, ranging between -11.3 and -12.3. During the deglaciation, Pb and Sr isotopes gradually increased to $^{206}Pb/^{204}Pb$ = 19.00 to 19.11, $^{207}Pb/^{204}Pb$ = 15.71 to 15.73, and $^{208}Pb/^{204}Pb$ = 39.16 to 39.26, while $^{87}Sr/^{86}Sr$ lie between

0.722 and 0.726. $^{87}Sr/^{86}Sr$ is anti-correlated with ε_{Nd}, which exhibits its most unradiogenic value of -13 at around 10 kyr BP.

Table 4.1 Nd, Sr and Pb isotopic composition of terrigenous fraction on core GeoB1523-1.

Depth in core (m)	Age (cal-kyr BP)	$^{143}Nd/^{144}Nd$ (2σ)	ε_{Nd} (2σ)	$^{87}Sr/^{86}Sr$ (2σ)	$^{206}Pb/^{204}Pb$ (2σ)	$^{207}Pb/^{204}Pb$ (2σ)	$^{208}Pb/^{204}Pb$ (2σ)
0.03	2.0	0.511988 (4)	-12.68 ± 0.09	0.725050 (8)	19.0220 (29)	15.7193 (35)	39.2104 (117)
0.13	7.7	0.511975 (6)	-12.93 ± 0.12	0.725138 (5)	19.0242 (47)	15.7171 (56)	39.2054 (188)
0.18	9.7	0.511984 (6)	-12.76 ± 0.12	0.724529 (7)	19.0081 (24)	15.7194 (30)	39.1875 (99)
0.28	13.8	0.512007 (5)	-12.31 ± 0.09	0.723408 (7)	18.9591 (50)	15.7158 (44)	39.0976 (117)
0.43	18.7	0.512043 (4)	-11.60 ± 0.07	0.722603 (6)	18.9888 (24)	15.7157 (27)	39.1371 (86)
0.58	21.4	0.512038 (6)	-11.71 ± 0.12	0.722449 (6)	18.9899 (34)	15.7107 (42)	39.1322 (140)
0.78	28.4	0.512035 (7)	-11.75 ± 0.14	0.722085 (5)	19.0291 (18)	15.7169 (22)	39.1598 (74)
1.18	42.5	0.512014 (6)	-12.17 ± 0.12	0.723371 (6)	19.0002 (42)	15.7134 (51)	39.1626 (171)
1.38	49.5	0.512004 (7)	-12.36 ± 0.13	0.723733 (6)	19.0635 (44)	15.7237 (53)	39.2085 (177)
1.63	62.0	0.512040 (4)	-11.66 ± 0.07	0.722587 (8)	19.0014 (33)	15.7171 (40)	39.1518 (134)
1.73	66.5	0.512038 (4)	-11.71 ± 0.07	0.723119 (6)	19.0162 (47)	15.7219 (57)	39.1773 (191)
1.98	74.0	0.512017 (3)	-12.12 ± 0.07	0.724707 (6)	18.9678 (65)	15.7143 (80)	39.0993 (266)
2.28	87.0	0.512014 (6)	-12.18 ± 0.11	0.724952 (6)	19.0692 (26)	15.7238 (31)	39.2133 (102)
2.58	99.0	0.512011 (4)	-12.23 ± 0.08	0.726143 (6)	19.1099 (60)	15.7315 (73)	39.2421 (243)
2.83	108.2	0.512022 (9)	-12.02 ± 0.17	0.724474 (8)	19.0579 (36)	15.7190 (44)	39.1877 (146)
3.13	122.0	0.511994 (6)	-12.56 ± 0.12	0.724760 (6)	18.9997 (26)	15.7145 (29)	39.1775 (94)
3.38	132.8	0.512027 (6)	-11.93 ± 0.12	0.723469 (7)	18.9894 (20)	15.7141 (24)	39.1459 (78)
3.63	142.1	0.512059 (6)	-11.29 ± 0.12	0.722462 (6)	19.0039 (41)	15.7107 (50)	39.1316 (167)
3.93	153.2	0.512024 (6)	-11.98 ± 0.12	0.722689 (6)	18.9666 (20)	15.7167 (23)	39.1354 (74)
4.23	166.6	0.512018 (7)	-12.08 ± 0.13	0.723507 (7)	19.0859 (26)	15.7362 (28)	39.2525 (87)
4.78	188.5	0.512021 (5)	-12.03 ± 0.10	0.724658 (7)	19.0616 (28)	15.7185 (34)	39.2168 (114)
5.13	205.0	0.512009 (5)	-12.27 ± 0.09	0.724831 (7)	19.0784 (31)	15.7246 (37)	39.2601 (124)

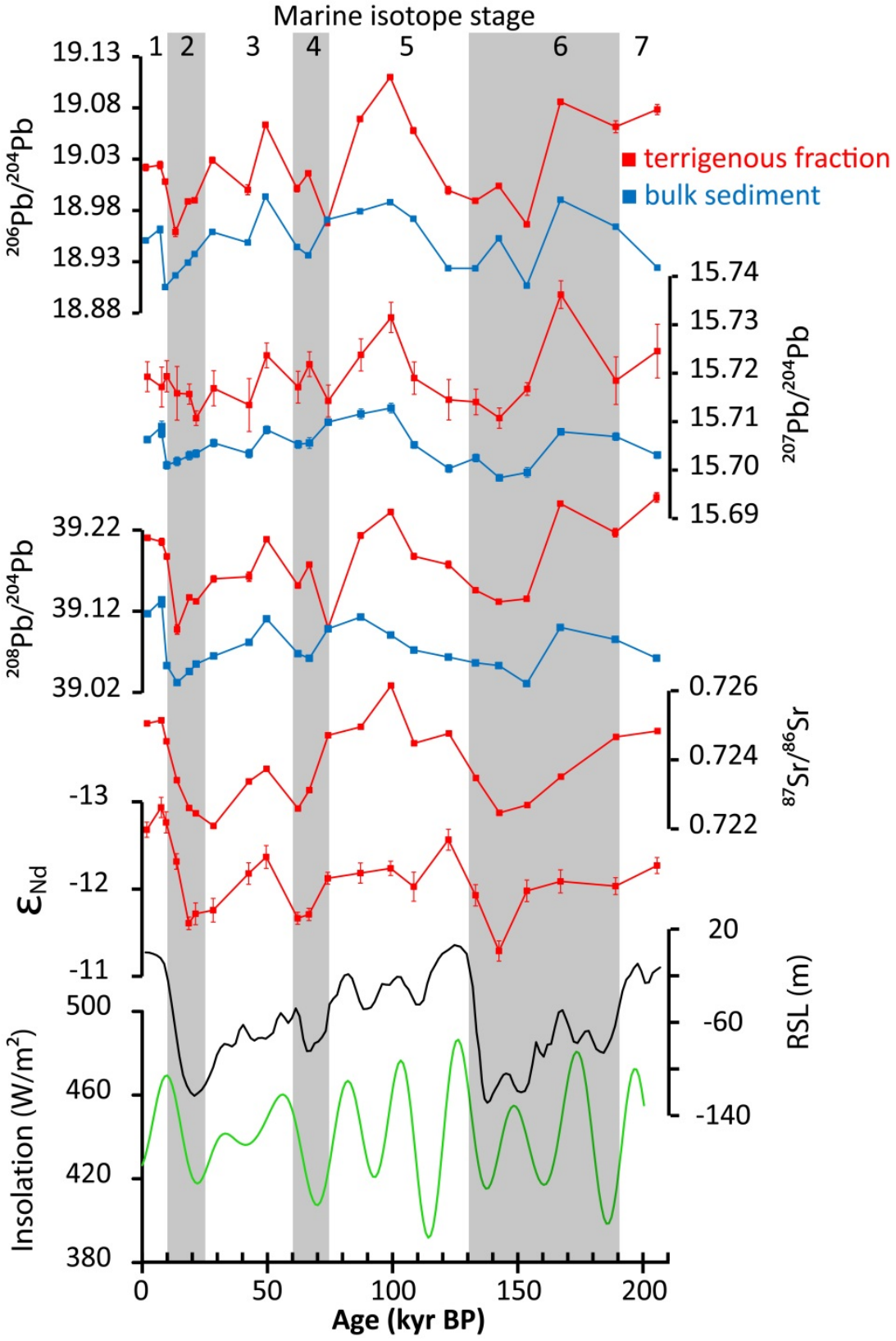

Fig. 4.4 Radiogenic isotopic variations of terrigenerous fraction (this study, red) and bulk sediment (Abouchami and Zabel, 2003, blue) from core GeoB1523-1. The relative sea level curve is built from global mean ocean $\delta^{18}O$ (Waelbroeck et al., 2002, black). The insolation curve is inferred from mid-month insolation 65°N for July in W/m^2 (Berger and Loutre, 1991; Berger, 1992, green). Marine Isotope Stage (MIS) is marked while grey presents cold glacial periods. The error bar on $^{206}Pb/^{204}Pb$, $^{208}Pb/^{204}Pb$ and $^{87}Sr/^{86}Sr$ is similar to the symbol size.

Pb isotopes measured on bulk sediments from the same core were presented in previous study (Abouchami and Zabel, 2003) and show ranges of $^{206}Pb/^{204}Pb$ = 18.91 to 18.99, $^{207}Pb/^{204}Pb$ = 15.70 to 15.71, and $^{208}Pb/^{204}Pb$ = 39.03 to 39.13; these values are systematically slightly less radiogenic than those we measure in the pure terrigenous fraction. Nevertheless, our data for the terrigenous fraction are generally quite consistent with the previous data for bulk sediments obtained by Abouchami and Zabel (2003) and basically exhibit the same trends (Fig. 4.4). The small offsets between the terrigenous fraction and bulk sediment data may reasonably be attributed to addtional authigenic and carbonate fractions, which bias towards a seawater composition in the bulk sediment (Bayon et al., 2002; Bayon et al., 2004).

4.4 Discussion

Previous studies have demonstrated the validity of using radiogenic isotopic records to trace the provenance and transport process of terrigenous sediments, which vary naturally due to the differences in the age, geologic history and geochemistry of continental terranes, and which are then transported upon weathering into the oceans via rivers, wind and ice (Abouchami and Zabel, 2003; Rutberg et al., 2005; Franzese et al., 2006; Bentahila et al., 2008; Franzese et al., 2009). Many factors ultimately can affect the isotopic signature preserved in terrestrial material deposited in marine sedimentary archives. These include changes in seasonal wind intensity and direction, terrestrial physical sorting, chemical weathering intensity, balance between aeolian and fluvial transport, as well as vegetation cover (Bayon et al., 2009; Cole et al., 2009; Chen et al., 2013; Garcin et al., 2014). As will be discussed below, at the Ceara Rise, relative sea level, climate variation and precipitation all influence radiogenic isotopic composition of the sediments.

4.4.1 Potential mixing end-members of the sediments

The simplest geochemical scheme for representing the composition of detrital sediment on the Ceara Rise is as a binary mixture between "highland Andes" and "lowland Shield" end-member compositions, as plotted in Fig. 4.5 alongside data from Amazon fan muds (McDaniel et al., 1997) and suspended loads from different tributaries (Allègre et al., 1996; Viers et al., 2008). This is based upon: (a) that the Ceara Rise is located in a high-lithogenic-flux region where the dominant source of suspended load is the Amazon River system, with smaller rivers only contributing an insignificant amount of material (Gibbs, 1974; Zabel et al., 1999; Dobson et al., 2001; Govin et al., 2014); (b) the Amazon River system passes through and drains most of northern South America, including the entire west coast Andean fold-belt mountains, as well as the ancient Brazilian and Guiana Precambrian Shields; (c) contributions from African wind-blown dusts at the Ceara Rise are likely to be neglible.

Allègre et al. (1996) have argued that the tributaries contributing to the main Amazon River can be divided into two groups: two are "Andean rivers" – Solimões and Madeira - draining mostly the Andes, while "lowland rivers" flow mostly over Precambrian Shield areas in eastern Brazil (Trombetas, Tapajos). A similar scheme was used by Abouchami and Zabel (2003). Following this idea, we could use either the Solimõs or the Madeira as our "Andean" endmember.

Suspended loads from these rivers have differences in isotopic composition, as can be seen in Fig. 4.5, which are likely to reflect gross north-south radiogenic isotope gradients seen along the Andean volcanic chain (e.g. Miller and Harris, 1989; Mamani et al., 2008). Unfortunately, the conventionally-obtained Pb isotope dataset of Allègie et al. (1996) is of far lesser quality than our own triple-spike dataset. On balance, we have opted to use data on suspended loads from the Rio Madeira as the "highland" Andes endmember. The Rio Madeira is the main southern and second biggest tributary to the Amazon. It drains approximately a quarter of the Amazon Basin and is responsible for around 50% of the suspended load

(roughly 550 × 10^6 t/year) released to the ocean from South America (Meade et al., 1985; Meade, 1994; Guyot et al., 1996).

The Trombetas has been chosen as the "lowland" Guiana Shield endmember, although it has the second smallest catchment of tributaries in the Amazon Basin. It is made up of the Poana, Anamu, and other headstreams originating in the Tumucumaque Uplands on the Guiana Shield (Vari et al., 2009). We assume that the Trombetas represents the isotopic composition of suspended load coming from the Guiana Shield (Allègre et al., 1996). The fact that the Trombetas has highly radiogenic Pb and Sr, and very unradiogenic Nd, is consistent with the old age of the Guiana Shield. We note that, even more extreme compositions have been documented in samples of Belterra clay from the region, which are locally-derived weathering products of the craton bedrock (Abouchami et al., 2013).

Thus, suspended load from the tributaries Madeira and Trombetas are used here as representative of the isotopic compositions of the Andes and Guiana Shield end-members, respectively. The changes in the Pb and Nd isotope ratios recorded in the terrigenous fraction in the Ceara Rise core will then reflect the relative proportions of materials, of different Pb and Nd isotopic compositions, from these two end-members. The ε_{Nd} at the Ceara Rise is more negative than that of highland Andes and more positive than that of the Guiana Shield, indicating that the Ceara Rise receives most of its detrital Nd from the Andes with an additional part from the older, cratonic regions, consistent with a former study (McDaniel et al., 1997). Our radiogenic isotope records for the study site are plotted together with those of various sources of materials in $^{207}Pb/^{204}Pb$ vs. $^{206}Pb/^{204}Pb$ (Fig. 4.5a), $^{208}Pb/^{204}Pb$ vs. $^{206}Pb/^{204}Pb$ (Fig. 4.5b), ε_{Nd} vs. $^{206}Pb/^{204}Pb$ (Fig. 4.5c) and $^{87}Sr/^{86}Sr$ vs. $^{206}Pb/^{204}Pb$ (Fig. 4.5d).

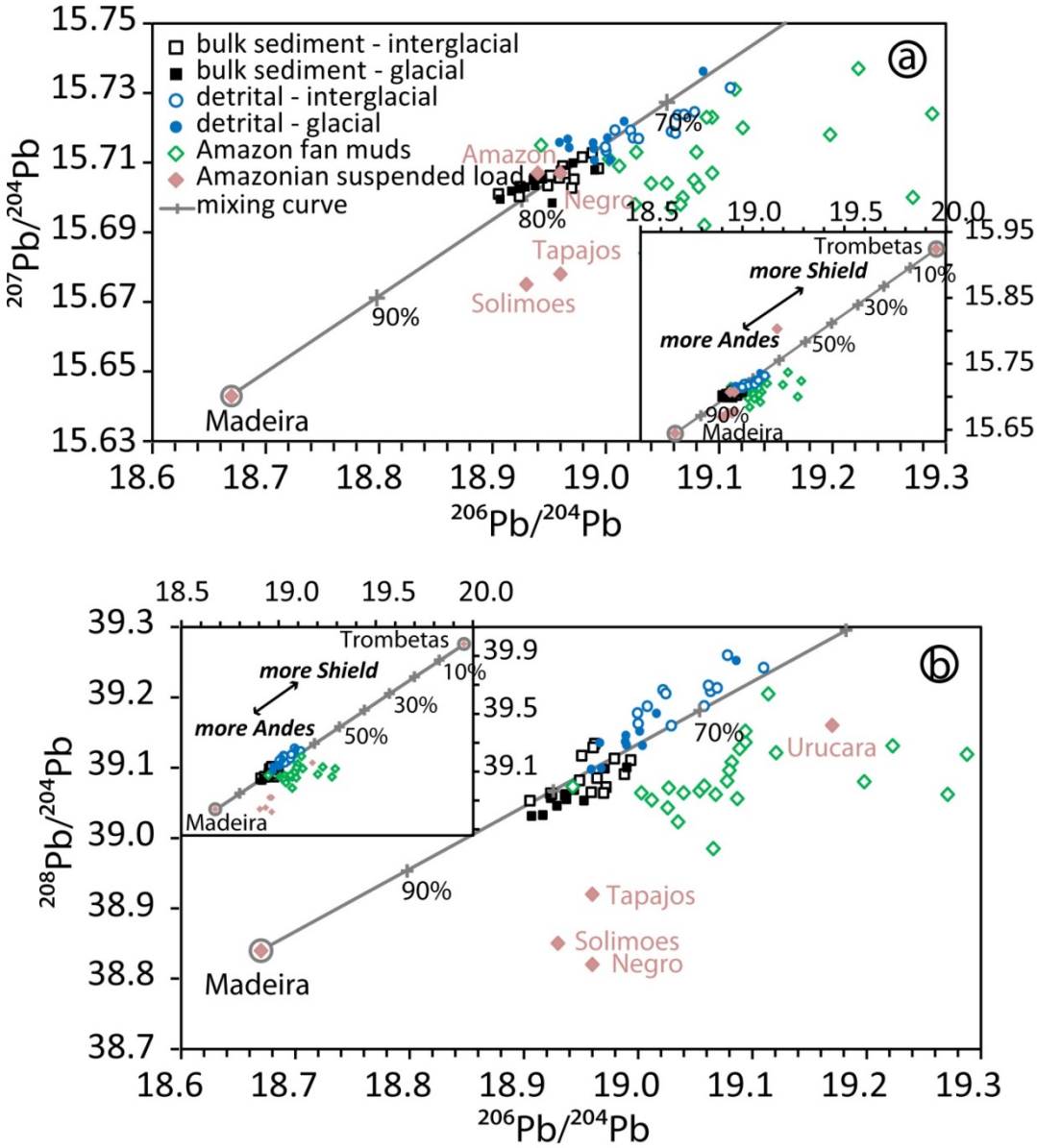

Fig. 4.5 Sr-Nd-Pb isotope cross plots. (a) $^{207}Pb/^{204}Pb$ vs. $^{206}Pb/^{204}Pb$, (b) $^{208}Pb/^{204}Pb$ vs. $^{206}Pb/^{204}Pb$, (c) $^{206}Pb/^{204}Pb$ vs. ε_{Nd}, (d) $^{206}Pb/^{204}Pb$ vs. $^{87}Sr/^{86}Sr$ isotope plots. Grey line in displays represent a simple binary mixing between 'Andes' and 'Shield' Pb isotopes. The Sr isotopic composition of Rio Solimoes and Pb isotope of Madeira have been used as the isotopic composition of Andes based on the proportions of the Andean component proposed in Allègre et al. (1996). Pb and Nd isotopic compositions of Amazon fan muds (McDaniel et al., 1997) and Amazonian suspended load from various tributaries and locations are worked (Allègre et al., 1996). Bulk sediment data of GeoB1523-1 from (Abouchami and Zabel, 2003).

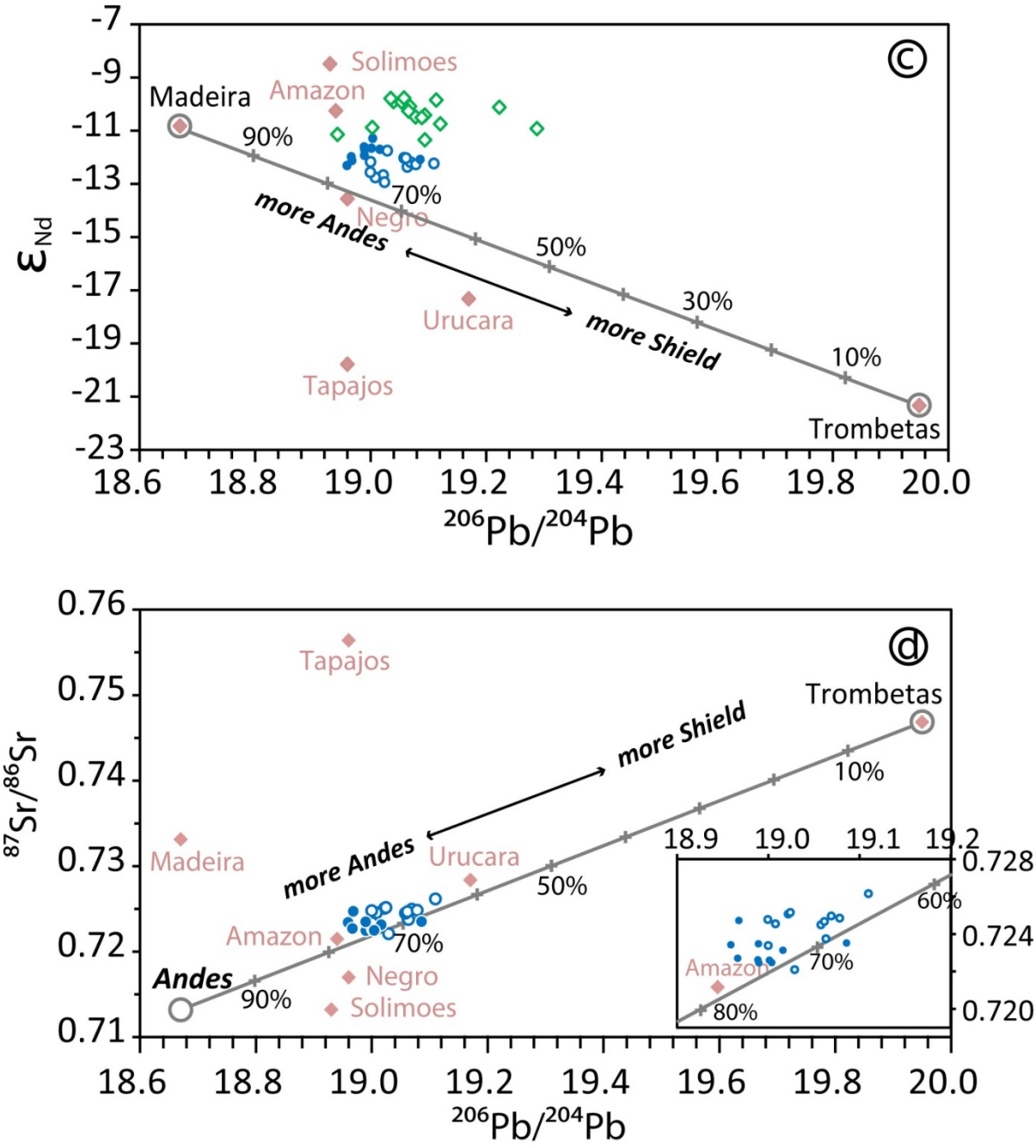

Continued **Fig. 4.5**

Most isotopic compositions of the detrital material from the Ceara Rise fall on or near the mixing curve between the two end-members (Fig. 4.5), while the interglacial data have generally lower ε_{Nd} values and more radiogenic Pb isotopic compositions compared to those in glacial periods. This shift can be explained by a 10% less contribution of the highland Andes end-member during interglacial periods. But overall it indicates that the Ceara Rise received its predominant sediment input from erosional weathering products of the Andes. According to Santos et al. (2015), the suspended load of the Andes controls the isotopic composition and flux from the Amazon River. This finding is consistent with concentrations of goethite and hematite found in the terrigenous fraction of sediments in the Ceara Rise (Harris and Mix, 1999), as well as isotopic compositions of mud samples taken from the Amazon Fan (McDaniel et al., 1997). ε_{Nd} and $^{87}Sr/^{86}Sr$ vs. $^{206}Pb/^{204}Pb$ suggest a similar picture, that the proportion of highland Andes versus lowland Guiana Shield to the Ceara Rise remained relatively stable (Fig. 4.5c and d). However, there are notable glacial-interglacial variations in Sr-Nd-Pb isotopes. The significant shift in isotopic composition between cold and warm periods seen in our dataset at the Ceara Rise is also mirrored in the Pb isotope data obtained previously on bulk sediments (Abouchami and Zabel, 2003).

Amazon Fan muds, composed primarily of Andean-derived sediments, have more radiogenic $^{206}Pb/^{204}Pb$ and $^{207}Pb/^{204}Pb$, and less radiogenic Nd isotopes than Andean igneous rocks, indicating that they have some component of Precambrian Pb in them (Milliman, 1979; Damuth et al., 1988; McDaniel et al., 1997). The isotopic composition of suspended load from the Rio Negro, plotted in Fig. 4.5, is consistent with such a notion that these sediments drain admixtures of Guiana Shield and Andean materials, as shown in the Nd-Sr isotopic cross-plot (Allègre et al., 1996; McDaniel et al., 1997; Latrubesse and Franzinelli, 2005). The Rio Negro is the largest black-water river and is ranked top ten for annual discharge in the world, draining highly chemically weathered soils. Thus, a simple binary mixing model seems to

successfully represent the mixing pattern seen in terrestrial-derived sediments at the Ceara Rise.

If we consider the Brazilian Shield as an additional source for the Ceara Rise, the suspended load from Tapajós River is a proper candidate to be used as a potential end-member. The Tapajós River is one of three major clear-water rivers in the Amazon system, which drains the central Brazilian Shield (Latrubesse and Franzinelli, 2005). It has higher ε_{Nd} and lower $^{207}Pb/^{204}Pb$ and $^{208}Pb/^{204}Pb$ isotopic compositions than those of the Guiana Shield, represented here by the Trombetas (Allègre et al., 1996). Figure 4.5 obviously shows that the Brazilien shield only can contribute a minor proportion of the material at the Ceara Rise based purely on its Nd and Sr isotopic composition, that resemble that of very old continental crust (McDaniel et al., 1997).

A gradual, and not subtle, shift in all isotope ratios is evident between cold and warm periods over the last 205 kyr (Fig. 4.5 and Fig. 4.6). This indicates an enhanced proportion of Andes highland, or decreased cratonic shield material during glacial periods. Other factors associated with climate variation may affect the input of sediment. For example, changes in relative sea level, alpine glaciation, precipitation and temperature (which influences weathering rates) may cause changes in the sedimentary contributions, even though the mechanisms are still not well understood (McDaniel et al., 1997).

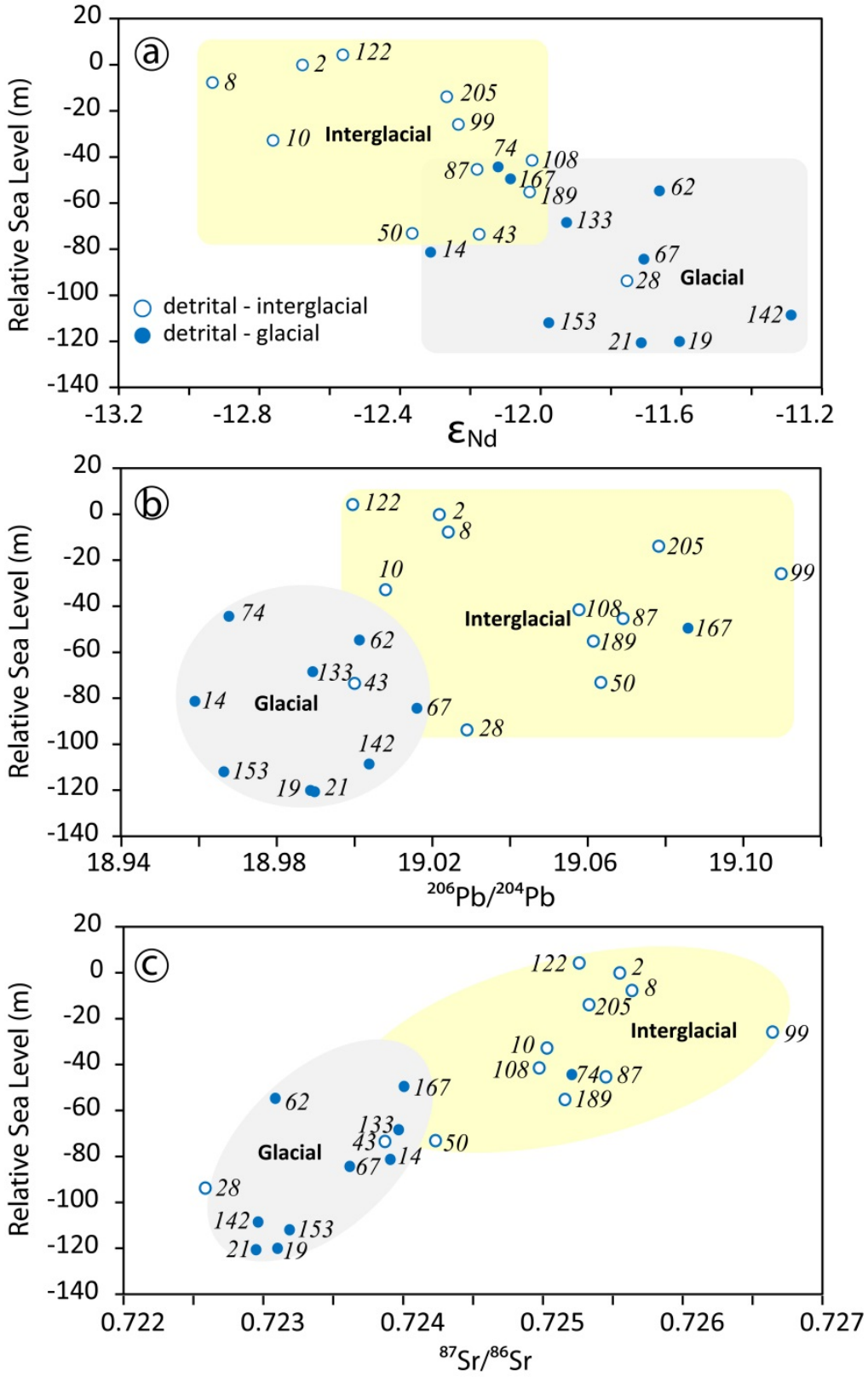

Fig. 4.6 Relationships between Sr-Nd-Pb and relative sea level (RSL). (a) ε_{Nd} vs. RSL, (b) $^{206}Pb/^{204}Pb$ vs. RSL, and (c) $^{87}Sr/^{86}Sr$ vs. RSL plots. Values in italic refer to the ages (kyr BP). Data have been subdivided into glacial and interglacial periods, and marked in grey and yellow respectively. The global sea level curve is constructed from the global mean ocean benthic $\delta^{18}O$ (Waelbroeck et al., 2002).

4.4.2 Relative sea level and changes in sediment sources

Relative sea level rise and fall is a global adjustment in the total volume of sea water contained within the ocean basins due to the formation of high-latitude ice sheets. It is one of the most fundamental factors impacting the rate and mode of sediment input from continental shelves into the deep ocean basins, as well as the rate of sediment accumulation on continental margins. Relative sea level has been widely used as a proxy record for millennial time-scale climate and tectonic processes (Vail et al., 1977; Major et al., 2006; Frigola et al., 2012; Lopes et al., 2014; Chang et al., 2015).

Govin et al. (2014) have discussed the contribution of different sedimentary sources at the Ceara Rise over the past 250 kyr, showing a relative increase in material originating from the highland Andes during intervals of sea level low stand. This suggests that sea level fluctuation is not the primary factor controlling the balance between highland Andes and lowland Shield contributions. Blum et al. (2013) concluded that there should be an increased contribution from lowland cratons during sea level low stands in glacial periods; this came from reviewing understanding of paleovalley systems: lowland rivers and flowing through low-lying sedimentary basins are more sensitive to valley incision and erosion than the Andean highlands upstream. Irion et al. (1995) suggested that non-Andean-sourced sediment was enhanced during the last glacial as a result of overall incision of the Amazon River caused by low global sea level.

In order to better understand the relative roles of sediment input and relative sea level change, we compare the isotopic compositions with the global sea level record in Figs. 4.4 and 4.6. The relative sea level shows increases passing from glacials to interglacials periods, varying from -120 m and 0 m, which is due to the influx of fresh water from glacial melt as the climate warms up (Waelbroeck et al., 2002). These changes are in the range of the global mean sea level variation of 125 m since the Last Glacial Maximum at around 20 kyr (Gornitz, 2009).

The comparison between Sr-Nd-Pb isotopes and relative sea level records in Fig. 4.6, shows a strong correspondance on glacial-interglacial timescales. During glacial periods, the relative sea level estimates lie within the range -120 m to -40 m, while ε_{Nd} values are between -12.3 and -11.3, $^{206}Pb/^{204}Pb$ ratios are below 19.09 and $^{87}Sr/^{86}Sr$ between 0.722 and 0.725. In contrast, in interglacial periods, relative sea levels lay between -80 m and 0 m (Fig. 4.6); associated isotopic compositions during these warmer times are less radiogenic ε_{Nd} (-12.9 and -11.8), and more radiogenic $^{206}Pb/^{204}Pb$ and $^{87}Sr/^{86}Sr$, ranging up to 19.11 and 0.726, respectively. There is overlapping between the glacial and interglacial fields seen in Figure 4.6 at 28 kyr, 74 kyr and 167 kyr - these represent a transition phase from glacial to interglacial periods or a shift between warm-cold substages (Sun and An, 2005; Kawamura et al., 2007). Either way, this probably represents a lag between global climate warming (with associated changes in precipitation and sediment delivery by the Amazon) and sea level rise (ice sheet melting).

Such a relationship shown in Fig. 4.6 indicates that changes in the source areas (i.e. different isotopic compositions) mostly vary synchronously with rise or drop in sea level. There is a strikingly similar behavior between different time periods over the past 200 kyr. This relationship appears robust and reflects the fundamental relation between global sea level changes and climate forcing of terrigenous inputs to the Ceara Rise.

Other studies have shown that the input of terrigenous material to the western Equatorial Atlantic bore some relation to fluctuations in relative sea level and fluvial runoff during the late Pleistocene (Damuth and Kumar, 1975; Nittrouer et al., 1995; Rühlemann et al., 1996; McDaniel et al., 1997; Harris and Mix, 1999; Rühlemann et al., 2001). As the sea regressed to more than -60 m below present, most of the Amazon-derived sediment would be transported directly to the deep sea by means of gravity-controlled sediment flows (turbidites) through small channels and the Amazon Submarine Canyon (Milliman et al., 1975). By contrast, during high stands in sea level, terrigenous sediment becomes trapped and stored in the

drainage basin and on the inner continental shelf off northeast Brazil since there is a more gentle slope at the land/ocean boundary (Damuth and Kumar, 1975; McDaniel et al., 1997).

It has been documented that at transitions from glacials to interglacials, the supply of terrigenous minerals from the Amazon River to the Ceara Rise dropped markedly due to a rapid increase of sea level (Damuth, 1977; Francois et al., 1990; Francois and Bacon, 1991; Rühlemann et al., 1996). This is further supported by high terrigenous fluxes coinciding with low sea levels, as inferred from low $\%CaCO_3$ and high $\delta^{18}O$ at the Ceara Rise (Harris and Mix, 1999).

Our results support the idea that a significant eustatic lowering of sea level in glacial cycles enhanced the proportion of terrigenous input to the core site and was associated with more radiogenic ε_{Nd}, unradiogenic Pb and Sr isotopic compositions. This may be because a declining sea level results in seaward progradation of the shoreline up to 350 km, approaching the shelf edge (Damuth and Kumar, 1975; Milliman et al., 1975; Nittrouer et al., 1995).

The large amount of arkosic sand is the most important piece of evidence to suggest that the highland Andes are the most major source of the sediment deposited at the Ceara Rise (Milliman et al., 1975; Meade et al., 1985; Guyot et al., 2007). Thus, the decreased interglacial supply from the highland Andes - marked by less radiogenic ε_{Nd} and more radiogenic Pb and Sr isotope ratios at the Ceara Rise - probably suggests a link between maximum sea level stands and contributions from lowland and highland source (Harris and Mix, 1999; Abouchami and Zabel, 2003). This fits the hypothesis, firstly, that Andean sediment may become trapped up the Amazon valley in response to postglacial eustatic sea level rises, effectively increasing the proportion of lowland sources. Secondly, during sea level low stands in glacial periods, a steepened gradient in the Amazon enhanced the transportation efficiency of sediment loads from the Andes, diluting the lowland craton signature by incising the channel and floodplain of the lower Amazon (Stallard, 1988; Harris and Mix, 1999; Aalto et al., 2003; Mertes and Dunne, 2008). The higher accumulation rate of

terrigenous material during glacials compared to interglacials is also suggested by excess ^{230}Th activity at the Ceara Rise (Rühlemann et al., 1996) and further supports this view.

4.4.3 Andean Glaciation and sediment delivery

Changes in eustatic sea level are tightly linked to the advance and retreat of continental ice sheets. During cold periods, water evaporating from the oceans at high latitudes became locked in glacier ice, leading to glacier advance and lowering of sea level; when the climate warmed up, the glaciers retreated and meltwater returned to the oceans, resulting in rising sea level (Nye, 1960; van de Wal and Oerlemans, 1995; Gardner et al., 2013).

Glaciers are extremely effective weathering and erosional agents, by abrading and plucking out of bedrock as they advance. The tropical Andes between Peru, Bolivia, Colombia and Ecuador are host to more than 98% of glaciers in the tropics principally due to the high elevation of the Andes mountains. The slopes of the tropical Andes are extensively eroded by mountain glaciers (Kaser, 1999; Thomson et al., 2010; Borsdorf et al., 2015). It has been shown that glacier expansion tends to enhance both mechanical and chemical denudation rates during glacial stages; further, glaciers erode more rapidly than rivers under similar conditions (Molnar and England, 1990; Raymo and Ruddiman, 1992; Hallet et al., 1996). Enhanced in stream loading and valley filling could potentially result from increased periglacial activity on mountain slopes (Damuth and Fairbridge, 1970).

The general occurrence of intervals of high lake level in glacial periods suggests cold and wet climate conditions in glacials versus interglacials in the tropical Andes, as exemplified by Lake Titicaca and shown by lacustrine pollen records (Baker et al., 2001b; Fritz et al., 2007; Punyasena et al., 2008; Fritz et al., 2012). This, combing with a snow line that dropped by 1 km in the Andes during glacials (Wilhelmy, 1957), implies that glacial expansion may have lead to a significantly enhanced terrigenous input from the Andes, which was then delivered by the Amazon into the Atlantic. This idea is further supported by

apparently diminished chemical weathering and terrigenous supply of Amazon lowland material to the Ceara Rise during glacial periods, owning to drier interglacial climate (Debrabant et al., 1997; Rühlemann et al., 2001). Increased terrigenous delivery is also clearly evident in the markedly higher accumulation rate during glacial stages (Francois and Bacon, 1991; Rühlemann et al., 1996).

In sharp contrast, Rimington (1999) has suggest that advancing ice would have substantially reduced sediment supply from the Andean region. Stable isotopes and biomarker proxies at Site 942 on the Amazon Fan are generally supportive of the conclusion that an increase in sediment supply from the Andes coincided with meltwater produced by the retreat of the Andean glaciers on glacial-to-interglacial transitions (Maslin et al., 2000; Bendle et al., 2010).

Overall, these studies cited are often confusing and contradictory. Nevertheless, it appears that one should expect a greater Andean versus lowland contribution to the Amazon suspended load during glacial times – and this is exactly what our radiogenic isotope data from the Ceara Rise imply. During glacials, there is a shift to more positive ε_{Nd} and less radiogenic $^{87}Sr/^{86}Sr$ and Pb isotopic composition (Figs. 4.5 and 4.6), consistent with more "younger" crustal components (i.e. Andes) present.

4.4.4 Precipitation in the Amazon Basin and ITCZ movement

The Amazon River basin is characterized by the fact that the major source areas of water discharge do not coincide with the main source areas supplying sediment. The highland Andes discharges less than 20% of all freshwater carried by the Amazon River, but contributes more than 80% of suspended load to the ocean (Gibbs, 1967; Milliman and Meade, 1983; Meade, 1994). A predominance of Andean-derived material in our core on the Ceara Rise throughout the last 205 kyr supports this (Fig. 4.5).

Changes in the distribution of precipitation within the Amazon Basin have the power to affect the relative balance of sedimentary contributions between the highland Andes and lowland Shield (Fig. 4.7). Indeed, there is evidence that the precipitation regime in these two regions are out of phase (McDaniel et al., 1997; Harris and Mix, 1999; Wang et al., 2006; Wang et al., 2007). Lake levels and speleothem oxygen isotope records document high precipitation in glacial periods and a shift to drier conditions during interglacial stages in the southern tropical Andes (Wirrmann and Mourguiart, 1995; Cross et al., 2000; Anhuf et al., 2006; Fritz et al., 2007; Cheng et al., 2013). Conversely, there appears to be increased precipitation passing from glacials to interglacials in lowland Amazonia (Cruz et al., 2005; Cruz et al., 2006; Wang et al., 2006; Wang et al., 2007).

Enhanced precipitation promotes intensified chemical weathering in both regions. A change in clay mineralogy would be expected, as lowland areas are characterized by highly weathered soils containing smectite, while the highland soils are less weathered and have illite (Gibbs, 1967; Debrabant et al., 1997; Rühlemann et al., 2001; Guyot et al., 2007). Illite/smectite ratios at our core site show a greater proportion of illite relative to smectite during the glacial versus interglacial periods (Rühlemann et al., 2001). This can be interpreted as reflecting drier lowland and wetter highland regions in the Amazon Basin during glacials versus interglacials. Thus, the evidence from clay mineralogy at the Ceara Rise site is supportive of an enhanced Andean contribution during glacials, which is entirely consistent with the glacial-to-interglacial radiogenic isotope shifts that we observe (Figs. 4.5 and 4.6).

The moisture availability over the Amazon Basin depends strongly on the north-south migration of the position of ITCZ, forced by Northern Hemisphere isolation, which affects the intensity of the South American summer monsoon (Harris and Mix, 1999; Baker et al., 2001b; Wang et al., 2004; Wang et al., 2006; Maslin et al., 2011). During the austral summer, there is increased rainfall in the Amazon Basin due to the South American monsoon resulting from an

enhanced land-ocean thermal gradient in which more moisture is transported onshore from the Atlantic Ocean (Fritz et al., 2004; Govin et al., 2014). In cold stages, there was a weaker ocean circulation and expanded ice coverage in the Northern Hemisphere, resulting from low high-latitude insolation. This then leads to a southward displacement of the ITCZ and strengthening of the Northeast-Trade Winds (Cruz et al., 2005; Cruz et al., 2006; Wang et al., 2006). As a result, there was enhanced moisture supply to the Amazon Basin (Cruz et al., 2006).

Changes in speleothem $\delta^{18}O$ records from southern and northern Brazil show that more moisture was being transported into the Amazon Basin during glacial periods, while the South American summer monsoon migrated southwards (Cruz et al., 2006; Wang et al., 2006; Wang et al., 2007). During glacial phases, the snow line dropped by 1 km in the Andes and there was increased precipitation and humidity at mid-elevations (Damuth and Fairbridge, 1970). Peterson et al. (2000) proposed that this phenomenon was caused by the southward displacement of the ITCZ with the rainbelt being blocked by the Andean mountain ranges (Gregory-Wodzicki, 2000). If correct, this would cause greater rainfall and river runoff in glacials, consistent with what we observed at the Ceara Rise (Fig. 4.6).

During transitions from glacials to interglacials, Andean glaciers retreated and rainfall increased sharply in the Amazon lowlands (Maslin et al., 2000; Maslin and Burns, 2000). This is seen in low levels in lake Titicaca in the Holocene which document decreased southward and westward advection of moisture into the central Andes and thus less runoff (Cross et al., 2000).

Rapid climate changes over the Amazon Basin may reflect shifts in the position of the ITCZ, forced by Northern Hemisphere insolation (Hays et al., 1976; Harris and Mix, 1999). It has been shown that June insolation at 65°N is the only climatic forcing that has an appropriate phase consistent with Amazon climate proxies (Harris and Mix, 1999).

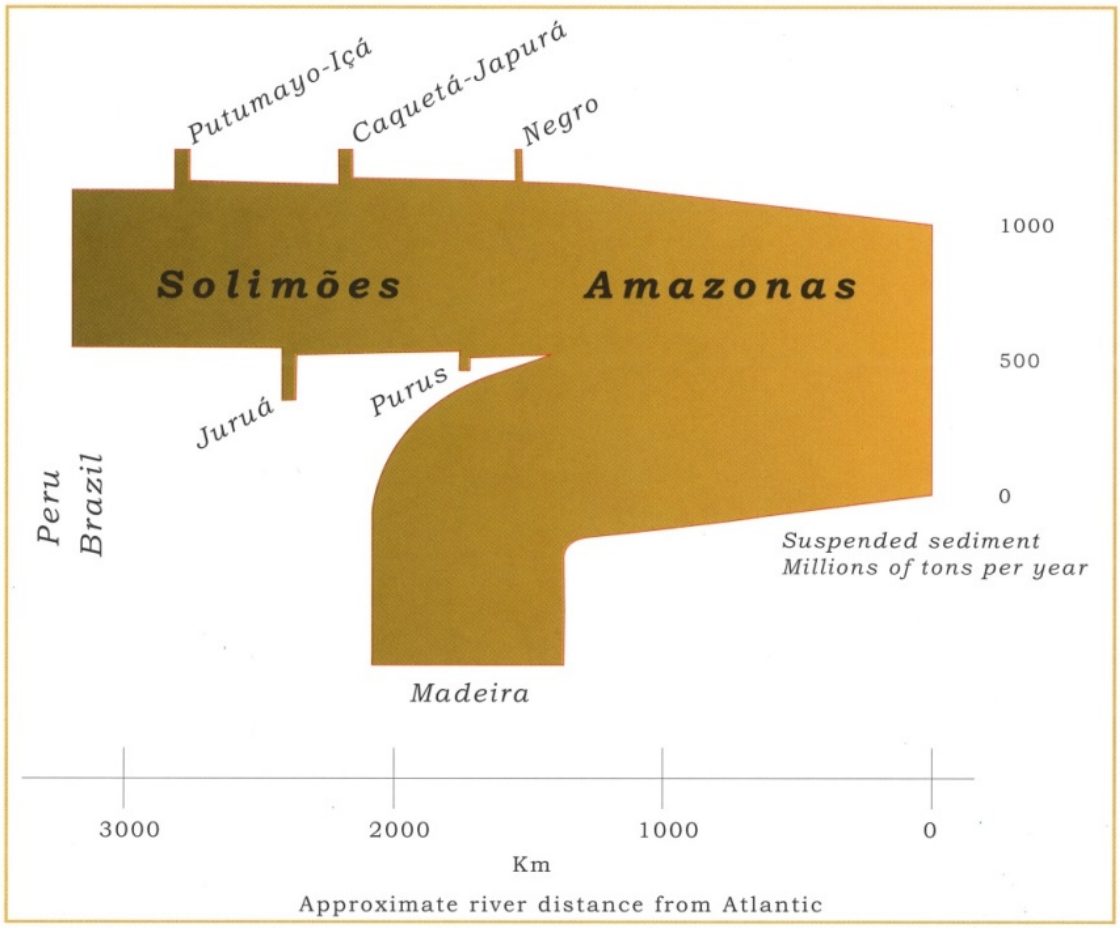

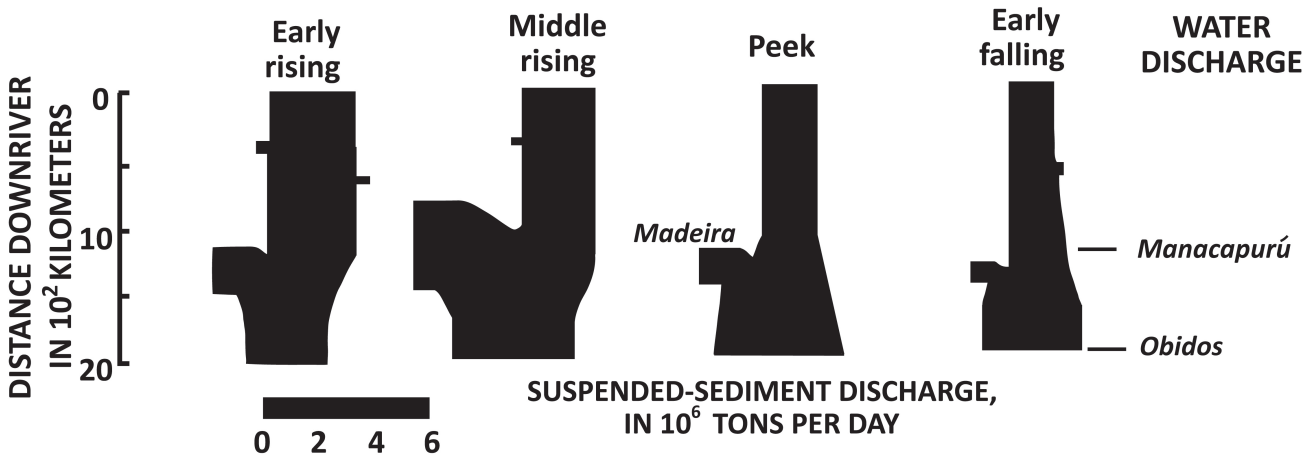

Fig. 4.7 **(a)** Distribution of sediment contributions from the Amazon's main stem and tributaries in Brazil (Goulding et al., 2003); **(b)** seasonality of storage and remobilisation of suspended loads at different water-discharge conditions in the main stem Amazon Rivers (Meade, 1994).

In order to examine whether precipitation in the Amazon Basin is forced by insolation, we compare the Sr and Pb isotopic compositions of our detrital record with July insolation at 65°N in Fig. 4.8. The 65°N insolation (Berger and Loutre, 1991; Berger, 1992) varies between 410 W/m^2 and 470 W/m^2. In Fig 4.8, the glacial-interglacial shifts in Pb and Sr isotopic composition are very clear. However, there is little or no correlation apparent with 65 °N summer insolation. At first, this is surprising given the strong correlations between radiogenic isotopes and relative sea level seen in Fig. 4.6. There appear to be two reasons for this. Firstly, low insolation occurs at 74 kyr, 167 kyr, 189 kyr and 205 kyr which are transitions between warm and cold periods, occurring at MIS5a-4, MIS7-6, MIS6e-6d, MIS7b-7a, respectively. Excluding these transitions, then in general, interglacials exhibit higher insolation than in glacials and this correlates positively, if poorly, with Pb and Sr isotope ratios. Secondly, the waxing and waning of continental ice sheets, reflected in the sea level curve, is in response to long-term forcings by high-latitude Northern Hemisphere isolation and not its short-term value (see Fig. 4.4).

Harris and Mix (1999) suggest that the latitudinal shifts of the ITCZ are triggered by an oceanic mechanism (forced by high-latitude insolation) with a lead in precipitation relative to ice volume, altering the erosion balance between highland and lowland regions in the Amazon Basin. Our results strongly support this view. During interglacial periods, higher insolation forced glacier melting, leading to an increased sea level stand; there was less rainfall over the Andes (on northward displacement of the ITCZ) and thus reduced Andean material entering the Amazon River system. Alternatively, postglacial eustatic sea level rise might have caused sediment build-up within the Amazon Basin, and thus less Andean contribution.

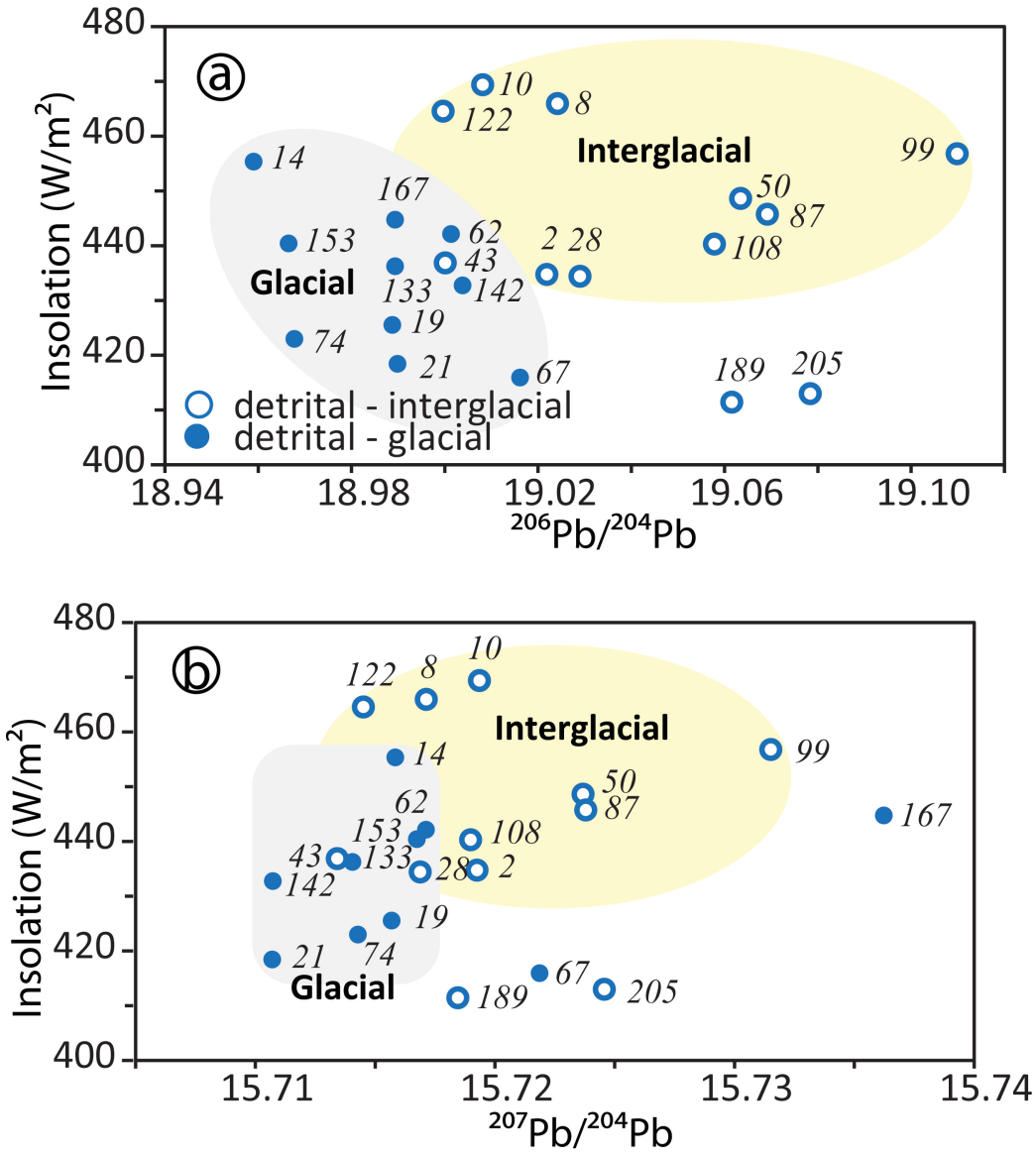

Fig. 4.8 Relationships between Sr-Nd-Pb isotopes and Insolation record. (a) $^{206}Pb/^{204}Pb$ vs. Insolation, (b) $^{207}Pb/^{204}Pb$ vs. Insolation, (c) $^{208}Pb/^{204}Pb$ vs. Insolation, and (d) $^{87}Sr/^{86}Sr$ vs. Insolation plots. Values in italic refer to the ages (kyr BP). Data have been subdivided into glacial and interglacial periods, and marked in grey and yellow respectively. The insolation data is inferred from mid-month insolation 65°N for July in W/m^2 (Berger and Loutre, 1991; Berger, 1992).

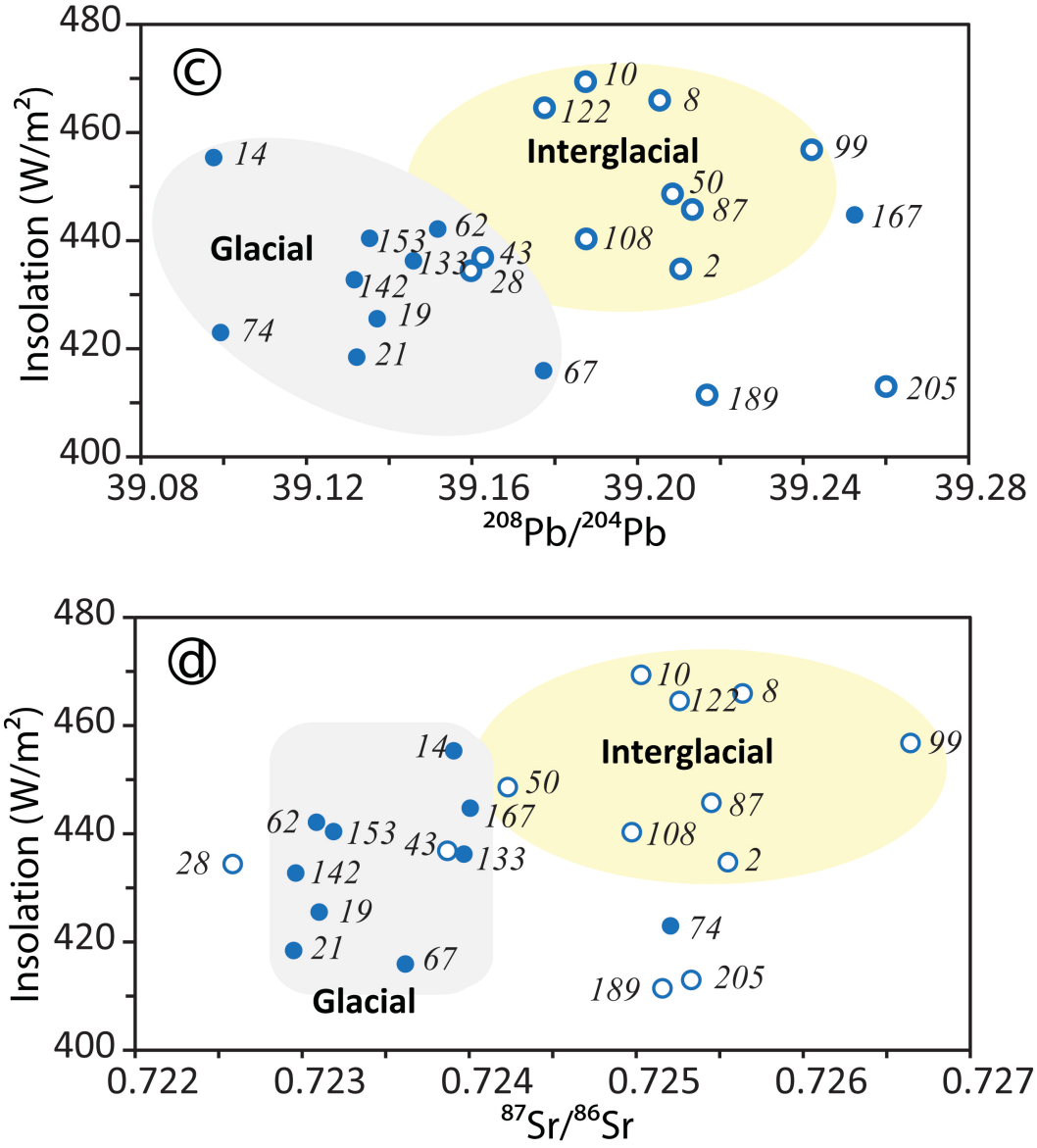

Continued **Fig. 4.8**

The former scenario seems more probable as several proxies indicate a wetter and colder climate over the Andes region when the Amazon lowlands were drier and colder during glacial times. These proxies include: stable isotopes in Amazon Fan sediments (Maslin et al., 2000; Maslin and Burns, 2000), speleothem oxygen isotope records from Brazil (Cruz et al., 2006; Wang et al., 2006; Wang et al., 2007), $\%CaCO_3$ and $\delta^{13}C$ of organic carbon records from Blivia, Peru (Fritz et al., 2007), as well as clay mineralogy and iron oxide concentration at the Ceara Rise (Harris and Mix, 1999; Rühlemann et al., 2001). This is also supported by speleothem oxygen isotope records from Amazonia, from which Cheng et al. (2013)

concluded that Amazon Basin precipitation follows Northern Hemisphere insolation, with a modest increase in rainfall in the west and a significant dying in the eastern part occurring during the last glacial.

4.4.5 Sediment transport to the Ceara Rise

In the western Equatorial Atlantic, terrigenous material delivered to the coast is dominated by the huge of suspended load of the Amazon River (Fig. 4.2) (Damuth and Kumar, 1975; Harris and Mix, 1999; Maslin and Burns, 2000; de Morais et al., 2006; Bendle et al., 2010; Govin et al., 2014). Most of this sediment becomes trapped offshore on the fan during sea level high stands, but enters the ocean freely when the sea level is low (McDaniel et al., 1997; Maslin and Burns, 2000; Mertes and Dunne, 2008). In our record, we see more radiogenic ε_{Nd}, and less radiogenic $^{87}Sr/^{86}Sr$ and Pb isotopes during glacials; this is associated with excess ^{230}Th at the Ceara Rise (Rühlemann et al., 2001) implying a greater sediment flux. Thus, sea level was lower, accumulation rates were higher and the contribution from the highland Andes increased during glacial stages.

The ^{230}Th mass balance at our core site suggests that postdepositional redistribution and lateral transport of sediment to the site were small over the last 180 kyr (Rühlemann et al., 2001). Moreover, the net flow of bottom water off the Amazon is landward, making it unlikely that sediment is transported from the Amazon to the Ceara Rise along the bottom (Gibbs, 1970; Damuth and Kumar, 1975). Similarly, the Ceara Rise lies over 1 km above the abyssal plain and cannot receive sediment from Amazon Fan turbidity currents (Rühlemann et al., 2001). Here, we suggest that the surface circulation in the western equatorial Atlantic may play an important role in modulating terrigenous sources reaching the Ceara Rise (see Fig. 4.3).

Many studies have already concluded that sediment transport to the Ceara Rise is controlled by the Trade Winds during annual migration of the ITCZ (Gibbs, 1970, 1973;

Rühlemann et al., 2001; Hu et al., 2004; Govin et al., 2014). During boreal winter, the NBC is strengthened by the NE-Trades as the ITCZ moves to its southernmost position (Fig. 4.3). This sweeps most of the Amazon plume suspended load northwestward along the coast. In boreal summer, strong SE-Trades (northernmost position of the ITCZ) force the NBC to turn eastward, away from the coast, between 5°N and 8°N. This retroflection of the NBC is known as the North Equatorial Counter Current (NECC; see Fig. 4.3). The NECC carries around 70% of the Amazon plume eastwards to the Ceara Rise (Lentz, 1995; Maslin and Burns, 2000; Rühlemann et al., 2001). It has been shown that enhanced zonal wind intensity would have increased the strength of the NBC retroflection during the last glacial period (Francois and Bacon, 1991; Maslin, 1998; Maslin and Burns, 2000; Rühlemann et al., 2001). It has also been suggested that during glacial stages, the southern boundary of the ITCZ migrated further south, causing an intensified NBC retroflection, deflecting more of the Amazon freshwater plume eastwards (Wilson et al., 2011; Govin et al., 2014). We propose here that the high sedimentation rate at the Ceara Rise during glacials was caused by two effects. First, the NBC retroflection was prolonged in duration or intensified, delivering more material (Wilson et al., 2011; Govin et al., 2014); second, as our GeoB1523-1 radiogenic isotope record suggests, the Andean sediment flux into the Amazon River system was greater in glacial times.

4.5 Conclusions

We present a 205-kyr record of Sr, Nd and Pb isotopic compositions on detrital fractions from sediment core GeoB1523-1 (3°49'N, 41°37'W, 3,292 m) located on the Ceara Rise in the western equatorial Atlantic. This is a record of the suspended load of the Amazon River entering the ocean, and thus the compositional mix of continental sources, and tributaries within the Amazon catchment over time. All radiogenic isotope systems display systematic shifts between warm and cold climatic periods. The principal isotopic variations seem to reflect the proportions of “highland” (Andean, young) and “lowland” (cratonic shields,

old) contributing sediment to the Amazon River system. There was an increased contribution of highland (Andes) materials during glacial compared to interglacial periods. Changes in terrigenous supply are correlated with and in phase with global relative sea levels. Correlation with Northern Hemisphere summer insolation at 65°N is poor, but improves if samples from glacial-interglacial transitions are excluded.

We suggest that the most important processes controlling changes in Amazon sediment provenance are variability in sea level, Andean glaciation and precipitation patterns within the Amazon Basin. During glacial periods, sea levels fell and southward displacement of the ITCZ caused enhanced moisture delivery to the Andes and build-up of Andean glaciers. This resulted in intensified Andean erosion and more "highland" material carried by the Amazon River. When the sea level regressed to more than -60 m, most of this suspended load enters the ocean directly, and more of it in the Amazon plume is transported to the Ceara Rise via the NBC retroflection. By contrast, during interglacial phases, sea levels rose, and there was greater rainfall over the Amazon lowland areas, associated with the northward displacement of the ITCZ. This caused intensification of chemical weathering in wet warm lowland regions and an enhanced contribution to the Amazon load. At high sea level stands, some terrigenous sediment is trapped and stored upriver in the drainage basin and on the inner continental shelf; this, combined with a less active NBC retroflection, gives rise to less Amazon material reaching the Ceara Rise in interglacial periods.

Acknowledgments

R.W. was funded by the Chinese State Scholarship Study Abroad Program for Graduate Studies and a Max Planck Society Research fellowship. We thank Matthias Zabel for supplying the GeoB1523-1 core material originally, and H. Feldmannn, S. Herrmann and R. Jotter for their help in the lab.

References

Aalto, R., Maurice-Bourgoin, L., Dunne, T., Montgomery, D.R., Nittrouer, C.A., Guyot, J.-L., 2003. Episodic sediment accumulation on Amazonian flood plains influenced by El Nino/Southern Oscillation. Nature 425, 493-497.

Abbott, M.B., Seltzer, G.O., Kelts, K.R., Southon, J., 1997. Holocene paleohydrology of the tropical Andes from lake records. Quaternary Research 47, 70-80.

Abouchami, W., Näthe, K., Kumar, A., Galer, S.J.G., Jochum, K.P., Williams, E., Horbe, A.M.C., Rosa, J.W.C., Balsam, W., Adams, D., Mezger, K., Andreae, M.O., 2013. Geochemical and isotopic characterization of the Bodélé Depression dust source and implications for transatlantic dust transport to the Amazon Basin. Earth and Planetary Science Letters 380, 112-123.

Abouchami, W., Zabel, M., 2003. Climate forcing of the Pb isotope record of terrigenous input into the Equatorial Atlantic. Earth and Planetary Science Letters 213, 221-234.

Allègre, C.J., Dupré, B., Négrel, P., Gaillardet, J., 1996. Sr-Nd-Pb isotope systematics in Amazon and Congo River systems: constraints about erosion processes. Chemical Geology 131, 93-112.

Anhuf, D., Ledru, M.P., Behling, H., Da Cruz Jr, F.W., Cordeiro, R.C., Van der Hammen, T., Karmann, I., Marengo, J.A., De Oliveira, P.E., Pessenda, L., Siffedine, A., Albuquerque, A.L., Da Silva Dias, P.L., 2006. Paleo-environmental change in Amazonian and African rainforest during the LGM. Palaeogeography, Palaeoclimatology, Palaeoecology 239, 510-527.

Arz, H.W., Pätzold, J., Wefer, G., 1999. Climatic changes during the last deglaciation recorded in sediment cores from the northeastern Brazilian Continental Margin. Geo-Marine Letters 19, 209-218.

Baker, P.A., Rigsby, C.A., Seltzer, G.O., Fritz, S.C., Lowenstein, T.K., Bacher, N.P., Veliz, C., 2001a. Tropical climate changes at millennial and orbital timescales on the Bolivian Altiplano. Nature 409, 698-701.

Baker, P.A., Seltzer, G.O., Fritz, S.C., Dunbar, R.B., Grove, M.J., Tapia, P.M., Cross, S.L., Rowe, H.D., Broda, J.P., 2001b. The history of South American tropical precipitation for the past 25,000 years. Science 291, 640-643.

Bayon, G., Burton, K.W., Soulet, G., Vigier, N., Dennielou, B., Etoubleau, J., Ponzevera, E., German, C.R., Nesbitt, R.W., 2009. Hf and Nd isotopes in marine sediments: Constraints on global silicate weathering. Earth and Planetary Science Letters 277, 318-326.

Bayon, G., German, C.R., Boella, R.M., Milton, J.A., Taylor, R.N., Nesbitt, R.W., 2002. An improved method for extracting marine sediment fractions and its application to Sr and Nd isotopic analysis. Chemical Geology 187, 179-199.

Bayon, G., German, C.R., Burton, K.W., Nesbitt, R.W., Rogers, N., 2004. Sedimentary Fe–Mn oxyhydroxides as paleoceanographic archives and the role of aeolian flux in regulating oceanic dissolved REE. Earth and Planetary Science Letters 224, 477-492.

Bendle, J.A., Weijers, J.W.H., Maslin, M.A., Sinninghe Damsté, J.S., Schouten, S., Hopmans, E.C., Boot, C.S., Pancost, R.D., 2010. Major changes in glacial and Holocene terrestrial temperatures and sources of organic carbon recorded in the Amazon fan by tetraether lipids. Geochemistry, Geophysics, Geosystems 11, Q12007.

Bentahila, Y., Ben Othman, D., Luck, J.-M., 2008. Strontium, lead and zinc isotopes in marine cores as tracers of sedimentary provenance: A case study around Taiwan orogen. Chemical Geology 248, 62-82.

Berger, A., 1992. Orbital Variations and Insolation Database. IGBP PAGES/World Data Center for Paleoclimatology, Boulder, CO.

Berger, A., Loutre, M.F., 1991. Insolation values for the climate of the last 10 million years. Quaternary Science Reviews 10, 297-317.

Bleil, U., von Dobeneck, T., 2004. Late Quaternary terrigenous sedimentation in the western Equatorial Atlantic South American versus African provenance discriminated by magnetic mineral analysis, in: Wefer, G., Mulitza, S., Ratmeyer, V. (Eds.), The South Atlantic in the Late Quaternary. Springer Berlin Heidelberg, pp. 213-236.
Blum, M., Martin, J., Milliken, K., Garvin, M., 2013. Paleovalley systems: Insights from Quaternary analogs and experiments. Earth-Science Reviews 116, 128-169.
Borsdorf, A., Stadel, C., Scott, B., 2015. The Andes: A geographical portrait. Springer International Publishing.
Chang, F., Li, T., Xiong, Z., Xu, Z., 2015. Evidence for sea level and monsoonally driven variations in terrigenous input to the northern East China Sea during the last 24.3 ka. Paleoceanography 30, 642-658.
Chen, T.-Y., Li, G., Frank, M., Ling, H.-F., 2013. Hafnium isotope fractionation during continental weathering: Implications for the generation of the seawater Nd-Hf isotope relationships. Geophysical Research Letters 40, 916-920.
Cheng, H., Sinha, A., Cruz, F.W., Wang, X., Edwards, R.L., d'Horta, F.M., Ribas, C.C., Vuille, M., Stott, L.D., Auler, A.S., 2013. Climate change patterns in Amazonia and biodiversity. Nat Commun 4, 1411.
Chester, R., Hughes, M.J., 1967. A chemical technique for the separation of ferro-manganese minerals, carbonate minerals and adsorbed trace elements from pelagic sediments. Chemical Geology 2, 249-262.
Clement, A.C., Hall, A., Broccoli, A.J., 2004. The importance of precessional signals in the tropical climate. Clim Dyn 22, 327-341.
Cole, J.M., Goldstein, S.L., deMenocal, P.B., Hemming, S.R., Grousset, F.E., 2009. Contrasting compositions of Saharan dust in the eastern Atlantic Ocean during the last deglaciation and African Humid Period. Earth and Planetary Science Letters 278, 257-266.
Colinvaux, P.A., De Oliveira, P.E., Moreno, J.E., Miller, M.C., Bush, M.B., 1996. A long pollen record from lowland Amazonia: Forest and cooling in glacial times. Science 274, 85-88.
Cross, S.L., Baker, P.A., Seltzer, G.O., Fritz, S.C., Dunbar, R.B., 2000. A new estimate of the Holocene lowstand level of Lake Titicaca, central Andes, and implications for tropical palaeohydrology. The Holocene 10, 21-32.
Cruz, F., Burns, S.J., Karmann, I., Sharp, W.D., Vuille, M., 2006. Reconstruction of regional atmospheric circulation features during the late Pleistocene in subtropical Brazil from oxygen isotope composition of speleothems. Earth and Planetary Science Letters 248, 495-507.
Cruz, F.W., Burns, S.J., Karmann, I., Sharp, W.D., Vuille, M., Cardoso, A.O., Ferrari, J.A., Silva Dias, P.L., Viana, O., 2005. Insolation-driven changes in atmospheric circulation over the past 116,000 years in subtropical Brazil. Nature 434, 63-66.
Cruz, F.W., Vuille, M., Burns, S.J., Wang, X., Cheng, H., Werner, M., Lawrence Edwards, R., Karmann, I., Auler, A.S., Nguyen, H., 2009. Orbitally driven east-west antiphasing of South American precipitation. Nature Geosci 2, 210-214.
Curry, W.B., Shackleton, N.J., Richter, C., et al., 1995. Proceedings of the Ocean Drilling Program, Initial Report 154, p. 1111.
Damuth, J.E., 1977. Late Quaternary sedimentation in the western equatorial Atlantic. Geological Society of America Bulletin 88, 695-710.
Damuth, J.E., Fairbridge, R.W., 1970. Equatorial Atlantic deep-sea arkosic sands and Ice-Age aridity in tropical South America. Geological Society of America Bulletin 81, 189-206.
Damuth, J.E., Flood, R.D., Kowsmann, R.O., Belderson, R.H., Gorini, M.A., 1988. Anatomy and growth pattern of Amazon deep-sea fan as revealed by long-range side-scan sonar (GLORIA) and high-resolution seismic studies. American Association of Petroleum Geologists Bulletin 72, 885-911.

Damuth, J.E., Kumar, N., 1975. Amazon Cone: Morphology, Sediments, Age, and Growth Pattern. Geological Society of America Bulletin 86, 863-878.
de Morais, J.O., Tintelnot, M., Irion, G., Souza Pinheiro, L., 2006. Pathways of clay mineral transport in the coastal zone of the Brazilian continental shelf from Ceará to the mouth of the Amazon River. Geo-Marine Letters 26, 16-22.
Debrabant, P., Lopez, M., Chamley, H., 1997. Clay mineral distribution and significance in Quaternary sediments of the Amazon Fan, Proceedings Ocean Drilling Program Scientific Results. National Science Foundation, pp. 177-192.
Dobson, D.M., Dickens, G.R., Rea, D.K., 2001. Terrigenous sediment on Ceara Rise: a Cenozoic record of South American orogeny and erosion. Palaeogeography, Palaeoclimatology, Palaeoecology 165, 215-229.
Dürkoop, A., Hale, W., Mulitza, S., Pätzold, J., Wefer, G., 1997. Late Quaternary variations of sea surface salinity and temperature in the western tropical Atlantic: Evidence from $\delta^{18}O$ of Globigerinoides sacculifer. Paleoceanography 12, 764-772.
Francois, R., Bacon, M.P., 1991. Variations in Terrigenous Input into the Deep Equatorial Atlantic During the Past 24,000 Years. Science 251, 1473-1476.
Francois, R., Bacon, M.P., Suman, D.O., 1990. Thorium-230 profiling in deep-sea sediments: High-resolution records of flux and dissolution of carbonate in the equatorial Atlantic during the last 24,000 years. Paleoceanography 5, 761-787.
Franzese, A.M., Hemming, S.R., Goldstein, S.L., 2009. Use of strontium isotopes in detrital sediments to constrain the glacial position of the Agulhas Retroflection. Paleoceanography 24, PA2217.
Franzese, A.M., Hemming, S.R., Goldstein, S.L., Anderson, R.F., 2006. Reduced Agulhas Leakage during the Last Glacial Maximum inferred from an integrated provenance and flux study. Earth and Planetary Science Letters 250, 72-88.
Frigola, J., Canals, M., Cacho, I., Moreno, A., Sierro, F.J., Flores, J.A., Berné, S., Jouet, G., Dennielou, B., Herrera, G., Pasqual, C., Grimalt, J.O., Galavazi, M., Schneider, R., 2012. A 500 kyr record of global sea-level oscillations in the Gulf of Lion, Mediterranean Sea: new insights into MIS 3 sea-level variability. Clim. Past 8, 1067-1077.
Fritz, S.C., Baker, P.A., Lowenstein, T.K., Seltzer, G.O., Rigsby, C.A., Dwyer, G.S., Tapia, P.M., Arnold, K.K., Ku, T.-L., Luo, S., 2004. Hydrologic variation during the last 170,000 years in the southern hemisphere tropics of South America. Quaternary Research 61, 95-104.
Fritz, S.C., Baker, P.A., Seltzer, G.O., Ballantyne, A., Tapia, P., Cheng, H., Edwards, R.L., 2007. Quaternary glaciation and hydrologic variation in the South American tropics as reconstructed from the Lake Titicaca drilling project. Quaternary Research 68, 410-420.
Fritz, S.C., Baker, P.A., Tapia, P., Spanbauer, T., Westover, K., 2012. Evolution of the Lake Titicaca basin and its diatom flora over the last ~ 370,000 years. Palaeogeography, Palaeoclimatology, Palaeoecology 317–318, 93-103.
Galer, S.J.G., 1999. Optimal double and triple spiking for high precision lead isotopic measurement. Chemical Geology 157, 255-274.
Garcin, Y., Schefuß, E., Schwab, V.F., Garreta, V., Gleixner, G., Vincens, A., Todou, G., Séné, O., Onana, J.-M., Achoundong, G., Sachse, D., 2014. Reconstructing C_3 and C_4 vegetation cover using *n*-alkane carbon isotope ratios in recent lake sediments from Cameroon, Western Central Africa. Geochimica et Cosmochimica Acta 142, 482-500.
Gardner, A.S., Moholdt, G., Cogley, J.G., Wouters, B., Arendt, A.A., Wahr, J., Berthier, E., Hock, R., Pfeffer, W.T., Kaser, G., Ligtenberg, S.R.M., Bolch, T., Sharp, M.J., Hagen, J.O., van den Broeke, M.R., Paul, F., 2013. A reconciled estimate of glacier contributions to sea level rise: 2003 to 2009. Science 340, 852-857.

Gibbs, R.J., 1967. The geochemistry of the Amazon river Ssystem: Part I. The factors that control the salinity and the composition and concentration of the suspended solids. Geological Society of America Bulletin 78, 1203-1232.
Gibbs, R.J., 1970. Circulation in the Amazon River estuary and adjacent Atlantic Ocean. Journal of Marine Research 28, 113-123.
Gibbs, R.J., 1973. The bottom sediments of the Amazon shelf and tropical Atlantic Ocean. Marine Geology 14, 39-45.
Gibbs, R.J., 1974. The suspended material of the Amazon shelf and tropical Atlantic Ocean, in: Gibbs, R. (Ed.), Suspended Solids in Water. Springer US, pp. 203-210.
Gornitz, V., 2009. Sea Level Change, Post-Glacial, in: Gornitz, V. (Ed.), Encyclopedia of Paleoclimatology and Ancient Environments. Springer Netherlands, Dordrecht, pp. 887-893.
Govin, A., Chiessi, C.M., Zabel, M., Sawakuchi, A.O., Heslop, D., Hörner, T., Zhang, Y., Mulitza, S., 2014. Terrigenous input off northern South America driven by changes in Amazonian climate and the North Brazil Current retroflection during the last 250 ka. Clim. Past 10, 843-862.
Govin, A., Holzwarth, U., Heslop, D., Ford Keeling, L., Zabel, M., Mulitza, S., Collins, J.A., Chiessi, C.M., 2012. Distribution of major elements in Atlantic surface sediments (36°N–49°S): Imprint of terrigenous input and continental weathering. Geochemistry, Geophysics, Geosystems 13, Q01013.
Gregory-Wodzicki, K.M., 2000. Uplift history of the Central and Northern Andes: a review. Geological Society of America Bulletin 112, 1091-1105.
Guyot, J.L., Filizola, N., Quintanilla, J., Cortez, J., 1996. Dissolved solids and suspended sediment yields in the Rio Madeira basin, from the Bolivian Andes to the Amazon IAHS Publication.
Guyot, J.L., Jouanneau, J.M., Soares, L., Boaventura, G.R., Maillet, N., Lagane, C., 2007. Clay mineral composition of river sediments in the Amazon Basin. CATENA 71, 340-356.
Hallet, B., Hunter, L., Bogen, J., 1996. Rates of erosion and sediment evacuation by glaciers: A review of field data and their implications. Global and Planetary Change 12, 213-235.
Harris, S.E., Mix, A.C., 1999. Pleistocene Precipitation Balance in the Amazon Basin Recorded in Deep Sea Sediments. Quaternary Research 51, 14-26.
Hays, J.D., Imbrie, J., Shackleton, N.J., 1976. Variations in the Earth's Orbit: Pacemaker of the Ice Ages. Science 194, 1121-1132.
Henehan, M.J., Rae, J.W.B., Foster, G.L., Erez, J., Prentice, K.C., Kucera, M., Bostock, H.C., Martínez-Botí, M.A., Milton, J.A., Wilson, P.A., Marshall, B.J., Elliott, T., 2013. Calibration of the boron isotope proxy in the planktonic foraminifera Globigerinoides ruber for use in palaeo-CO_2 reconstruction. Earth and Planetary Science Letters 364, 111-122.
Hu, C., Montgomery, E.T., Schmitt, R.W., Muller-Karger, F.E., 2004. The dispersal of the Amazon and Orinoco River water in the tropical Atlantic and Caribbean Sea: Observation from space and S-PALACE floats. Deep Sea Research Part II: Topical Studies in Oceanography 51, 1151-1171.
Imbrie, J., Hays, J.D., Martinson, D.G., McIntyre, A., Mix, A.C., Morley, J.J., Pisias, N.G., Prell, W.L., Shackleton, N.J., 1984. The orbital theory of Pleistocene climate: Support from a revised chronology of the marine $\delta^{18}O$ record, Milankovitch and climate: Understanding the response to astronomical forcing, p. 269.
Irion, G., Müller, J., Nunes de Mello, J., Junk, W.J., 1995. Quaternary geology of the Amazonian Lowland. Geo-Marine Letters 15, 172-178.
Jacobsen, S.B., Wasserburg, G.J., 1980. Sm-Nd isotopic evolution of chondrites. Earth and Planetary Science Letters 50, 139-155.

Kaser, G., 1999. A review of the modern fluctuations of tropical glaciers. Global and Planetary Change 22, 93-103.
Kawamura, K., Parrenin, F., Lisiecki, L., Uemura, R., Vimeux, F., Severinghaus, J.P., Hutterli, M.A., Nakazawa, T., Aoki, S., Jouzel, J., Raymo, M.E., Matsumoto, K., Nakata, H., Motoyama, H., Fujita, S., Goto-Azuma, K., Fujii, Y., Watanabe, O., 2007. Northern Hemisphere forcing of climatic cycles in Antarctica over the past 360,000 years. Nature 448, 912-916.
Kinkel, H., Baumann, K.H., Čepek, M., 2000. Coccolithophores in the equatorial Atlantic Ocean: response to seasonal and Late Quaternary surface water variability. Marine Micropaleontology 39, 87-112.
Kumar, A., Abouchami, W., Galer, S.J.G., Garrison, V.H., Williams, E., Andreae, M.O., 2014. A radiogenic isotope tracer study of transatlantic dust transport from Africa to the Caribbean. Atmospheric Environment 82, 130-143.
Kumar, N., Embley, R.W., 1977. Evolution and origin of Ceará Rise: An aseismic rise in the western equatorial Atlantic. Geological Society of America Bulletin 88, 683-694.
Kutzbach, J.E., Liu, X., Liu, Z., Chen, G., 2008. Simulation of the evolutionary response of global summer monsoons to orbital forcing over the past 280,000 years. Clim Dyn 30, 567-579.
Latrubesse, E.M., Franzinelli, E., 2005. The late Quaternary evolution of the Negro River, Amazon, Brazil: Implications for island and floodplain formation in large anabranching tropical systems. Geomorphology 70, 372-397.
Lentz, S.J., 1995. Seasonal variations in the horizontal structure of the Amazon Plume inferred from historical hydrographic data. Journal of Geophysical Research: Oceans 100, 2391-2400.
Leyden, B.W., Brenner, M., Hodell, D.A., Curtis, J.H., 1993. Late Pleistocene climate in the central American lowlands, Climate Change in Continental Isotopic Records. American Geophysical Union, pp. 165-178.
Li, T., Xu, Z., Lim, D., Chang, F., Wan, S., Jung, H., Choi, J., 2015. Sr–Nd isotopic constraints on detrital sediment provenance and paleoenvironmental change in the northern Okinawa Trough during the late Quaternary. Palaeogeography, Palaeoclimatology, Palaeoecology 430, 74-84.
Lopes, R.P., Dillenburg, S.R., Schultz, C.L., Ferigolo, J., Ribeiro, A.M., Pereira, J.C., Holanda, E.C., Pitana, V.G., Kerber, L., 2014. The sea-level highstand correlated to marine isotope stage (MIS) 7 in the coastal plain of the state of Rio Grande do Sul, Brazil. Anais da Academia Brasileira de Ciências 86, 1573-1595.
Major, C.O., Goldstein, S.L., Ryan, W.B.F., Lericolais, G., Piotrowski, A.M., Hajdas, I., 2006. The co-evolution of Black Sea level and composition through the last deglaciation and its paleoclimatic significance. Quaternary Science Reviews 25, 2031-2047.
Mamani, M., Tassara, A., Wörner, G., 2008. Composition and structural control of crustal domains in the central Andes. Geochemistry, Geophysics, Geosystems 9, Q03006.
Maslin, M., 1998. Equatorial western Atlantic Ocean circulation changes linked to the Heinrich events: deep-sea sediment evidence from the Amazon Fan. Geological Society, London, Special Publications 131, 111-127.
Maslin, M., Durham, E., Burns, S., Platzman, E., Grootes, P., Greig, S., Nadeau, M., Schleicher, M., Pflaumann, U., Lomax, B., 2000. Palaeoreconstruction of the Amazon River freshwater and sediment discharge using sediments recovered at Site 942 on the Amazon Fan. Journal of Quaternary Science 15, 419-434.
Maslin, M.A., Burns, S.J., 2000. Reconstruction of the Amazon Basin Effective Moisture Availability over the Past 14,000 Years. Science 290, 2285-2287.

Maslin, M.A., Ettwein, V.J., Wilson, K.E., Guilderson, T.P., Burns, S.J., Leng, M.J., 2011. Dynamic boundary-monsoon intensity hypothesis: evidence from the deglacial Amazon River discharge record. Quaternary Science Reviews 30, 3823-3833.
McDaniel, D.K., McLennan, S.M., Hanson, G.N., 1997. Provenance of Amazon muds: constraints from Nd and Pb isotopes. Proc. ODP Sci. Results 155, 169-176.
Meade, R.H., 1994. Suspended sediments of the modern Amazon and Orinoco rivers. Quaternary International 21, 29-39.
Meade, R.H., Dunne, T., Richey, J.E., De M. Santos, U., Salati, E., 1985. Storage and remobilization of suspended sediment in the lower Amazon river of Brazil. Science 228, 488-490.
Mertes, L.A.K., Dunne, T., 2008. Effects of tectonism, climate change, and sea-level change on the form and behaviour of the modern Amazon River and its floodplain, Large Rivers. John Wiley & Sons, Ltd, pp. 115-144.
Meyer, I., Davies, G.R., Stuut, J.-B.W., 2011. Grain size control on Sr-Nd isotope provenance studies and impact on paleoclimate reconstructions: An example from deep-sea sediments offshore NW Africa. Geochemistry, Geophysics, Geosystems 12, Q03005.
Miller, J.F., Harris, N.B.W., 1989. Evolution of continental crust in the Central Andes; constraints from Nd isotope systematics. Geology 17, 615-617.
Milliman, J.D., 1979. Morphology and structure of Amazon upper continental margin. AAPG Bulletin 63, 934-950.
Milliman, J.D., 2015. Bianchi, T.S., Allison, M.A., and Cai, W.-J. (eds.). Biogeochemical Dynamics at Major River-Coastal Interfaces. Linkages with Global Change. PB - Cambridge University Press . ISBN: 9781107022577. Limnology and Oceanography Bulletin 24, 55-85.
Milliman, J.D., Meade, R.H., 1983. World-Wide Delivery of River Sediment to the Oceans. The Journal of Geology 91, 1-21.
Milliman, J.D., Summerhayes, C.P., Barretto, H.T., 1975. Quaternary sedimentation on the Amazon continental margin: A model. Geological Society of America Bulletin 86, 610-614.
Molnar, P., England, P., 1990. Late Cenozoic uplift of mountain ranges and global climate change: chicken or egg? Nature 346, 29-34.
Mulitza, S., Rühlemann, C., Bickert, T., Hale, W., Pätzold, J., Wefer, G., 1998. Late Quaternary $\delta^{13}C$ gradients and carbonate accumulation in the western equatorial Atlantic. Earth and Planetary Science Letters 155, 237-249.
Muller-Karger, F.E., McClain, C.R., Richardson, P.L., 1988. The dispersal of the Amazon's water. Nature 333, 56-59.
Nittrouer, C.A., Kuehl, S.A., Sternberg, R.W., Figueiredo Jr, A.G., Faria, L.E.C., 1995. An introduction to the geological significance of sediment transport and accumulation on the Amazon continental shelf. Marine Geology 125, 177-192.
Nye, J.F., 1960. The response of glaciers and Ice-sheets to seasonal and climatic changes. Proceedings of the Royal Society of London A: Mathematical, Physical and Engineering Sciences 256, 559-584.
Parra, M., Pujos, M., 1998. Origin of late Holocene fine-grained sediments on the French Guiana shelf. Continental Shelf Research 18, 1613-1629.
Peterson, L.C., Haug, G.H., Hughen, K.A., Röhl, U., 2000. Rapid Changes in the Hydrologic Cycle of the Tropical Atlantic During the Last Glacial. Science 290, 1947-1951.
Placzek, C., Patchett, P.J., Quade, J., Wagner, J.D.M., 2006. Strategies for successful U-Th dating of paleolake carbonates: An example from the Bolivian Altiplano. Geochemistry, Geophysics, Geosystems 7, Q05024.

Punyasena, S.W., Mayle, F.E., McElwain, J.C., 2008. Quantitative estimates of glacial and Holocene temperature and precipitation change in lowland Amazonian Bolivia. Geology 36, 667-670.
Raymo, M.E., Ruddiman, W.F., 1992. Tectonic forcing of late Cenozoic climate. Nature 359, 117-122.
Rimington, N., 1999. Depositional history of sands on the Amazon Fan. University of Wales, Cardiff, U. K.
Rühlemann, C., Diekmann, B., Mulitza, S., Frank, M., 2001. Late Quaternary changes of western equatorial Atlantic surface circulation and Amazon lowland climate recorded in Ceará Rise deep-sea sediments. Paleoceanography 16, 293-305.
Rühlemann, C., Frank, M., Hale, W., Mangini, A., Mulitza, S., Müller, P.J., Wefer, G., 1996. Late Quaternary productivity changes in the western equatorial Atlantic: Evidence from ^{230}Th-normalized carbonate and organic carbon accumulation rates. Marine Geology 135, 127-152.
Rühlemann, C., Müller, P.J., Schneider, R.R., 1999. Organic carbon and carbonate as paleoproductivity proxies: Examples from high and low productivity areas of the tropical Atlantic, in: Fischer, G., Wefer, G. (Eds.), Use of Proxies in Paleoceanography. Springer Berlin Heidelberg, pp. 315-344.
Rutberg, R.L., Goldstein, S.L., Hemming, S.R., Anderson, R.F., 2005. Sr isotope evidence for sources of terrigenous sediment in the southeast Atlantic Ocean: Is there increased available Fe for enhanced glacial productivity? Paleoceanography 20, PA1018.
Rutberg, R.L., Hemming, S.R., Goldstein, S.L., 2000. Reduced North Atlantic Deep Water flux to the glacial Southern Ocean inferred from neodymium isotope ratios. Nature 405, 935-938.
Santos, R.V., Sondag, F., Cochonneau, G., Lagane, C., Brunet, P., Hattingh, K., Chaves, J.G.S., 2015. Source area and seasonal ^{87}Sr/^{86}Sr variations in rivers of the Amazon basin. Hydrological Processes 29, 187-197.
Schlitzer, R., 2014. Ocean Data View. *http://odv.awi.de*.
Stallard, R.F., 1988. Weathering and erosion in the humid tropics, in: Lerman, A., Meybeck, M. (Eds.), Physical and Chemical Weathering in Geochemical Cycles. Springer Netherlands, Dordrecht, pp. 225-246.
Sun, Y., An, Z., 2005. Late Pliocene-Pleistocene changes in mass accumulation rates of eolian deposits on the central Chinese Loess Plateau. Journal of Geophysical Research: Atmospheres 110, D23101.
Sylvestre, F., Servant, M., Servant-Vildary, S., Causse, C., Fournier, M., Ybert, J.-P., 1999. Lake-Level chronology on the southern Bolivian Altiplano (18°–23°S) during late-glacial time and the early Holocene. Quaternary Research 51, 54-66.
Thomson, S.N., Brandon, M.T., Tomkin, J.H., Reiners, P.W., Vasquez, C., Wilson, N.J., 2010. Glaciation as a destructive and constructive control on mountain building. Nature 467, 313-317.
Vail, P.R., Mitchum, J.B., Thompson, S., 1977. Seismic Stratigraphy and Global Changes of Sea Level: Part 4. Global Cycles of Relative Changes of Sea Level. American Association of Petroleum Geologists 26, 83-97.
van de Wal, R.S.W., Oerlemans, J., 1995. Response of valley glaciers to climate change and kinematic waves: a study with a numerical ice-flow model. Journal of Glaciology 41, 142-152.
Vari, R.P., Ferraris, C.J., Radosavljevic, A., Funk, V.A., 2009. Checklist of the Freshwater Fishes of the Guiana Shield. Bulletin of the Biological Society of Washington 17, 1-95.
Viers, J., Roddaz, M., Filizola, N., Guyot, J.-L., Sondag, F., Brunet, P., Zouiten, C., Boucayrand, C., Martin, F., Boaventura, G.R., 2008. Seasonal and provenance controls on Nd–Sr isotopic compositions of Amazon rivers suspended sediments and implications for

Nd and Sr fluxes exported to the Atlantic Ocean. Earth and Planetary Science Letters 274, 511-523.
Vink, A., Brune, A., Höll, C., Zonneveld, K.A.F., Willems, H., 2002. On the response of calcareous dinoflagellates to oligotrophy and stratification of the upper water column in the equatorial Atlantic Ocean. Palaeogeography, Palaeoclimatology, Palaeoecology 178, 53-66.
Waelbroeck, C., Labeyrie, L., Michel, E., Duplessy, J.C., McManus, J.F., Lambeck, K., Balbon, E., Labracherie, M., 2002. Sea-level and deep water temperature changes derived from benthic foraminifera isotopic records. Quaternary Science Reviews 21, 295-305.
Wang, X., Auler, A.S., Edwards, R.L., Cheng, H., Cristalli, P.S., Smart, P.L., Richards, D.A., Shen, C.-C., 2004. Wet periods in northeastern Brazil over the past 210 kyr linked to distant climate anomalies. Nature 432, 740-743.
Wang, X., Auler, A.S., Edwards, R.L., Cheng, H., Ito, E., Solheid, M., 2006. Interhemispheric anti-phasing of rainfall during the last glacial period. Quaternary Science Reviews 25, 3391-3403.
Wang, X., Auler, A.S., Edwards, R.L., Cheng, H., Ito, E., Wang, Y., Kong, X., Solheid, M., 2007. Millennial-scale precipitation changes in southern Brazil over the past 90,000 years. Geophysical Research Letters 34, L23701.
Wilhelmy, H., 1957. Eiszeit un eiszeitklima in den feucht tropischen Anden. Pet. Geogr. Mitt. Erg.-H 262, 281-310.
Wilson, K.E., Maslin, M.A., Burns, S.J., 2011. Evidence for a prolonged retroflection of the North Brazil Current during glacial stages. Palaeogeography, Palaeoclimatology, Palaeoecology 301, 86-96.
Wirrmann, D., Mourguiart, P., 1995. Late Quaternary spatio-temporal limnological variations in the Altiplano of Bolivia and Peru. Quaternary Research 43, 344-354.
Zabel, M., Bickert, T., Dittert, L., Haese, R.R., 1999. Significance of the sedimentary Al:Ti ratio as an indicator for variations in the circulation patterns of the equatorial North Atlantic. Paleoceanography 14, 789-799.

Chapter 5

Conclusions

The three previous chapters of this thesis examine three very contrasting temporal records from Atlantic sedimentary cores using radiogenic isotope systems as tracers of provenance. Chapter 2 concerns the AMOC, while chapters 3 and 4 examine how sources of African dust and suspended loads from the Amazon River, respectively, have changed over time.

New constraints on changes in the Atlantic Meridional Overturning Circulation (AMOC) since the Last Glacial Maximum (LGM ~18 - 24 ka) were obtained using radiogenic isotopes measured on hydrogenetic Fe-Mn oxide leachates from bulk sediments in a core from the Cape Basin, which reflect the composition of deep waters. The reliability of Nd isotopes in the Fe-Mn oxides of bulk sediments as a deep water signal was confirmed by measuring planktonic foraminifera and fish debris records from the same core. Combined with $^{231}Pa/^{230}Th$ and benthic $\delta^{13}C$ records, these data were used to reconstruct the variation in deep water circulation in the southeast Atlantic over the past 24 ka. We can now say with a high degree of certainty that in glacial times, Southern Component Water (SCW) flowed at shallower depths and penetrated further northwards, based upon the depth and latitudinal gradient in ε_{Nd}. The AMOC became progressively invigorated through the Holocene, reaching its full strength at the present day. The controversial idea of a "reversed" flow of Atlantic deep water during the LGM, due to more northward penetration of SCW, is supported by our study.

We also investigated changes in the provenance, delivery and oceanic transport of eolian dusts and riverine suspended loads in relation to terrestrial climate variations. We obtained Sr, Nd and Pb isotopic records on the detrital, terrigeous fraction of sediment cores from which we are able to characterize variations in source provenance in the eastern at 5° N (the Sierra Leone Rise) and western at 4°N equatorial Atlantic (the Ceara Rise) over last 200 ka that are

clearly climate related. Our records demonstrate that the responses of terrigenous inputs in the eastern and western equatorial Atlantic as a result of climate changes were quite different. In the east, the isotopic records imply there are three major sources of eolian dust contributing, derived from the Sahara-Sahel region of western North Africa. The relative contributions among these sources are controlled by differences in North African humidity and vegetation cover; during African Humid Periods there are observable shifts in radiogenic Pb isotope composition implying changes in the sources of dust supplied. By contrast, there is no significant response to latitudinal shift of the southern and northern boundary of the Intertropical Convergence Zone (ITCZ) during glacial-interglacial cycles.

The record of Amazon River suspended loads in the western Atlantic (Ceara Rise) is quite different. The supply of Amazon sediment to the Ceara Rise was greater during glacials due to a more prolonged seasonal North Brazil Current retroflection, which deflects the Amazon plume offshore, delivering terrigenous material to the Ceara Rise. The Pb, Nd and Sr radiogenic isotope data show systematic shifts during glacial-interglacial cycles and are strongly correlated with the deep-ocean benthic $\delta^{18}O$ record, which reflects global average temperature. These variations imply a shift in relative contributions from highland Andes and lowland Guiana Shield suspended loads areas contributing to the Amazon River system that are then reaching the Ceara Rise. We suggest that changes in sea level, Andean glaciation, precipitation and high-latitude insolation all play a role in modulating the sedimentary loads contributed by the Amazon, but ultimately the main driver is migration of the ITCZ. The sediment supply to the top of Ceara Rise is stronger during glacials due to a more prolonged North Brazil Current retroflection, which results in a stronger deflection of the suspended load of the Amazon River and shortens the distance of terrigenous material supply to the Ceara Rise site.

List of Figures

List of Table